LA-UR-96-3472

CONF-9608192--10

Title: QUEST FOR THE QUANTUM LIMIT IN THREE DIMENSIONAL METALS

Author(s): J. S. Brooks, J. S. Qualls, L. W. Engel, R. G. Clark, A. S. Dzurak, B. E. Kane--Univ. of New S. Wales, Australia
O. Tatsenko, V. Platinov, A. Bykov, M. Dolotenko-- VNIIEF, Russia
Clarence M. Flowler, Johdale C. Solem, James C. King, William D. Zerwekh, Dwight G. Rickel, Jeffrey D Goette--LANL
Lawrence J. Campbell -- MST-10, LANL
M. Tokumoto, N. Kinoshita, T. Kinoshita and Y. Tanaka--Electrotechnical Laboratory, Japan
H. Anzai -- Himeji Institute, Japan

Submitted to: "7TH International Conference on Megagauss Field Generation and Related Topics", Sarov, Russia August 5-10, 1996

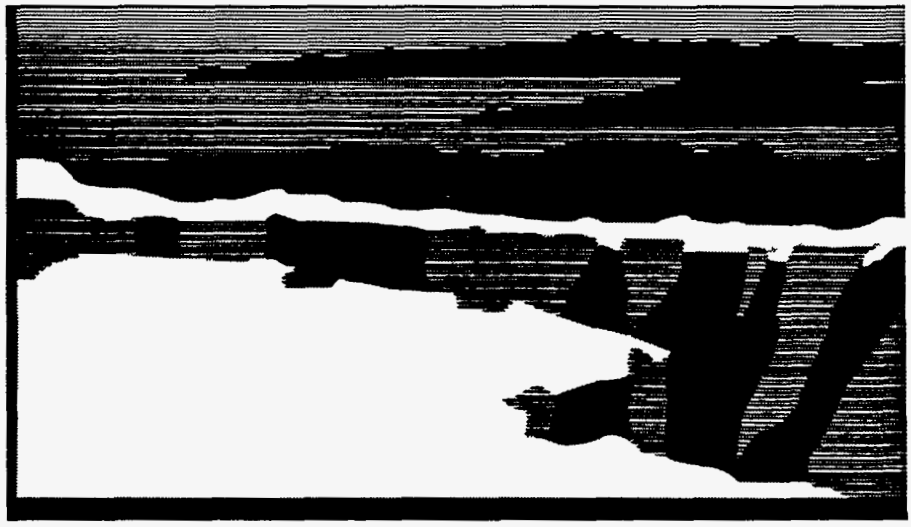

Los Alamos
NATIONAL LABORATORY

QUEST FOR THE QUANTUM LIMIT IN THREE DIMENSIONAL METALS

J. S. Brooks, J. S. Qualls, L. W. Engel, R.G. Clark[1], A. S. Dzurak[1], B. E. Kane[1], O. Tatsenko[2], V. Platinov[2], A. Bykov[2], M. Dolotenko[2], C.M. Fowler[3], J. C. Solem[3], J. King[3], W. Zerwekh[3], D. Rickel[4], J.D. Goettee[4], L. J. Campbell[4], M. Tokumoto[5], N. Kinoshita[5], T. Kinoshita[5], and Y. Tanaka[5], H. Anzai[6], N. Miura[7], H. Yokoi[8]

Florida State University and National High Magnetic Field Laboratory, Tallahassee FL USA
[1]University of New South Wales, Sydney Australia
[2]VNIIEF, Sarov, Russia
[3]Los Alamos National Laboratory, Los Alamos NM USA
[4]National High Magnetic Field Laboratory, Los Alamos National Laboratory, Los Alamos NM USA
[5]Electrotechnical Laboratory, Tsukuba Japan
[6]Himeji Institute, Hyogo, Akahogun, Japan
[7]ISSP, University of Tokyo, Tokyo, Japan
[8]NIMC, Tsukuba, Japan

September 16, 1996

ABSTRACT

The purpose of this work is to exploit ultra-high, flux compression type magnetic fields to achieve magnetic energies which are on the same or greater scale of the electronic structure in metallic systems. Under such conditions a metal may become an insulator, may acquire a completely new electronic structure, or may develop novel configurations of electronic order. In this paper we consider experiments on quasi-two dimensional molecular conductors in both non-destructive pulsed fields to 60 T and in destructive flux compression fields to 700 T at low temperatures. New results on the molecular conductors α-(BEDT-TTF)$_2$NH$_4$Hg(SCN)$_4$ and (TMTSF)$_2$ClO$_4$ are discussed in experiments up to 60 T at low temperatures, and preliminary results on α-(BEDT-TTF)$_2$NH$_4$Hg(SCN)$_4$ in the 700 T MC1 series flux compression generators are presented. We argue that true direct dc electrical transport measurements in these materials at low temperatures up to 700 T appear to be within reach.

Submitted to the "7th Int. Conf. on Megagauss Magnetic Field Generation and Related Topics - MG-VII", Sarov, , Russia, Aug. 5-10, 1996.

DISCLAIMER

I Introduction

The problem of the effects of very high magnetic fields on metals is one of fundamental importance. By definition, a metal has a Fermi surface. What do we mean by a metal? We mean a material in which the building blocks (atoms or molecules) are in a strictly periodic lattice structure, and in which electrons and/or holes are free to move along trajectories in one, two, or three dimensions as long as their energy remains constant. This is the Fermi energy, and these trajectories, when depicted in momentum space, make up what we call a Fermi surface. The energetics of the electrons in a metal become quantized in the plane perpendicular to the magnetic field. When this quantized energy, the cyclotron energy $E_c = \hbar\omega_c (\upsilon + 1/2)$ is coincident with the Fermi energy, all properties of the material related to the free energy or to the density of states are affected. And since $w_c = eB / m^*$, as the field is increased, the quantum number υ which satisfies the relation $E_F = E_c$ decreases. Hence there will be some field above which $\upsilon < 1$, and this is what is called the quantum limit. At this stage mother nature has to make a decision. One is that there is no longer any electrons in states at the Fermi level, and the material becomes an insulator. Another is that she finds new clever ways to arrange the electrons, as has been discovered in the fractional Hall effect. And a third is that since any real material is by no means as simple as the above picture suggests, other mechanisms for electron behavior which are enhanced by magnetic field (e.g. magnetic breakdown) kick in. The cyclotron energy is plotted vs. magnetic field in Fig. 1a. In the molecular crystals which we study, above 10 megagauss (1000 T) the magnetic energy is of the same order as the energy band-width, and are in the quantum limit of the material. Also the coulomb energy $\kappa e^2 / a \approx 140$ meV for a 10 Å lattice, so it is even possible that the crystal structure would change!

There is another interesting possibility which involves the magnetic length scale. There is a competition between the lattice periodicity (which gives rise to the Fermi surface character and to the Landau level scheme) and the periodicity induced by the magnetic field. In the lattice the "quantum" of space is the area of one unit cell. In the magnetic field, the "quantum" is the magnetic field flux quantum ϕ_0. The ratio of the flux in a unit cell to the flux quantum is $\phi/\phi_0 = Ba^2/h/e$. where a is the length of the unit cell. When the ratio is unity, $\phi/\phi_0 = 1$, and we may define $\ell_0 = \sqrt{h / eB}$, the magnetic length associated with this condition. To make a long story short, when the magnetic field is high enough so that it is of the order of one flux quantum per unit cell, the energy spectrum splits up into the most marvelous set of sub levels, the so-called Hofstadter Butterfly diagram[1]. The point at which this occurs vs. characteristic lattice constant is given in Fig. 1b. Hence, if one wished to observe such behavior in a metal such as copper, one would have to go the magnetic fields of order 100,000 T, but again, in the case of molecular crystals 1000 (i.e. 10 MG) is enough.

So, how do we go about looking for these remarkable effects of magnetic fields on metals? The easiest thing to do is to make a semiconductor heterostructure where one can study the to dimensional electron gas at the interface. This is nice since the electron gas is already quantized in the z- direction due to the spatial confinement, and the magnetic field quantizes the rest. And since the number of electrons is small, the Fermi level is small, and the magnetic field (less than 20 T) needed to get into the quantum limit is also small! It is important to note that the marriage of these semiconductors with high magnetic fields have yielded many "new states of matter" [2] at special quantum numbers υ, including the integer and fractional quantum Hall effect ($\upsilon < 10$ and $\upsilon < 1$) , composite Fermions ($\upsilon = 1/2$), Skyrmions ($\upsilon = 1, 1/3$), and Wigner crystallization ($\upsilon << 1$). At the other extreme, conventional metals are tough. They are three dimensional (no quantization along z), and the Fermi level is high (lots of electrons), so again very very high magnetic fields are

needed to get them into a quantum limit situation. But, there is another class of metals, which we call molecular conductors. The share the positive aspects of both the semiconductor and the conventional metal systems. On one hand, they are highly anisotropic. Usually their molecular structure is one of conducting layers separated by nearly insulating layers - hence they are at least quasi-two dimensional - in the spirit of the 2DEG. On the other hand, they have a Fermi surface, but the number of electrons is not so large. And in light of the Hofstadter picture, the unit cell is 100 times larger than in say copper, so the magnetic field needed to get into the Hofstadter regime in molecular conductors, as shown in Fig. 1, is in principle 100 times less!

Given the above discussion, we have decided to focus on the molecular conductors as the best candidates for studying novel effects of ultra high magnetic fields on metals[3]. They are nearly two dimensional, they come as very high quality single crystals, and their quantum limits can be reached in flux compression generators of the 1000 T class. Equally important is a peculiar feature of their anisotropic character. For some reason which is not yet clear, if one measures the resistance along the least conducting direction (see Fig. 9 below) , which is along the magnetic field direction, one observes a large magnetoresistance and quantum oscillation behavior, nearly a factor of 1000 times larger than the similar signals observed by studying the in-plane x-y resistance. This is a practical advantage. By only putting two leads on the sample, one above and below, and carefully aligning them along the magnetic field direction, one can get an enormous magnetoresistance signal from a very tiny sample. This reduces open loops in the leads which can pick up an unwanted emf when the magnetic field is changed rapidly, as in the case of pulsed and flux compression experiments.

The rest of this paper is organized as follows. First we show the experimental setup we have used in both pulsed and in the MC1 generator experiments. The message here is that by thinking about the extremes of the MC1 environment, we have made advances in noise reduction which are useful in pulsed, non-destructive applications. By looking backwards, this has given us new, very clean data in the pulsed field environment. We show our pulsed field results on several different materials. Next we show the results from the MC1 series. Finally we address considerations and designs for future MC1 shots.

II Simulation of signal and heating effects

What should we expect for a molecular conductor in a 700 T magnetic field? To examine this issue we consider the material α-(BEDT-TTF)$_2$NH$_4$Hg(SCN)$_4$. It is a highly anisotropic superconductor at 1.2 K, but is otherwise has no known magnetic field induced phase transitions. Its magnetoresistance is large at low magnetic fields, but saturates above 10 T. Its Fermi surface consists of a closed hole orbit and an open electron-like orbit. Measurements up to 50 T show only a marginal tendency for magnetic breakdown between the closed and open orbits. Magneto-oscillations are very prominent above 10 T for temperature in the range below 2 K, and the closed orbit Shubnikov de Haas (SdH) frequency is about 580 T. Hence this material should reach the quantum limit by 600 T, within the range of the MC1 system. Typical performance factors for the rate of change of magnetic field dB/dt and total field B for (1) pulsed magnets, (2) strip generator magnets, and (3) the MC1 class generators are shown in Fig. 2 vs. time.

To simulate the SdH signal of α-(BEDT-TTF)$_2$NH$_4$Hg(SCN)$_4$ in the MC1 system we have used the standard Lifshitz Kosevich expression[4, 5] to compute the oscillatory magnetoresistance

$$R_{osc} = [\exp(14.7 T_D m^* / m_0 B)(14.7 m^* T / m_0 B) / \sinh(14.7 m^* T / m_0 B)] \cos(2\pi F_0 / B)$$

where T_D is the Dingle temperature (~ 1 K), m^* is the effective mass (~ 2.1 m_0), and F_0 is the SdH frequency (~ 580 T).

The results for a typical temperature of 1.5 K is shown in Fig. 3a for the signal vs. time and also in Fig. 3b vs. field. Here we have used the data of Fig. 2c as input. We note that since the oscillations are periodic in inverse field, their period in linear field increases with field. Due to the very non-linear nature of the increase in field of the MC1 generators, the frequency of the

oscillations in the time domain is relatively uniform, going from about 4 MHz to 1 MHz over the duration of the pulse. As we will see, this makes it very difficult to separate electronic ringing in the lines from the actual signal.

Fig. 3 does not include the effects of heating due to the power introduced to the sample by the induced emf. To estimate this we first compute the integrated power introduced at any time according to the expression $Q_{tot} = \int_0^t \frac{(\dot{B}w)^2}{12\rho} dt$ where w is the characteristic width of the sample (of order 100 mm) and r is the resistivity. In the present case, the resistivity of the sample above 10 T is about an order of magnitude greater than the zero field value of r = 4.5 x 10^{-8} Ω-m. Hence we have taken the simple approximation that ρ has saturated between 10 and 700 T, and have not included the rise in temperature of the sample. The predicted heat input for a sample in the MC1 generator with the above parameters is shown in Fig. 4a. vs. time.

To determine the resulting rise in temperature of the sample we must compute the enthalpy $E = \int_{T=0}^{T} C_P dT$. Here C_P is the isobaric specific heat which we have taken[6] as $C_P = \gamma T + \beta T^3$ where γ = 1200 J/m^{3}K and β = 22 J/m^{3}K^3.

By comparison of Q_{tot} in Fig. 3a for a specific time with β in Fig. 3b, we can determine the temperature of the sample at any given time.
In the example shown, we estimate a 100 mm sample would rise to about 15 K by 700 T. Although this may seem extreme, if it is the parameter B/T which controls the amplitude of quantum oscillations, then we may compare the favorable case of say, 50 T at 1 K (B/T = 50) with the MC1 situation of 700/15 = 46. So in principle because of the extreme fields, the higher temperatures do not preclude observation of quantum limit effects.

In summary of this section, we note that the estimates above are approximate in the sense that we do not figure in the temperature dependence of the resistivity. Since the heating effects are worse for low resistance samples, a large magnetoresistance counteracts this effect. Also, as the temperature increases, so does the
resistance, and this again is in the right direction to counteract the power input to the sample. Secondly, we have not included the effect of thermal conductivity between the sample and the surrounding liquid helium, which should reduce the total heat input to the sample.

III. Experimental set up for the MC1 series.

An overview of the experimental set up is shown in Fig. 5. We have employed co-planar strip lines [7] on printed circuit boards to provide electrical contact to our samples. The sample holder is placed in a miniature plastic, super insulated dewar[8] specifically constructed for the MC1 environment. Another sample holder was placed back to back for the purpose of contactless measurements with a similar co-planar configuration, as will be described elsewhere[9]. Coaxial connections are made to the top of the dewar, which are some 30 m in length, and which run to the bunker down below. Fig. 6 shows the shape of the printed circuit board and Fig. 7 shows a detail of one of the co-planar transmission line patterns. For the dc transport measurements, holes were drilled through the center conductor at the positions shown, and the samples were inserted in the holes. The connecting lowest region of the transmission line was removed, and the center and outer conductors of each leg were shorted together with gold or silver paint. (See Fig. 8 for resulting electrical connection scheme.) In Fig. 8 and 9 we show details of the sample mounting configuration. In all, six samples can be mounted at one time on the sample holder, one on each leg of the co-planer transmission line pattern. Typically a sample was mounted by first drilling a 200 μm hole through the center conductor and PCB material. Then silicon rubber (RTV) was applied to the inside of the hole, and on the outer conductor lines surrounding the hole. This facilitates

getting the sample into the proper position, since RTV cures very slowly. It also keeps the sample and gold paint from shorting to the outer conductor. Gold wires are then attached to the center conductor and to the sample by gold paint. This assembly was reasonably resistant to discontinuities which can result from differential thermal contraction upon cool down. The center and outer conductors were shorted together below the sample, there by terminating the coaxial connection.

The electronic configurations for MC1-A, B, and C are shown in Figs. 10, 11, and 12 respectively. Of most importance is the way the co-planar transmission line is connected. In the event that the PCB is not absolutely parallel to the magnetic field, induced emf's will appear in the two loops created by the inner and two outer conductor pairs. The net result of the connections (see Fig. 11 and 12) is that the emf's will cancel in the center conductor, and will only appear in the outer, grounded conductor. As we will see below, the residual emf's across the sample were generally less than 10 V in the MC1 experiments, and were essentially eliminated in pulsed fields. The circuit of Fig. 10 had no 50 Ω termination, and was not otherwise optimized, and did not give reasonable results. In the example shown in Fig. 11 the 50 Ω termination at the scope was virtual in the sense that it was also used as the series resistor for the sample. Since there is a capacitance of about 3 nF in the coax which goes from the current source to the sample, the 50 Ω series resistor allowed a response of the current source of the order of 7 MHz. However, considerable ringing in the signal lines was still observed, even with the 50 Ω termination, as will be discussed below.

An updated electronics configuration is given in Fig. 12. Here a line driver is used to solve the 3nF coax loading problem, which thereby also directly terminates the coax at 50 Ω at each end. However, there is still about 140 pF in the co-planar lines. In choosing the optimum circuit, there are several considerations which must be addressed. First is how much current can the sample sustain without heating or degrading the low temperature behavior? As we show below, even several milliamps can be tolerated in the temperature range around 1.7 K. Hence the series resistance for the current source may be kept at a lower value, thereby keeping the time constant small enough to allow the current source to respond to rapid changes in the in the sample resistance. For completeness, we show the response of the various circuits vs. sample resistance in Fig. 13 In the analysis, the series resistance must be accounted for since it is not in a constant current limit. Here we see that as the sample resistance rises, the current decreases. Hence the optimum values for the compliance voltage and series resistance must be "customized" so that the sample does not get too much current, and so the RC time constant is not too large.

IV. Pre-tests of the various configurations in the 50 and 60 T class magnets.

To optimize the experimental parameters prior to the destructive MC1 experiments, we assembled the sample holder and dewar arrangement and performed experiments in the pulsed field magnets (< 60 T, 209 ms duration) at liquid helium temperatures. We now discuss these pre-test experiments. Not only could we anticipate the performance of the experimental setup when the MC1 was used, but we observed new physical properties in some of the samples in pulsed fields.

IV. a Experiments on α-(BEDT-TTF)$_2$NH$_4$Hg(SCN)$_4$

The molecular conductor α-(BEDT-TTF)$_2$NH$_4$Hg(SCN)$_4$ is a superconductor below about 1 K. When the magnetic field is applied perpendicular to the conducting BEDT-TTF layers, the critical field is reached by less than a tesla. For higher magnetic fields the magnetoresistance first rises rapidly, then saturates. With increasing field oscillations in the magnetoresistance appear which are called Shubnikov de Haas oscillations, as described in Fig. 3. In Fig. 14 we show a typical result based on the circuit of Fig. 10 for a sample mounted as in Fig. 9, and cooled to 1.7K. Fig. 14a shows the time dependence of signal, Fig. 14b shows the field dependence of the complete trace, and Fig. 14c shows the correction for resistance based on the divider circuit of Fig. 10

according to $R_{sample} = \frac{R_{series} V_{sample}}{(V_0 - V_{sample})}$. Here we make the following observations. First the measurements are two terminal. This means that the lead and contact resistance is in series with the sample. Ideally, the gold wire and paint assembly will contribute only 10 to 100 Ω to the sample resistance, but for larger contact resistance, the two terminal method tends to enhance the negative effects of dB/dt pick up. Secondly, except for a spike at the start of the pulse which be believe to be EMI from the ignitron switch, the data for both increasing and decreasing field lie essentially upon each other when plotted vs. field instead of time. Hence the effects of induced emf's due to the dB/dt have been essentially eliminated. Finally we note that although the signal voltage and resistance (computed from the series circuit) appear similar, for high values of resistance, such as at the peaks of the oscillations, the wave form in the voltage signal will appear attenuated. Hence the resistance must be computed to get the actual wave form. We further note that the compliance voltage V_0 must be known accurately for high resistance values, since the denominator ($V_0 - V_{sample}$) diverges as the sample resistance becomes large.

In Fig. 15 a comparison between the 50 Ω and a 2000 Ω series resistance in the current source is shown for one sample at 1.7 K. Although there is some are is nearly the same, particularly for the quantum oscillation amplitudes at high fields. Hence currents in the several mA range do not preclude the observation of quantum oscillations at these temperatures.

In Fig. 16 all signals for the 5 samples studied in the pretest are shown. The behavior is relatively uniform among them. However, a new feature not previously observed in these materials is the envelope associated with the quantum oscillation behavior. The frequency of the envelope is of order 50 T, and was first observed in the material only under hydrostatic pressure[10], and then later in uniaxial stress[11]. At present we have no explanation for the consistent observation of this feature in all of the samples studied, save that the extremely small size of the samples may cause them to be placed under some strain by the RTV and gold paint and wire contacts used in the sample mount.

In Fig. 17 we show the Fourier transform of the quantum oscillation data. At temperatures above 1 K, the oscillation amplitude begins to be attenuated (see Eq. 1) , and only a few harmonics of the fundamental frequency F_0 appear. The variation in F_0 from sample to sample is due to uncertainty in the orientation with respect to magnetic field (tilt increases the apparent F_0) and also perhaps strain on the sample.

We next turn to the second pretest where the electronics of Fig. 11 were used in general, but were we also employed an ac, amplitude modulation method similar to that of Clark et al.[Clark, 1996 #439] in one of the samples. The basic idea of the ac method is to put a 750 MHz carrier through the co-planar transmission line with the sample in series with the center conductor (see Fig. 18). The carrier is then rectified and recorded. To calibrate the rectified ac signal, we used a series of resistor values in shielded boxes. We found that over the range of 50 Ω to 2000 Ω the response of the ac signal was essentially linear , with only a small quadratic term, with resistance. Hence the rectified signal (which is large and negative at low resistance) increases towards zero with increasing resistance. Here again α-(BEDT-TTF)$_2$NH$_4$Hg(SCN)$_4$ was studied. In Fig. 19 data to 52 T is shown where we compare the ac vs. the dc method. This data was taken with no amplification of the rectified ac signal, and at low resolution in the data acquisition system. In Fig. 20 similar results to 14 T with an optimized ac circuit, which included leaving the VCO reference floating, is shown. Here the signal to noise for both DC and DC measurements are quite comparable, except that in the ac method the magnetoresistance rises much more rapidly at low fields (The same behavior is observable in Fig. 19.). In Figure 21a we show again comparisons of ac and dc measurements to 27 T, and in Fig. 21b we show an ac measurement to 50 T. In all cases the ac signal (even when the resistance is calculated from the ac signal as is shown in Fig. 21b) increases more rapidly at low fields than does the dc resistance signal. This must be due to characteristics of the ac electronics. The precise value of the zero field signal with respect to zero signal (which would correspond to a maximum resistance) appear to be dependent on the frequency of the oscillator, and perhaps other factors. Hence the relationship between the sample

resistance and the output voltage may be more complicated than the simple calibration indicated. More work is needed to fully understand the details of the ac circuit, but the conclusion is that the ac and dc methods are comparable. The ac method has the added advantage of being able to filter out, with a high pass filter, the types of ringing seen in the DC measurements.

IV. b Experiments on $(TMTSF)_2ClO_4$ in the quenched state.

A more complex molecular conductor, which is quasi - one dimensional in its electronic structure, is the Bechgaard salt[12] $(TMTSF)_2ClO_4$. Recently we have studied this material in pulsed fields up to 50 T[13] in the so-called relaxed state of the material. In this case the zero field superconducting state, the magnetic field induced spin density wave (FISDW) states, and an anomalous high field phase boundary are seen. The magnetic field is applied perpendicular to the conducting layers of the material. Superimposed on the background of the magnetoresistance at low temperatures is a phenomenon called "rapid oscillations" which have a characteristic frequency of 250 T with a second harmonic of 500 T. The second harmonic is strongly influenced in the FISDW states and is dependent on how well ordered the sample is. A relaxed sample is cooled very slowly (10 mK/min) through the anion ordering temperature at 24 K, and is well ordered. A quenched sample is one which is cooled as quickly as possible (300K/min) so that the anions do not order. Such samples will be non superconducting, and may show insulating behavior at low temperatures. Since the anion order halves the unit cell along one axis, the electronic structure of the quenched and ordered states are quite different.

A study of the ultra high field state, which may be an optimally nested FISDW state, and where above 250 T the rapid oscillation phenomena would be in the quantum limit, is very desirable. However, due to the complication of the slow cooling process, which ideally takes many hours with a controlled temperature sweep, it is not well suited to the MC1 experiments which must be done from room temperature to 1.7 K in a matter of 1/2 hour or so. Nevertheless, we decided to do MC1 type configuration pre-tests with this material anyway for two reasons. The first is that in a preliminary experiment[3] we found that a quenched sample of $(TMTSF)_2ClO_4$ the magnetoresistance had a very different character, and that the rapid oscillation frequency was about 190 T, significantly different from that of the ordered state. The second reason is that we wished to try to find a new, more convenient way to order the sample by self heating the sample with a high current while the sample was in the helium bath. The idea was to monitor the resistance of the sample vs. power input to see if ordering could be achieved by first bringing the power (temperature) of the sample above 24 K, and then reducing the power slowly back to zero. Our single attempt was not adequate to see if the method would work, but we do know that 10 mA will not seriously affect the material, and more work is in progress.

Samples of $(TMTSF)_2ClO_4$ were mounted in the manner of Fig. 9, with the c-axis parallel to the field and current directions, and various divider circuits were used to supply current. Signals to 57 T are shown in Fig. 22 for one of the samples studied as a function of temperature. Aside from the increasing magnetoresistance with decreasing temperature, quantum oscillations of low frequency are quite apparent at higher temperatures. In Fig. 23 we show the derivative signal for the 4 K and the 1.7 K data. Apparent here is the following. First, at higher temperatures a quantum oscillation frequency of about 190 T, very similar to that previously reported for a quenched sample[3] , is observed. At 1.7 K, this low frequency is attenuated, and the standard second harmonic of the "rapid oscillation" frequency, of order 500 T dominates. From the derivative signal we can also see that the FISDW state is formed below 10 T, and there is hysteresis between the up and down sweeps of the field. Hence the 1.7 K data shows that the sample is partially ordered. For a fully ordered sample, the first harmonic of the rapid oscillation frequency[13, 14] will dominate above 28 T. The signals from other samples are shown in Figs. 24 and 25 at 1.7 K with similar behavior.

The new result of this work is that in quenched samples of $(TMTSF)_2ClO_4$ there is a new quantum oscillation frequency which is smaller than that previously observed in ordered samples. We interpret this in the following way. The nesting of the Fermi surface induced by quenching the $(TMTSF)_2ClO_4$ system gives rise to smaller remaining pockets on the Fermi surface than those which are induced by magnetic breakdown/Stark interference effects in ordered samples. This may

be a result of the larger, non-reconstructed Fermi surface of the quenched material as compared to the reconstructed Fermi surface of the ordered material. Secondly, the amplitude of this new oscillation seems to have a maximum at intermediate temperatures, as is the case of the rapid oscillation frequency within the FISDW phase[15], and in $(TMTSF)_2PF_6$ which has an ambient temperature SDW phase. Finally, in the present data on two samples, we note that at 1.7 K the 500 T rapid oscillation amplitude appears to be attenuated above 45 T, and the 190 T period seems to reappear. Because of the relatively high (of order 1 mA) current in the sample, we cannot at this time rule out heating of the sample at higher fields as a cause of this second effect (switching from the 500 to the 190 T frequency at 45 T) since the 500 T oscillation amplitude is less on the down sweep.

We end this section by discussing brief experiment to see if self heating of a $(TMTSF)_2ClO_4$ sample with a high current density might be employed to allow us to change the quenched sample into an ordered sample, or in some manner to change the degree of order. The test was run with the samples at about 4 K in liquid helium, and the current along the c-axis was increased in small steps, and then decreased in the same way. The resistance vs. current relations for two different samples are shown in Fig. 24 a and b. A very large dependence of c-axis resistance on current was observed in the two cases studied. At present we are not sure if it is intrinsic to the c-axis conductivity, or due to contact resistance effects. Nevertheless, we found that t he magnetoresistance data at 1.7 K before and after the heating was almost identical. Hence current densities of order 10^5 to 10^7 A/m^2 do not change the state of the sample when in helium at 4 K. More work is needed to address the problem of obtaining well ordered samples on a short time scale, if these materials are to be properly studied in the MC1 type systems.

V. First results on molecular conductors in the MC1 series.

We now turn to the main goal of this work, namely to go into the quantum limit of the molecular conductor materials by using the MC1 series flux compression magnets.

V. a Strip Line Shot #3.

In this first shot to 134 T in a strip line generator, we used a constant current source with a 300 V compliance behind the blast shield to bias the samples, and gain 10 high frequency pre-amps to drive the signal through the coaxial lines to the scopes. Since we had no idea how much dB/dt pick up we were going to get, we divided down the signal by 50 before amplification. We were pleased to learn that the dB/dt pick-up was generally less than a few volts, that and such a division was not needed. Also, there was no 50 ohm termination on the scopes, and the coupling was dc. However in anticipation of large induced voltages, the scopes were not set in a sensitive manner, and due to the 8 bit resolution of the scopes, very little useful information was recovered.

V. b MC1 - A.

The electronics used for this first MC1 shot are shown in Fig. 22 and the performance of the generator is shown in Fig. 27. Here we show the dB/dt and B vs. time , and also the dB/dt vs. field for this shot. A typical result for an α-$(BEDT\text{-}TTF)_2NH_4Hg(SCN)_4$ sample is shown in Fig. 28. Here the coupling to the scope was dc, and because of the configuration of the electronics (see Fig. 10), the bias circuit was near the sample, and the 3nF coax was between the circuit and the scopes, it seems that the magnetoresistance signal was not picked up. Further more, ringing of the signal at around 3 MHz was observed. This ringing was triggered by events which are related to the seed field and cascade process of the generator, it would appear. The time constant of the ring down is consistent with the RC time constant of the 2000 ohm series resistance and the 3nF capacitance of the coax. When the signal is plotted vs. magnetic field, the wave forms look temptingly like quantum oscillations, which are periodic in inverse field. However, this is just an artifact of the rapidly increasing magnetic field vs. a periodic signal at 3 MHz. Since this is what the data would look like (see Fig. 3) the ringing is a serious problem which must be addressed.

It was clear, however, that the dB/dt pick up was not more that a few volts, and this information was useful for subsequent designs.

V. c MC1 - B.

In the second MC1 shot, we addressed the problem of the 50 ohm termination, the dc coupling, and the RC time constant. The electronics are shown in Fig. 11. Here the idea was to use a "virtual" 50 ohm termination, and also to use the 50 ohm resistor as the series resistor. By using a 1.5 V compliance, the sample current could be kept within reasonable bounds, especially as the sample resistance rises in field. (See Fig. 13 c). The bias circuit was connected at the scope input, and the coax lines went directly to the sample probe. The scopes were configured as follows: each scope was set with each of the four channels on a different sensitivity to cover different ranges of signal. The most sensitive scale (1 V) was ac coupled so there was no offset needed. The other scales (i.e., 2.5 V, 8 V, 20 V) were dc coupled.

Typical data is shown for an α-(BEDT-TTF)$_2$NH$_4$Hg(SCN)$_4$ sample in Fig. 29. In this case The dc sample signal level before the trigger is clearly visible in the dc coupled signal. The rise in resistance of the sample can be seen in the raw dc data at higher sensitivity by comparing the 5 ms base line signal with the 30 to 40 μs region where the seed field has nearly saturated at about 15 T. However, as in the MC1 results, the 3 MHz ringing is still present, and it is triggered by the events associated with the various stages of the cascade.

To further analyze the data of Fig. 29, we have employed Fourier transform filtering to remove the high frequency ringing from the background signal. This has been done by first smoothing the data with a single pass of a binomial algorithm to remove the digital noise. Then a Fourier transform was performed, and the high frequency part was removed. A reverse Fourier transform was next applied to the truncated spectrum. The resulting signal is shown in Fig. 26 vs. both time and field. Clearly, when the cascade starts at around 50 μs, the ringing is too great to make a meaningful assessment of the sample resistance beyond that point. In the raw data, any signal beyond 1.5 V cannot arise from the sample since that is the compliance of the bias circuit.

To conclude this section, we note that in general we could follow the magnetoresistance of the sample until the cascade fires at 50 μs after which point the ringing made it difficult to determine any further features. However it appeared in most cases of the 6 samples measured that the dc resistance of the sample remained finite throughout most of the pulse, superimposed on the background of the ringing.

V. d MC1 - C.

The final MC1 - C shot further confirmed the conclusions of the last section, namely that the sample resistance appears finite in many cases throughout the duration of the shot, that the sample voltage stays below the compliance voltage, and that during the seed field period, the magnetoresistance follows that seen in the pulsed field measurements (up to about 18 T). For MC1-C we re-configured our electronics along the lines shown in Figs. 12 (dc) and 18 (ac). In the dc bias circuits, the series resistance is kept low, the compliance voltage is greater, and the coax lines are driven with a unity gain buffer with a 50 ohm output impedance. (The input voltage can be as high as +/- 10 V, so there is no problem with dB/dt induced voltages saturating the buffer.) We also operate in a better region of dynamic range in the bias circuits. The dc circuit was also been employed, but only yielded results in the pre-test (Fig. 21). Due to considerable delays between the sample mounting,. and subsequent thermal cycling of the apparatus due to two pre-test sessions with a month in between, some samples lost leads in the final stage before the MC1-C shot. Furthermore, unusually high levels of EMI were experienced when the capacitor bank fired, and more samples were lost at this point, probably due to induced currents. Nevertheless, one sample "survived" the t = 0 EMI, and the results are shown in Fig. 31.

In Fig. 31 a we can compare the zero field and seed field signals and note that the resistance in the seed field is higher. Hence the magnetoresistance due to the seed field is

evident. There is also very high noise when the capacitor bank fires, but this attenuates reasonably quickly. Further indications of new noise appear at later times, but unlike the MC1-B shot (Fig. 29), there is no substantial noise signal when the generator fires at about 56 μs. In general, the noise in MC1-C in Fig. 31a is significantly less than in MC1-B in Fig. 29. The use of the line driver amplifier and the conventional manner in which the 30 m of coax is terminated at both ends with 50 ohms may be the reason for this reduction in noise.

In Fig. 31 b we show the simulation of the oscillatory magnetoresistance and the magnetic field vs. time, and in Fig. 31 c we show the simulation and the raw signal vs. magnetic field. The high frequency and higher amplitude oscillations are clearly noise, but it is possible that the background signal, which has a much lower frequency variation of the order of the simulation, and which stays below the compliance voltage of the bias circuit, may be partially attributeable to the presence of sample's magnetoresistance and SdH oscillation behavior.

Hence Fig. 31 really defines the state of the problem. First the initial EMI when the bank fires is detrimental. Sometimes it may destroy the sample and/or its leads, or may cause the sample to warm significantly. Nevertheless, the observation of magnetoresistance in the seed field tells us that the sample has survived this first trauma. Secondly, although better 50 ohm termination helps the signal-to-noise, further reduction of the background noise is needed before one can determine with certainly the high field resistance and/or the magneto oscillatory behavior. The nature of the noise when the second and third segments of the MC1 cascade become active, and whether or not it can be attenuated, is not known at this stage. The cancellation of the dB/dt induced emf seems to be quite good. One can however see that the average value of the signal does increase monotonically when the generator fires, and then levels off above about 300 T. Some of the monotonic increase could be due to some form of induced emf, but there is no direct comparison which can be made between the signal and the dB/dt wave form of, for instance Fig. 27 b.

VI. Conclusions.

We have made the first attempts to do direct dc measurements on low dimensional organic conductors to magnetic fields up to 700 T at low temperatures. We have developed methods of mounting these samples in such a way that the signals expected from the magnetoresistance are measurable against the background of the induced emf due to dB/dt effects. Indeed, the layered nature of the materials lend themselves in a crucial way to make these measurements possible. By carefully adjusting the many parameters of the dc bias circuit and signal amplification, we believe that it should indeed be possible to follow quantum oscillation phenomena in these materials up to 700 T.

There are a number of issues which should be considered for future experiments on molecular conductor type materials.

A. Generator optimization - It would be useful if the rise time of the field could be reduced without too large a compromise of the maximum field. Further, it would be good if the cost of such generators, and the involvement of personnel and other resources could be reduced to make them more accessible and less expensive.

B. Electrical and Magnetic Interference - On the scale of millivolt level signals, which are necessary for these experiments, the types of noise we experienced are astronomical. These effects are a combination of the ground plane, the initiation of the capacitor bank, and also the cascade behavior. At least the first two are in principle solvable.

C. Innovation in Instrumentation. There is more room for innovation in the following areas.

1) cryogenics
2) dc and dc resistance and conductivity measurements
3) magnetization - optimally balanced coils
4) mm wave (microwave) dielectric guides and cavities
5) application of visible optics to enhance the reduction of EMI in

measurements.
6) structure - x-ray and other probes of changes in crystal structure

D. Theory and simulation.

1) As higher magnetic fields become practical for use in condensed matter studies, theoretical issues concerning the effects of high magnetic fields on both the ground states and on the physical and electronic structure of materials is needed.
2) Because of the highly dynamic nature of the experiments, better simulations of sample heating, temperature rises, and simulation of the anticipated signals would be highly desirable.

E. Samples and materials.

1) It is desirable to learn how to further miniaturize the sample volume used in experiments. Samples in the 10 micron or less range will greatly reduce heating problems.
2) New materials should be considered which are ideal for both addressing the scientific issues of interest and which lend themselves to the high field environment.

As a final note, we wish to point out that in working out the problems with doing experiments in the megagauss environment, we have made significant improvements in some aspects of less aggressive pulsed field studies. An example is the almost negligible level of dB/dt pick-up observed in the many pre-test shots up to 60 T, where there is no need to subtract out an induced emf background to extract the data. Another is the dc method of transport measurements, which when optimized, gives a very high degree of noise rejection.

VI. ACKNOWLEDGMENTS.

Research by JSB is sponsored by NSF-DMR- 95-10427. Work in the non-destructive pulsed magnets was carried out at the National High Magnetic Field Laboratory - Pulsed Field Lab at Los Alamos National Laboratory, and the MC1 work was carried out in collaboration with DX Division at the Ancho Canyon Site at Los Alamos National Laboratory. The MC1 generators were fabricated at VNIIEF, Sarov Russia.

FIGURE CAPTIONS

Fig. 1. Comparison of magnetic length and energy scales for materials. a) The magnetic length for one flux quantum per unit cell vs. magnetic field. Arrows point to corresponding lattice constants and magnetic fields for different materials. b) Comparison of cyclotron energy (effective mass = 2 m_0), quantum limit, and band width for α-(BEDT-TTF)$_2$NH$_4$Hg(SCN)$_4$.

Fig. 2. Rate of change of field (a) and magnetic field (b) derived from integration of pick up coil for a non-destructive pulsed field magnet, a destructive stripline magnet, and a MC1-A cascade generator magnet.

Fig. 3. Computation of the oscillatory part of the magnetoresistance for α-(BEDT-TTF)$_2$NH$_4$Hg(SCN)$_4$ vs. time (t = 0 is when the cascade fires, not the seed field initiation) (a) and magnetic field (b) at 1.5 K in an MC1 flux compression generator system. Indicated in (a) is the approximate real time frequency of the signal which results from the inverse field periodicity of the quantum oscillations. Indicated in (b) is the regime of the quantum limit which is where the lowest Landau level is reached in the system near 580 T.

Fig. 4. Computation of the energy input to a α-(BEDT-TTF)$_2$NH$_4$Hg(SCN)$_4$ sample vs. time for the MC1 system (a) and the enthalpy vs. temperature (b) for sample. The temperature at any point may be determined by equating the energy input with the enthalpy, which corresponds to a particular temperature.

Fig. 5. Overview of the test site and experimental equipment. Cryostat was pumped from a distance through PVC pipe to 1.7 K prior to firing the shot, and a safety valve was shut on the pump when the shot was triggered. Details of the capacitor bank and detonator system are not shown. Sample monitor circuits were only engaged to check sample properties before the shots.

Fig. 6. Printed circuit board template.

Fig. 7. Detail of lower section of co-planer transmission line pattern. Three nested patterns with similar design terminate within 3 cm of each other near the bottom of the sample holder.

Fig. 8. Schematic of sample positions for the modified co-planar pattern.

Fig. 9. Detailed schematic of sample mount.

Fig. 10. Bias circuit for MC1 - A shot.

Fig. 11. The 50 Ω terminator/resistor circuit used in MC1-B. C1 and C1 allow a virtual ground, and the small value of C2 is to circumvent inductance in the larger capacitor. The crosses represent flux which may arise due to miss-alignment of the PCB, and the arrows represent the resulting path of induced emf's. 30 m of 50 Ω coax are connected between the bias circuit and the scopes, which represents about 3 nF of capacitive loading.

Fig. 12. Schematic of optimized bias circuit with unity gain buffer used in MC1-C. Bias circuit is be behind the blast shield, and the buffer drives the 30 m length of coax to the scopes.

Fig. 13. Current and voltage curves for different divider configurations vs. sample resistance. a) 3 V compliance, 1500 W series resistor, b) 9 V compliance, 2500 W series resistor, c) 1.5 V compliance, 50 W series resistor.

Fig. 14. Signal from an α-(BEDT-TTF)$_2$NH$_4$Hg(SCN)$_4$ at 1.7 K.
a) vs. time, b) vs. field, and c) resistance computed from signal (down sweep only).

Fig. 15. Comparison of different bias arrangements with different currents for α-(BEDT-TTF)$_2$NH$_4$Hg(SCN)$_4$ at 1.7 K.

Fig. 16. Five samples of α-(BEDT-TTF)$_2$NH$_4$Hg(SCN)$_4$ run in 52 T pre-test before MC1 - B experiment.

Fig. 17. Fourier transform spectrum of oscillations in Fig. 14. The variation in fundamental SdH frequency is probably due to miss-alignment.

Fig. 18. Schematic of co-planar transmission line arrangement and circuit for DC measurement. (The high pass filter was not used in the pretest data shown in this paper.)

Fig. 19. Comparison of DC bias and DC measurement (to 52 T) of two samples of α-(BEDT-TTF)$_2$NH$_4$Hg(SCN)$_4$ prior to optimization of DC circuit.

Fig. 20 Comparison of DC bias and DC measurement (only to 14 T) of two samples of α-(BEDT-TTF)$_2$NH$_4$Hg(SCN)$_4$ after optimization of DC circuit. Both signal voltage and derived sample resistance are shown for the DC measurement.

Fig. 21. a) Comparison of ac and dc measurements on two samples of α-(BEDT-TTF)$_2$NH$_4$Hg(SCN)$_4$ to 30 T. b) dc measurement of α-(BEDT-TTF)$_2$NH$_4$Hg(SCN)$_4$ and corresponding derived resistance value. Inset: relationship between calibrated resistance and rectified ac output.

Fig. 22. Temperature dependence of magnetoresistance of (TMTSF)$_2$ClO$_4$ in quenched state. Note that the low frequency oscillation is most observable at higher temperatures. Faster oscillations are observable in the 1.7 K data in the range 20 to 35 T.

Fig. 23. High (a) and low (b) temperature magnetoresistance signal and its derivative for (TMTSF)$_2$ClO$_4$ in quenched state. Details discussed in text.

Fig. 24. a) Zero field R-I curves for two samples for current along the c-axis at 4 K. e) data similar to b) for another sample at 1.7 K.

Fig. 25. Similar analysis to Figs. 23 and 24 for a third sample of (TMTSF)$_2$ClO$_4$.

Fig. 26. DC data on two related materials. a) Magnetoresistance of h-Mo$_4$O$_{11}$. Here the quantum limit is reached at only 20 T, and anomalous new oscillations appear at the highest fields. b) Magnetoresistance of α-(BEDT-TTF)$_2$NH$_4$Hg(SCN)$_4$. Here the low temperature ground state is broken at about 22.5 T.

Fig. 27 . Performance of MC1 - A shot. a) dB/dt and B vs. time. b) dB/dt vs. B. The lower panel gives an indication as to how a signal would look vs. field if there was significant dB/dt induced emf's in the leads.

Fig. 28. Typical data on α-(BEDT-TTF)$_2$NH$_4$Hg(SCN)$_4$ for the MC1 - A test.

Fig. 29. Typical data on α-(BEDT-TTF)$_2$NH$_4$Hg(SCN)$_4$ for the MC1 - B test. a) High sensitivity with dc coupling. b) Lower sensitivity with dc coupling.

Fig. 30. Fourier transform - filtered signal a) vs. field and b) vs. time with resistance computed from divider circuit.

Fig. 31. Results on α-(BEDT-TTF)$_2$NH$_4$Hg(SCN)$_4$ from MC1-C. a) Raw data from dc coupled scope trace showing fiducial before trigger. Note that there are 10 nS/channel. b) Simulation and data vs. magnetic field. Details discussed in the text. c) Detail of low field part of signal (smoothed) with standard magnetoresistance fit to the data.

REFERENCES

[1] D. R. Hofstadter, Phys. Rev. B 14, 2239 (1976).
[2] See papers in the *Wuerzburg Conference* (eds. G. Landwehr and W. Ossau) (World Scientific, Wurzburg, Germany, 1996).
[3] J. S. Brooks, R. G. Clark, R. P. Starrett, R. Newbury, R. H. McKenzie, A. V. Skougarevsky, N. Kinoshita, T. Kinoshita, Y. Tanaka, H. Anzai, S. Takasaki, J. Yamada, M. V. Kartsovnik, A. I. Schegolev, G. J. Athas, and P. Sandhu, Physica B 216, 380 (1996).
[4] I. M. Lifshitz and A. M. Kosevich, Zh. eksp. teor. fiz. 29, 730 (1955).
[5] D. Shoenberg, *Magnetic Oscillations in Metals* (Cambridge University Press, Cambridge, 1994).
[6] P. Henning, J. S. Brooks, J. E. Crow, Y. Tanaka, T. Kinoshita, N. Kinoshita, M. Tokumoto, and H. Anzai, Solid State Commun. 95, 691 (1995).
[7] LABTECH. (David Lantham; Broadaaxe Park, Presteigne, Powys LD8 2UF Great Britain Tel. 44-1544-260093; Fax. 44-1544-260310).
[8] D. Rickel. in *Megagauss VII (these proceedings)* (ed. O. Tasenko) (Sarov, Russia, 1996).
[9] R. G. Clark et al. in *Megagauss VII (these proceedings)* (ed. O. Tatsenko) (Sarov, Russia, 1996).
[10] S. J. Klepper, J. S. Brooks, X. Chen, I. Bradaric, M. Tokumoto, N. Kinoshita, Y. Tanaka, and C. C. Agosta, Physical Review B 48, 9913-9916 (1993).
[11] C. E. Campos, J. S. Brooks, P. J. M. v. Bentum, J. A. A. J. Perenboom, S. J. Klepper, P. Sandhu, S. Valfells, Y. Tanaka, T. Kinoshita, N. Kinoshita, M. Tokumoto, and H. Anzai, Phys. Rev. B (RC) 52, R7014 (1995).
[12] T. Ishiguro and K. Yamaji, *Organic Superconductors* (Springer-Verlag, Berlin-Heidelberg, 1990).
[13] J. S. Brooks, R. G. Clark, R. McKenzie, R. Newbury, R. P. Starrett, A. V. Skougarevsky, M. Tokumoto, S. Takasaki, J. Yamada, H. Anzai, and S. Uji, Phys. Rev. B 53, 14406 (1996).
[14] C. C. Agosta, Physica B (to be published) (1995).
[15] S. Uji, T. Terashima, H. Aoki, J. S. Brooks, M. Tokumoto, S. Takasaki, J. Yamada, and H. Anzai, Physical Review B 53, 14399 (1996).

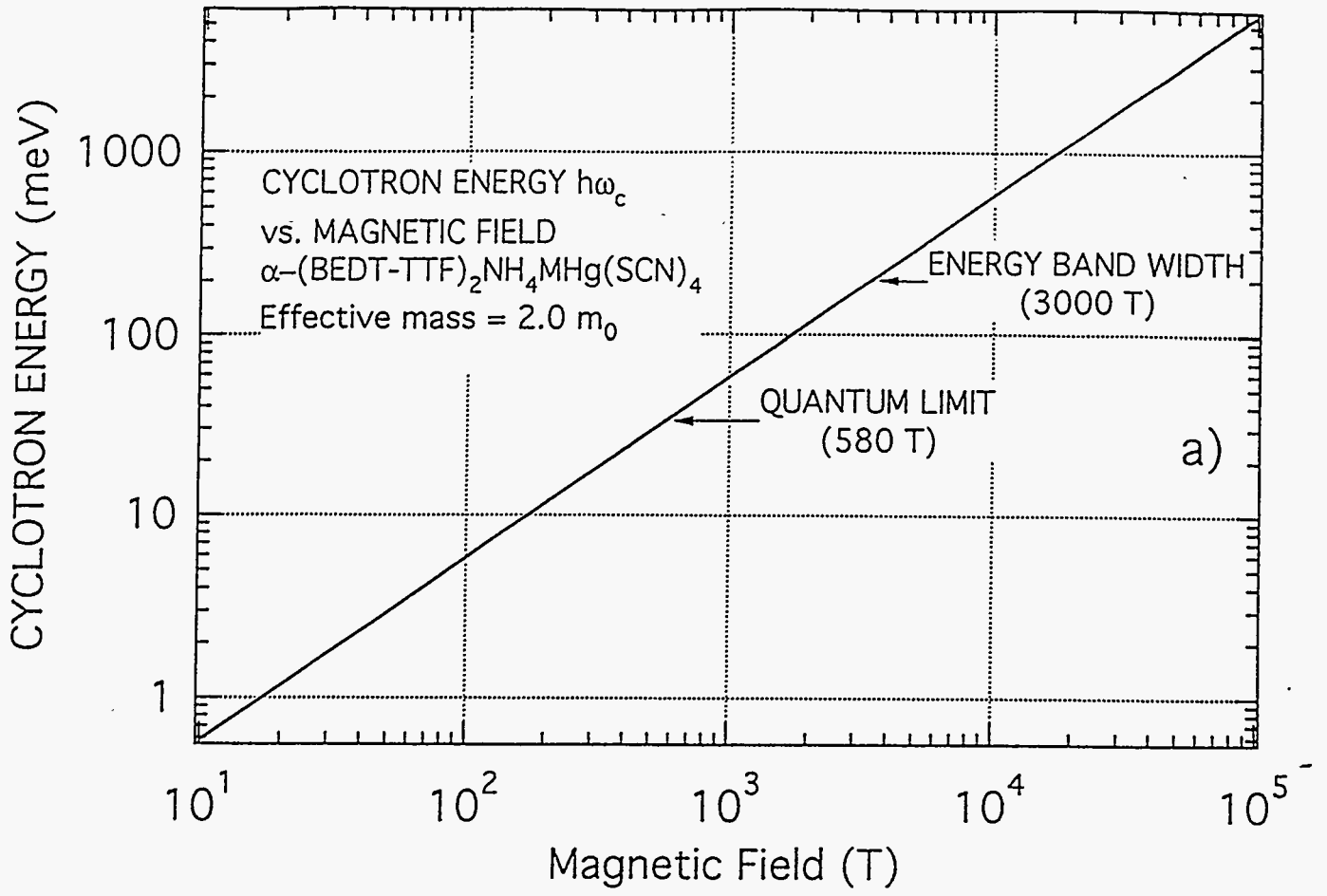
CYCLOTRON ENERGY (meV)
1000
100
10
1
CYCLOTRON ENERGY $h\omega_c$
vs. MAGNETIC FIELD
α-(BEDT-TTF)$_2$NH$_4$MHg(SCN)$_4$
Effective mass = 2.0 m_0
ENERGY BAND WIDTH
(3000 T)
QUANTUM LIMIT
(580 T)
a)
10^1
10^2
10^3
10^4
10^5
Magnetic Field (T)

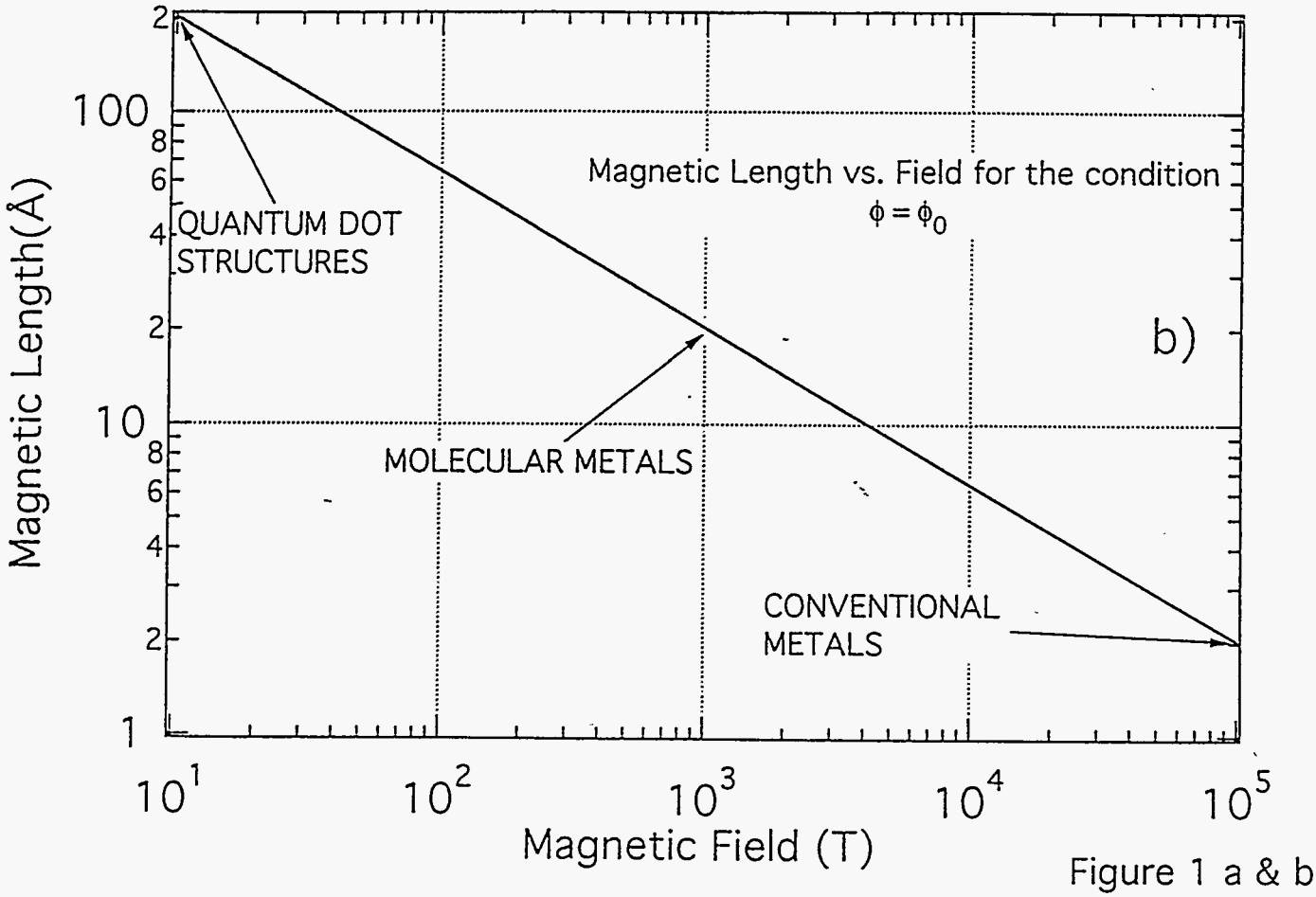
Magnetic Length(Å)
2
100
8
6
4
2
10
8
6
4
2
1
Magnetic Length vs. Field for the condition
$\phi = \phi_0$
QUANTUM DOT
STRUCTURES
MOLECULAR METALS
CONVENTIONAL
METALS
b)
10^1
10^2
10^3
10^4
10^5
Magnetic Field (T)

Figure 1 a & b

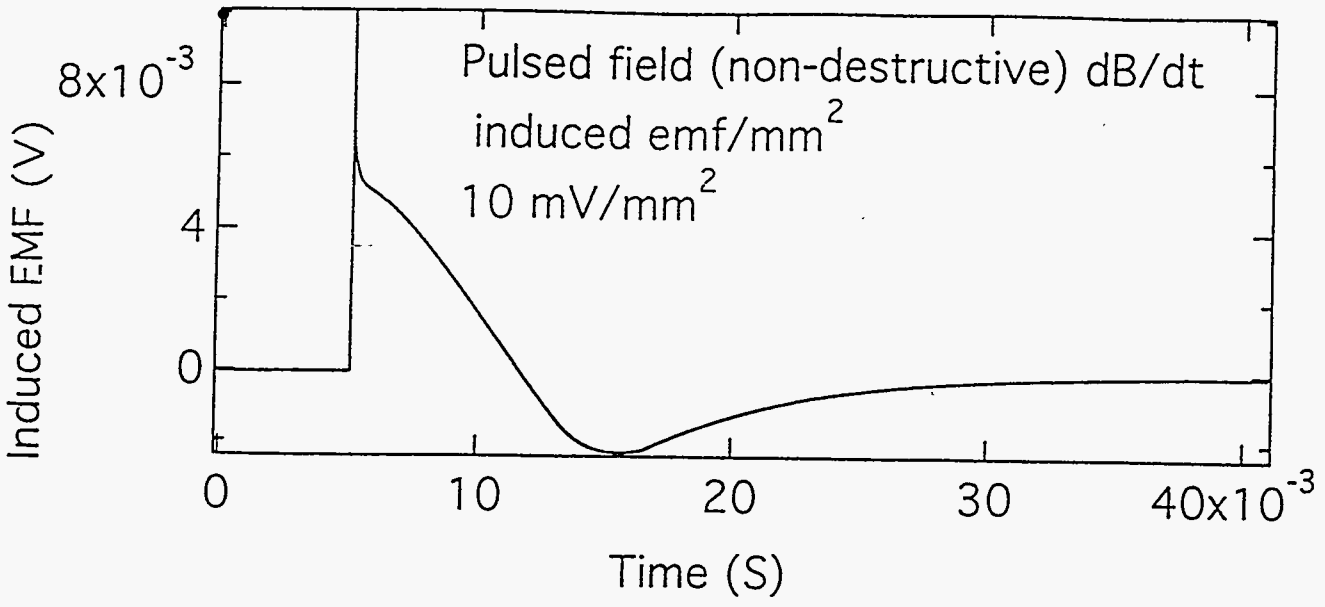
Pulsed field (non-destructive) dB/dt
induced emf/mm^2
10 mV/mm^2
Induced EMF (V)
8x10^{-3}
4
0
0
10
20
30
40x10^{-3}
Time (S)

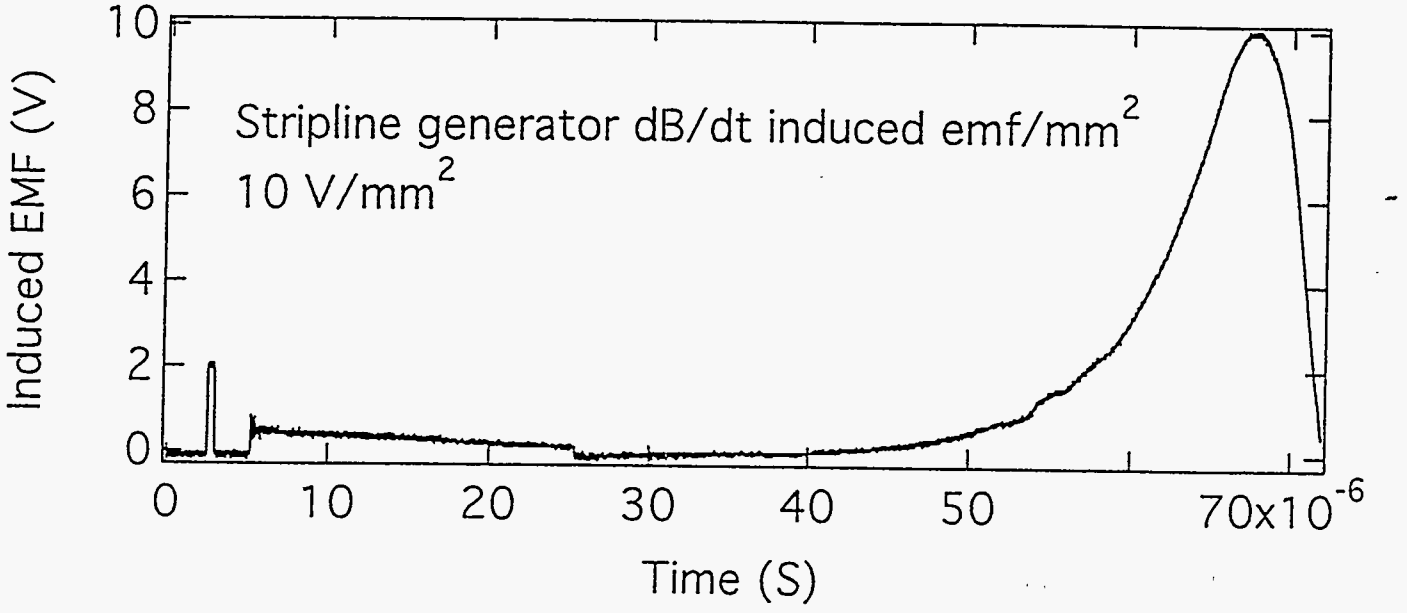
Stripline generator dB/dt induced emf/mm^2
10 V/mm^2
Induced EMF (V)
10
8
6
4
2
0
0
10
20
30
40
50
70x10^{-6}
Time (S)

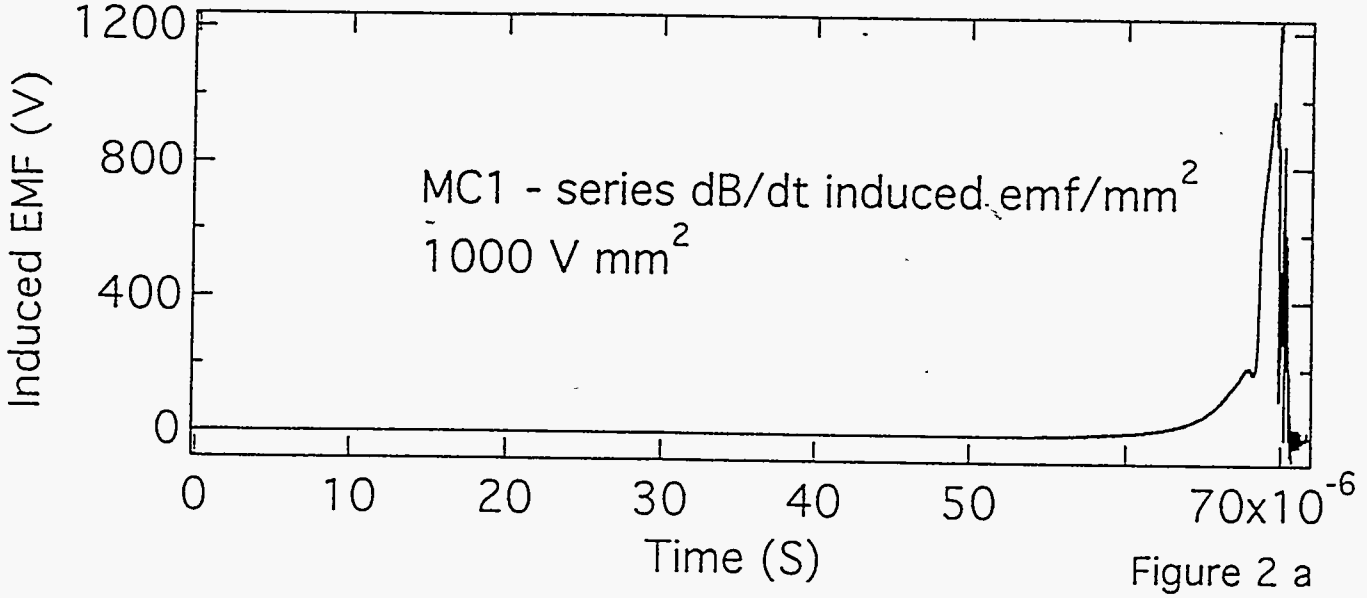
MC1 - series dB/dt induced emf/mm^2
1000 V mm^2
Induced EMF (V)
1200
800
400
0
0
10
20
30
40
50
70x10^{-6}
Time (S)

Figure 2 a

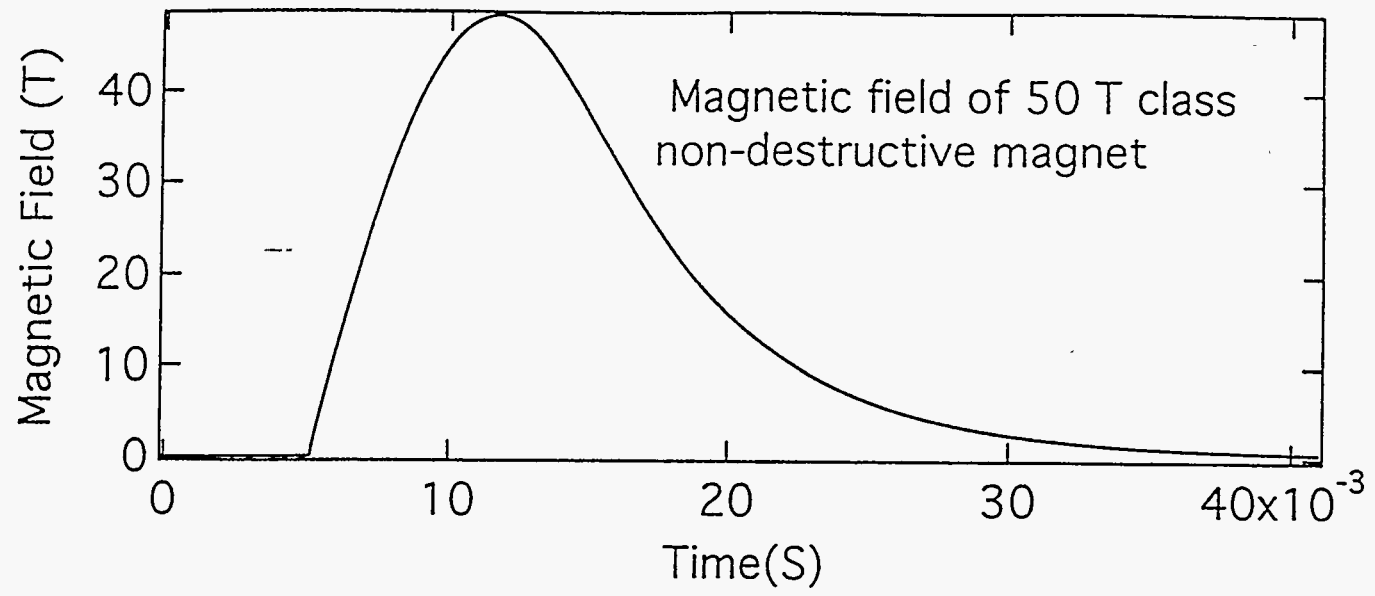
Magnetic field of 50 T class
non-destructive magnet
Magnetic Field (T)
0
10
20
30
40
0
10
20
30
40x10-3
Time(S)

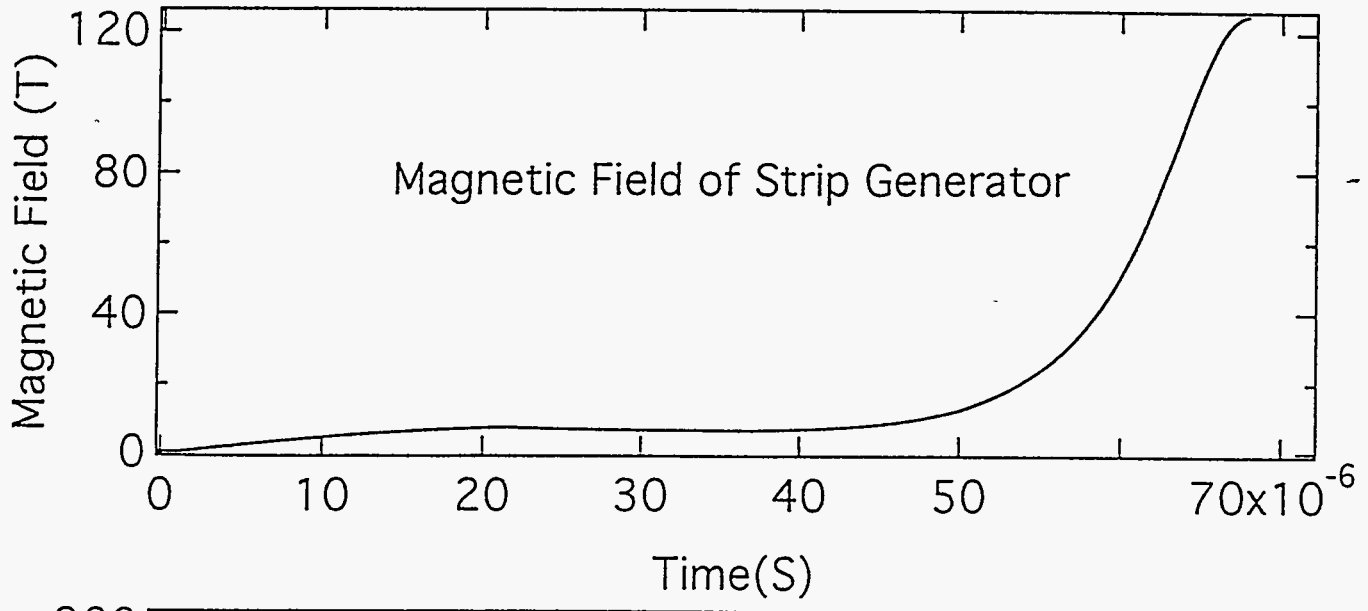
Magnetic Field of Strip Generator
Magnetic Field (T)
0
40
80
120
0
10
20
30
40
50
70x10-6
Time(S)

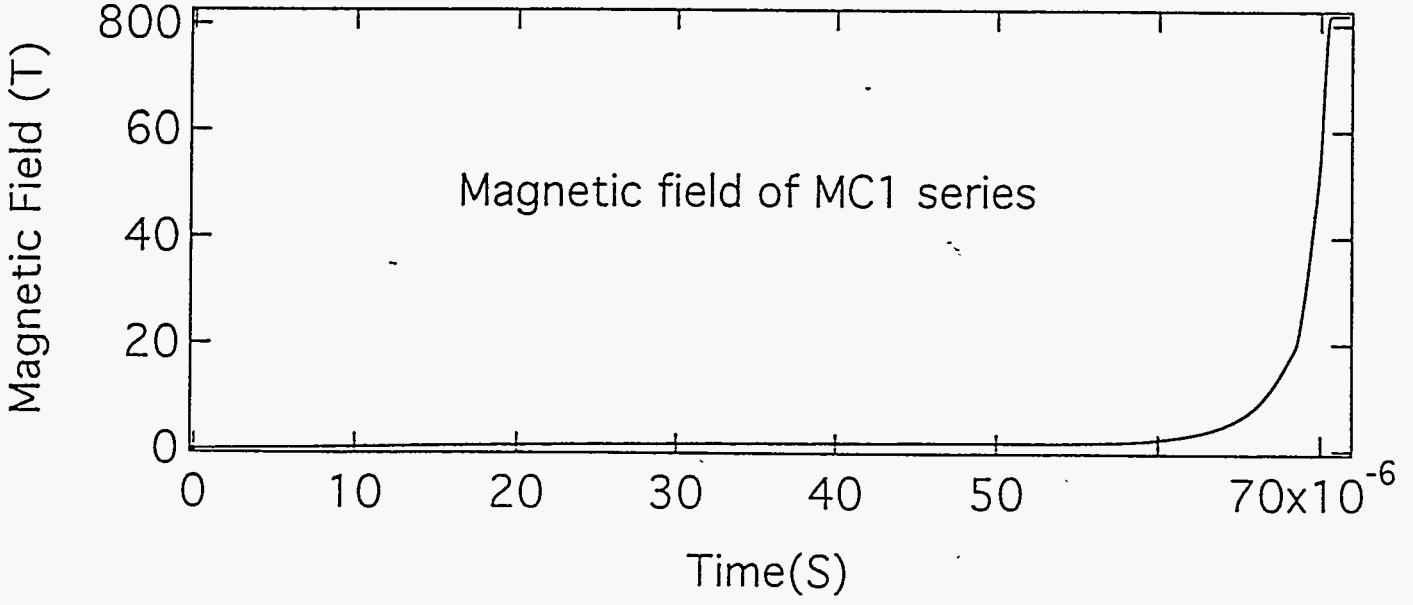
Magnetic field of MC1 series
Magnetic Field (T)
0
20
40
60
800
0
10
20
30
40
50
70x10-6
Time(S)

Figure 2 b

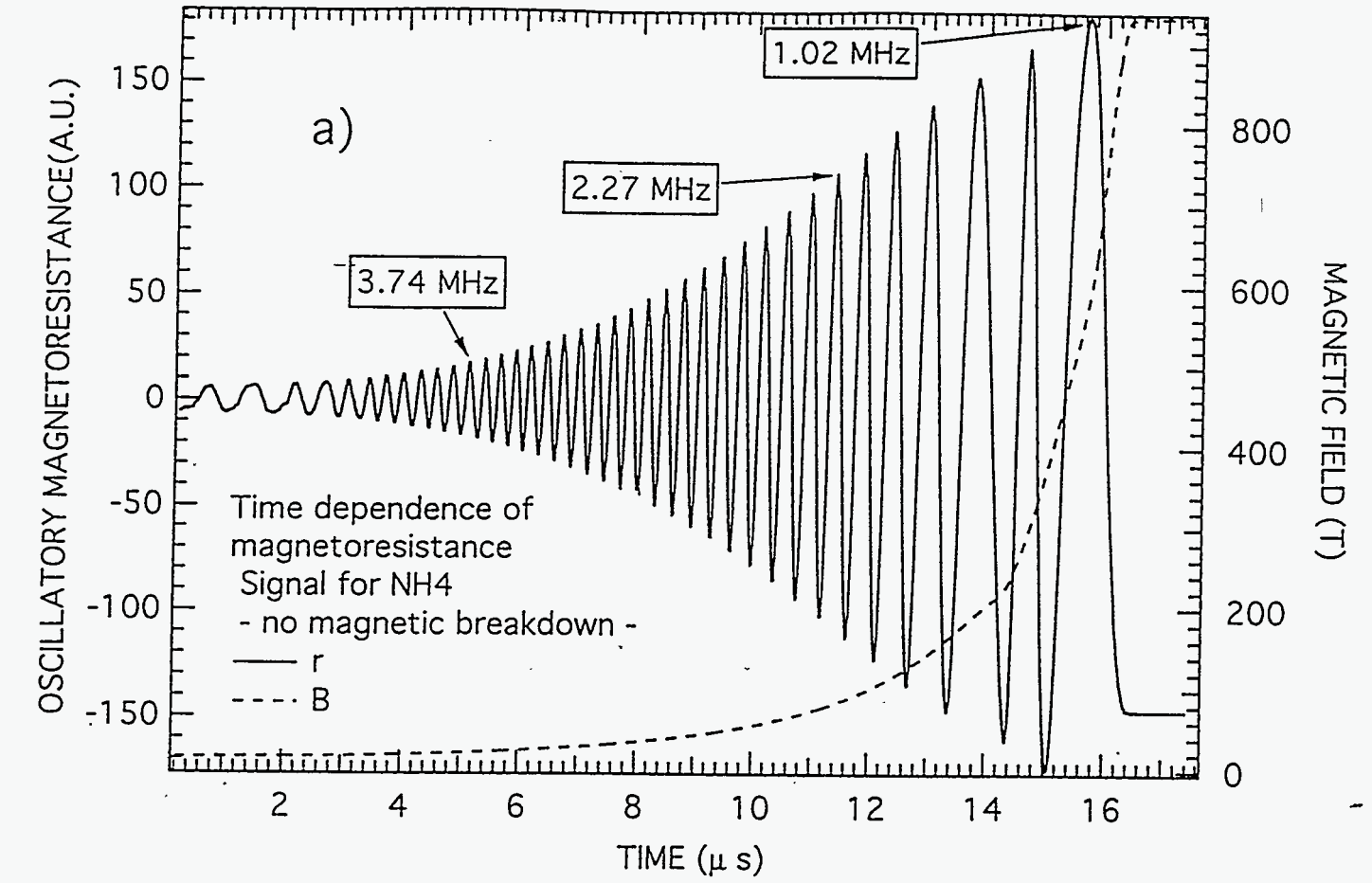
a)
1.02 MHz
2.27 MHz
3.74 MHz
Time dependence of
magnetoresistance
Signal for NH4
- no magnetic breakdown -
r
B
OSCILLATORY MAGNETORESISTANCE(A.U.)
MAGNETIC FIELD (T)
TIME (μ s)
150
100
50
0
-50
-100
-150
800
600
400
200
0
2
4
6
8
10
12
14
16

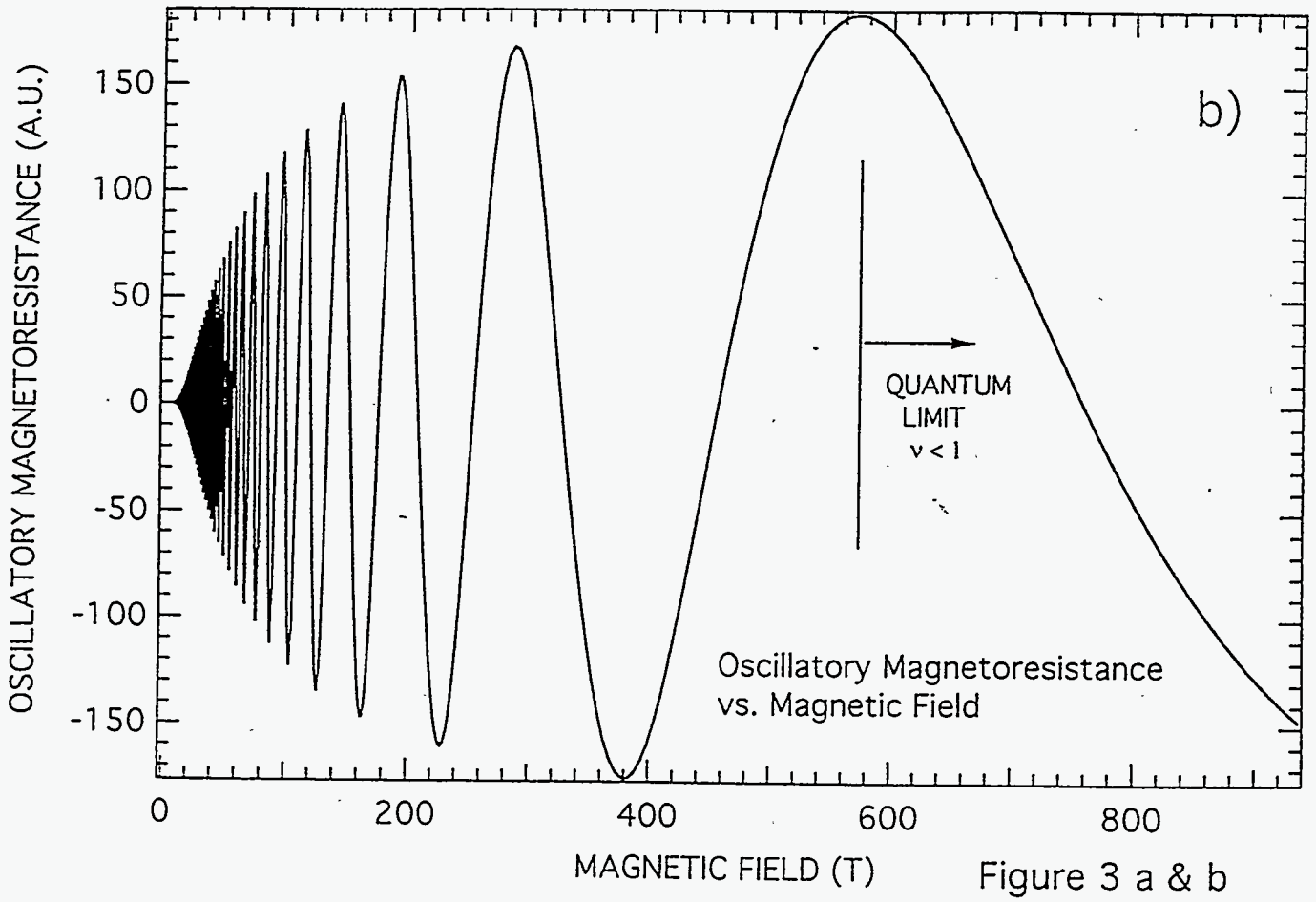
b)
QUANTUM
LIMIT
ν < 1
Oscillatory Magnetoresistance
vs. Magnetic Field
OSCILLATORY MAGNETORESISTANCE (A.U.)
MAGNETIC FIELD (T)
150
100
50
0
-50
-100
-150
0
200
400
600
800

Figure 3 a & b

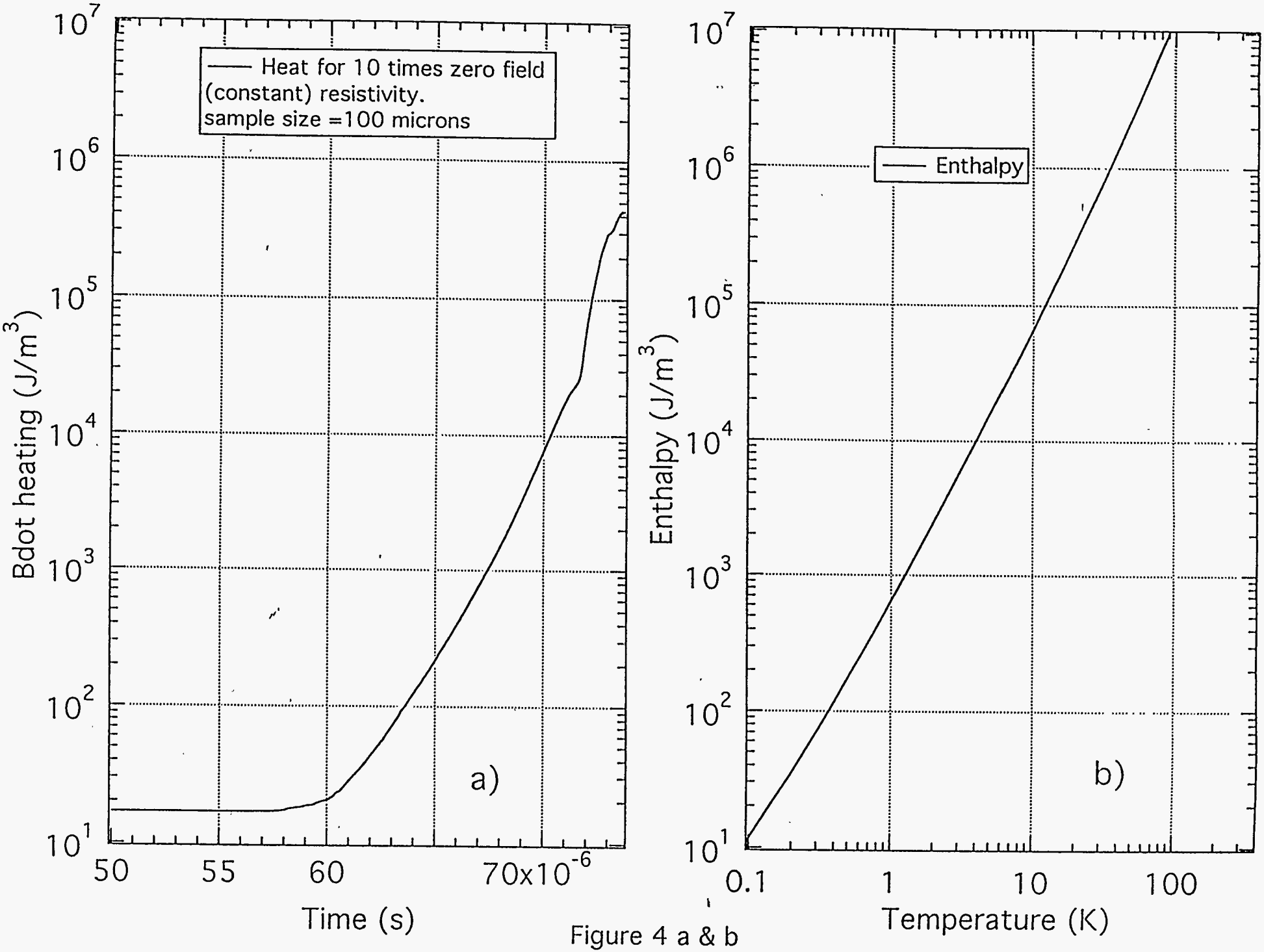
Heat for 10 times zero field
(constant) resistivity.
sample size =100 microns
Bdot heating (J/m3)
Time (s)
a)
Enthalpy
Enthalpy (J/m3)
Temperature (K)
b)

Figure 4 a & b

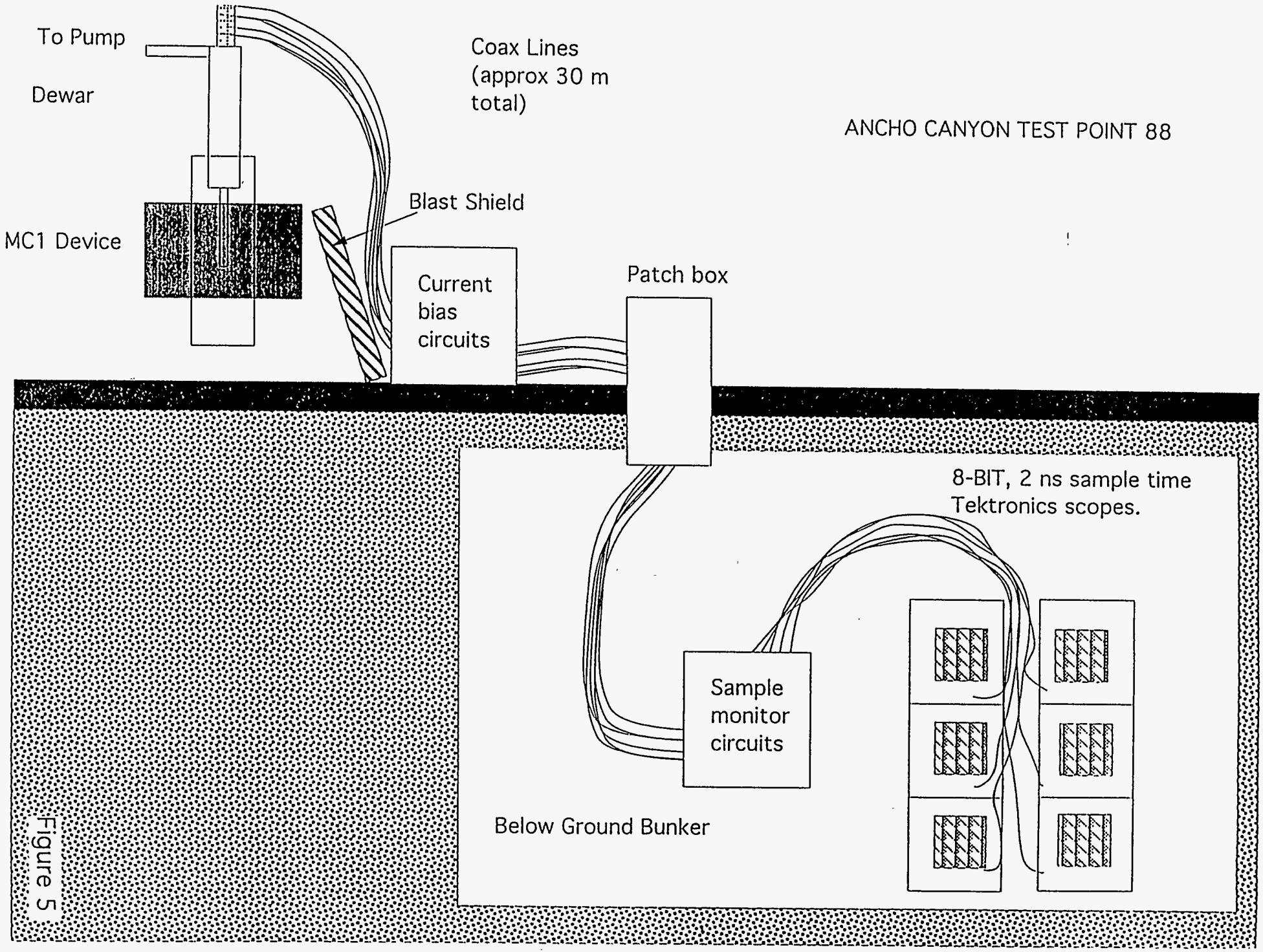
To Pump
Dewar
Coax Lines
(approx 30 m
total)
ANCHO CANYON TEST POINT 88
Blast Shield
MC1 Device
Current
bias
circuits
Patch box
8-BIT, 2 ns sample time
Tektronics scopes.
Sample
monitor
circuits
Below Ground Bunker

Figure 5

Printed circuit board overview

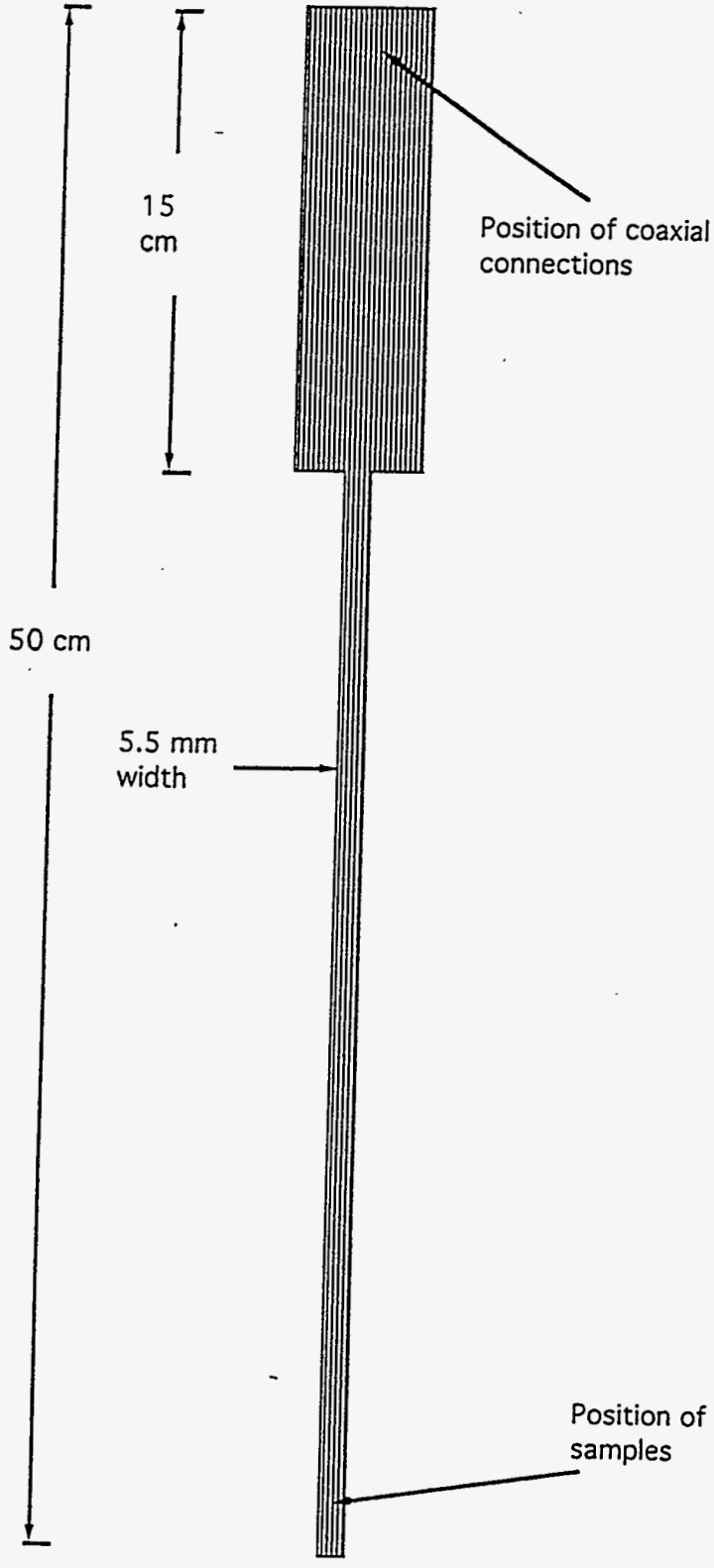

Figure 6

Detail of 18 μm thick gold coated copper co-planer transmission line pattern.

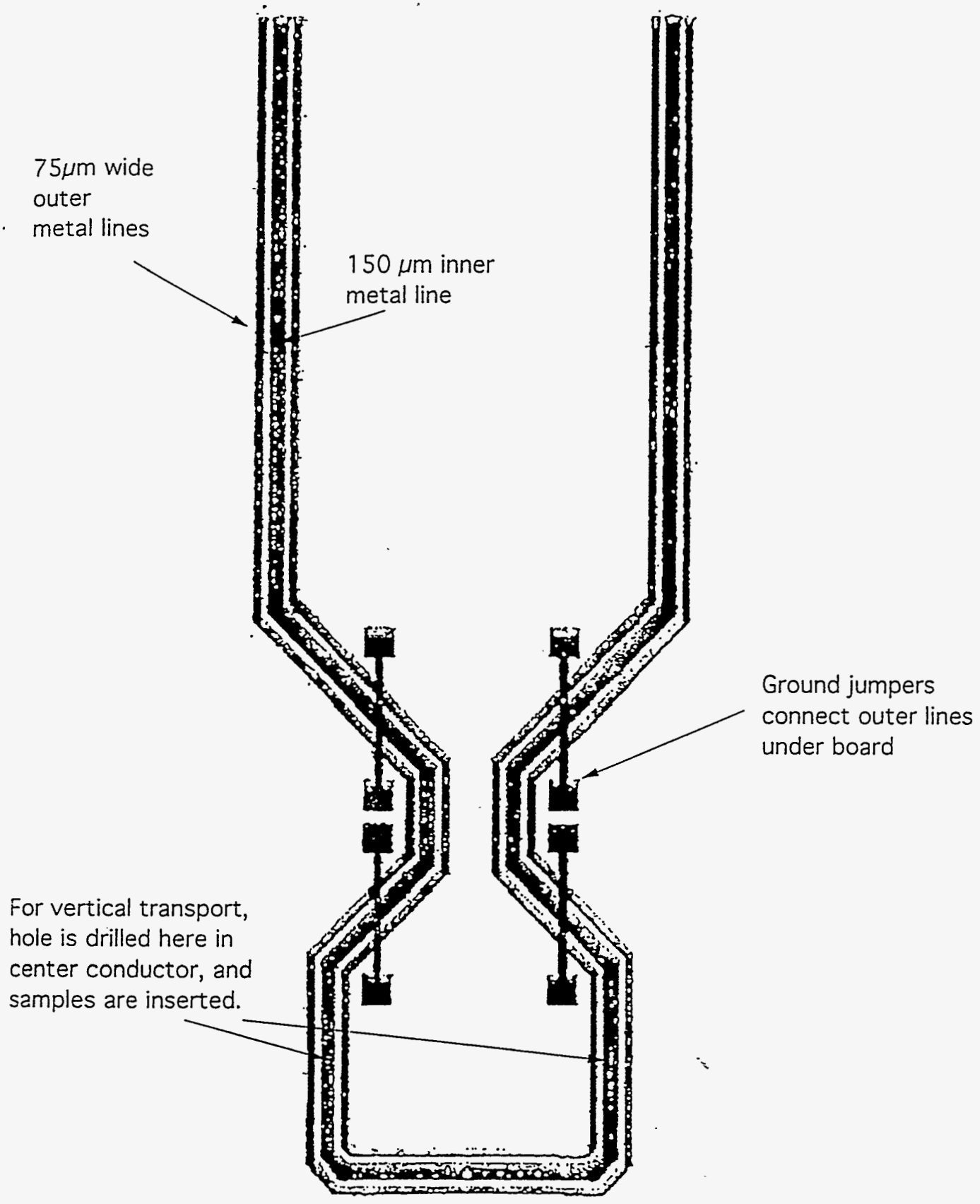

Figure 7

ORGANIC CRYSTAL ARRANGEMENT - ONLY ONE
STRIPLINE SEGMET SHOWN (OF THREE)
TOTAL OF 6 SAMPLES WILL BE MOUNTED

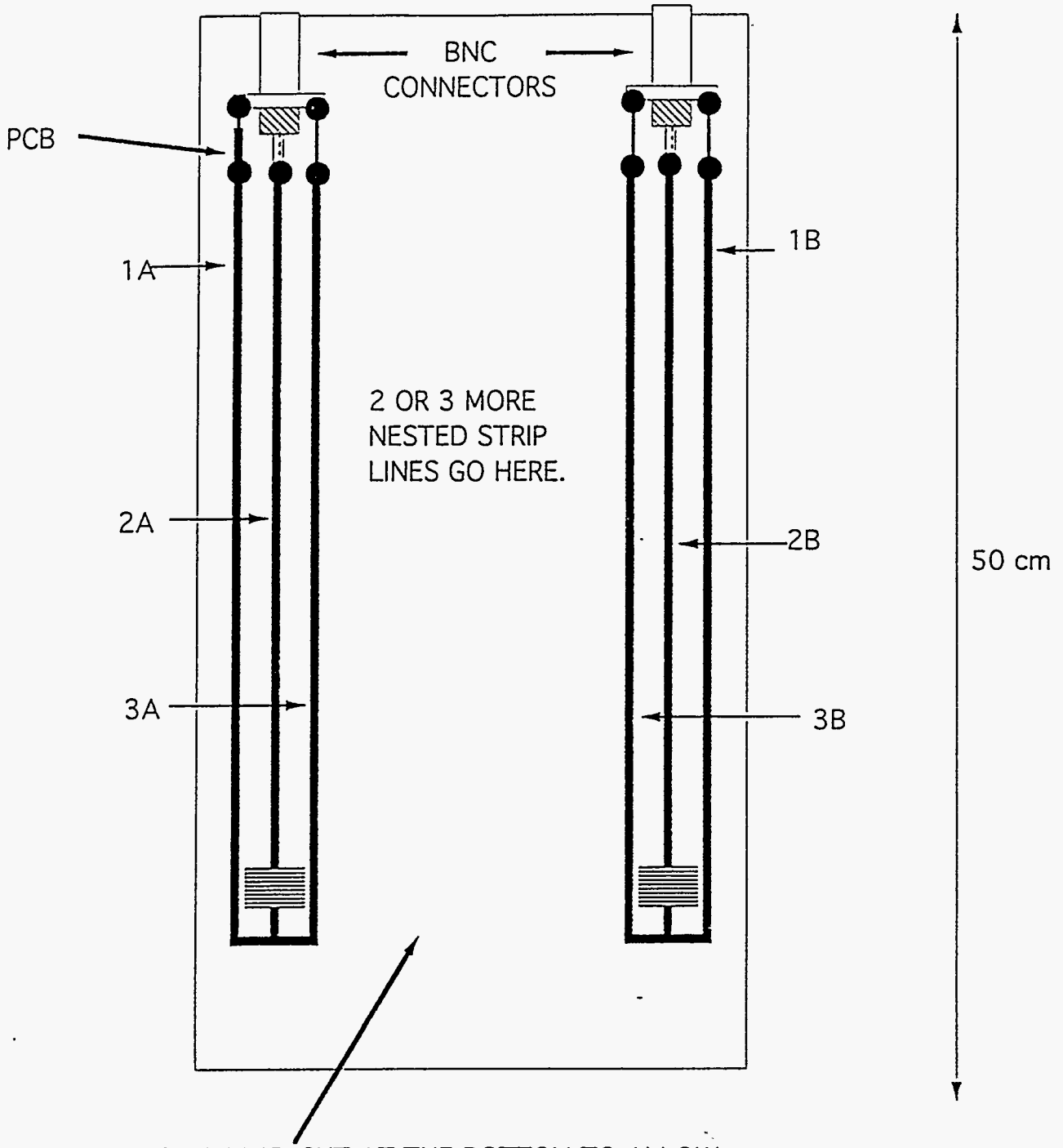

NOTE: STRIPLINE CUT AT THE BOTTOM TO ALLOW
TWO TERMINAL CONNECTIONS TO SAMPLES ON EACH
SEGMENT VIA SILVER OR GOLD PAINT.

Figure 8

DETAIL OF SAMPLE MOUNTING

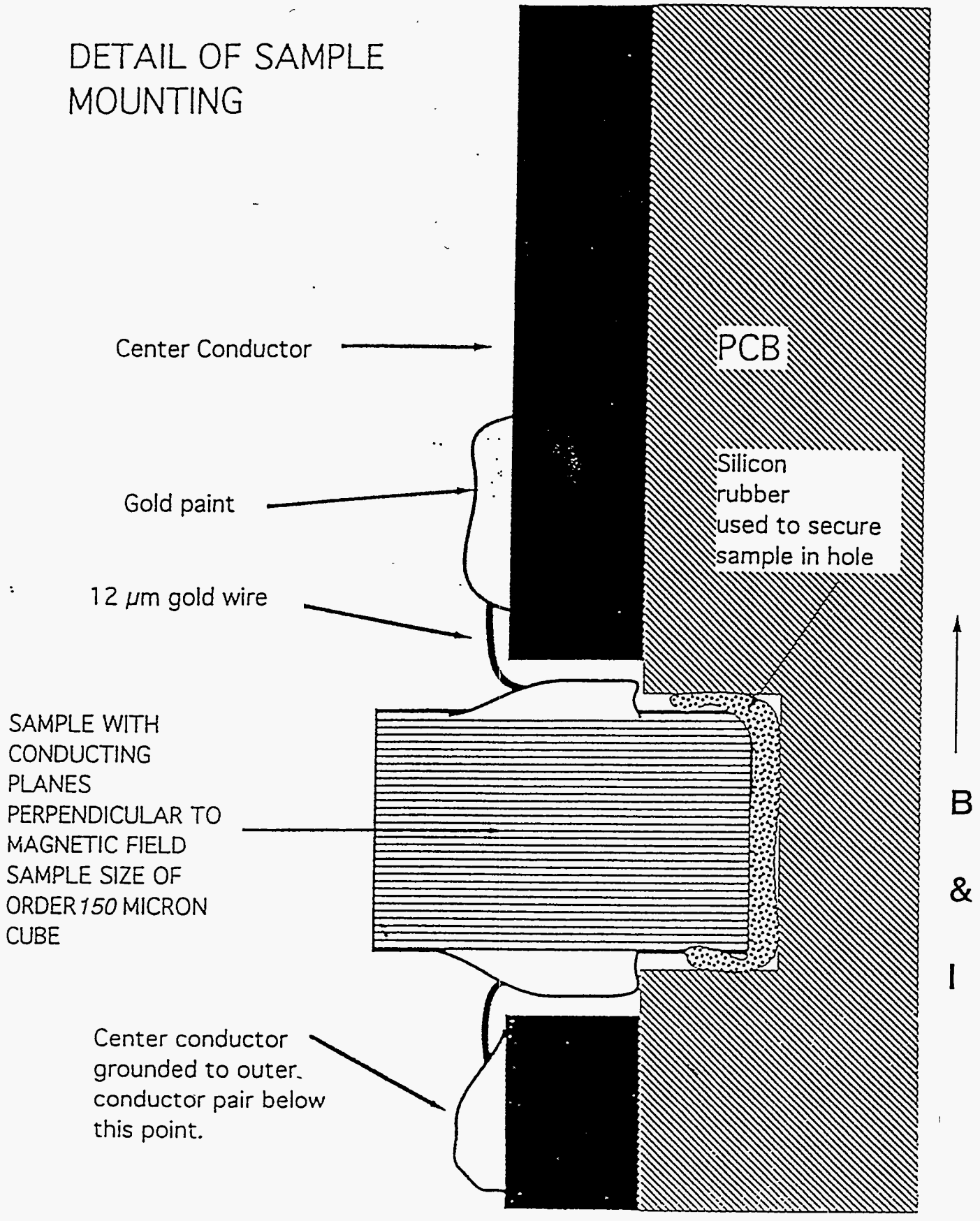

Figure 9

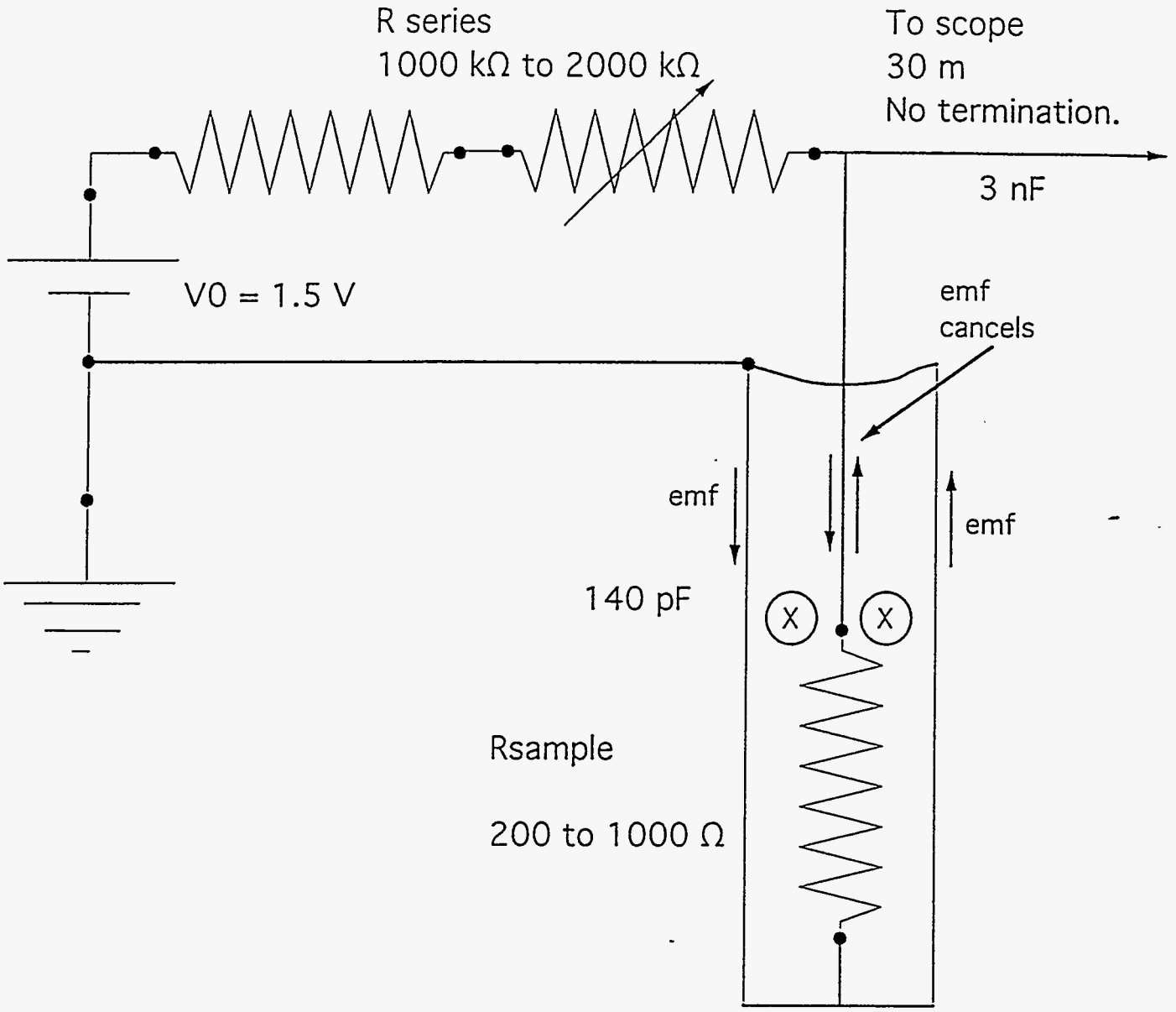

Electronics set up for MC1-A

Figure 10

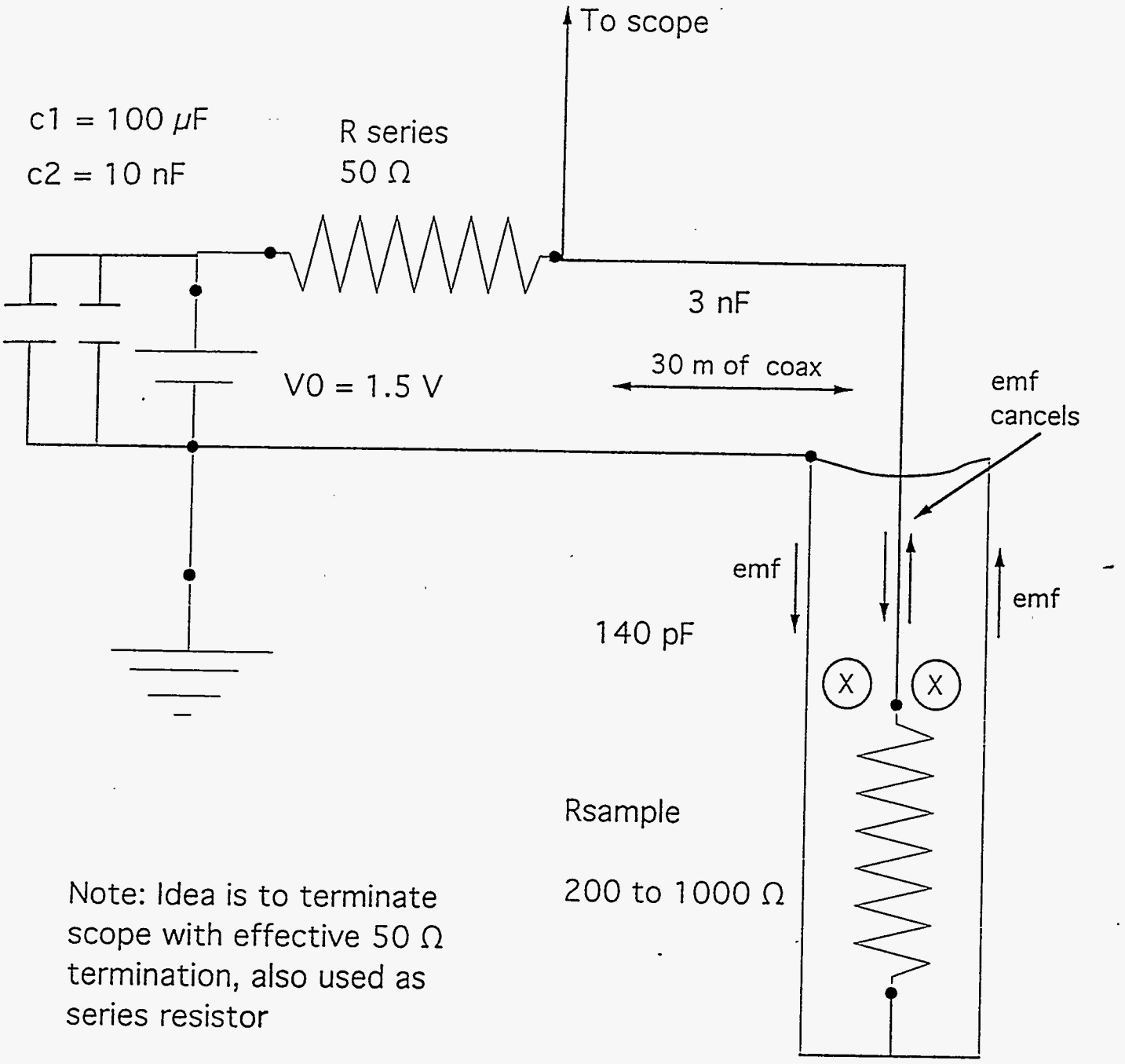

Note: Idea is to terminate scope with effective 50 Ω termination, also used as series resistor

Electronics set up for MC1-B

Figure 11

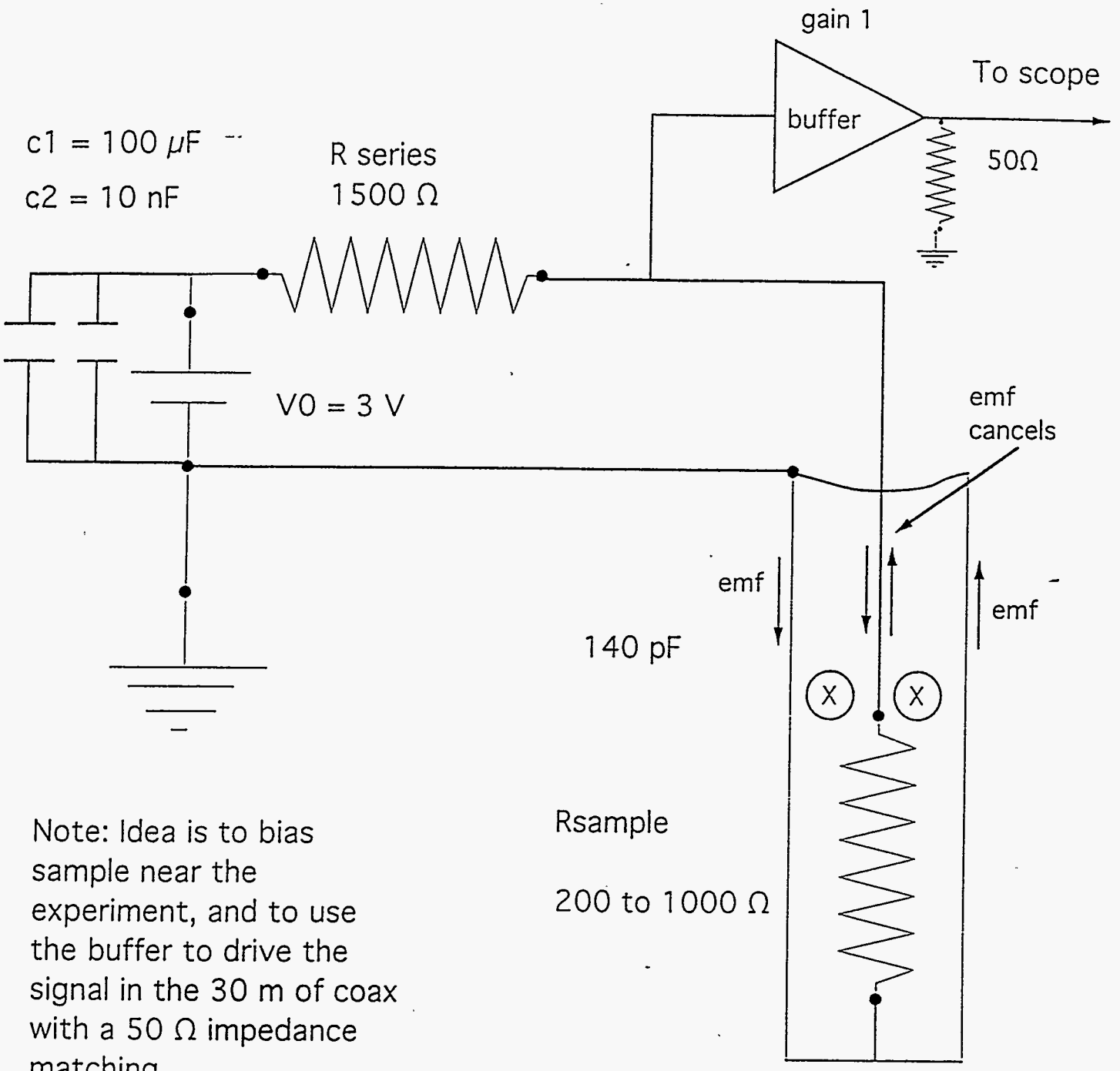

Note: Idea is to bias sample near the experiment, and to use the buffer to drive the signal in the 30 m of coax with a 50 Ω impedance matching

Electronics set up for MC1-C

Figure 12

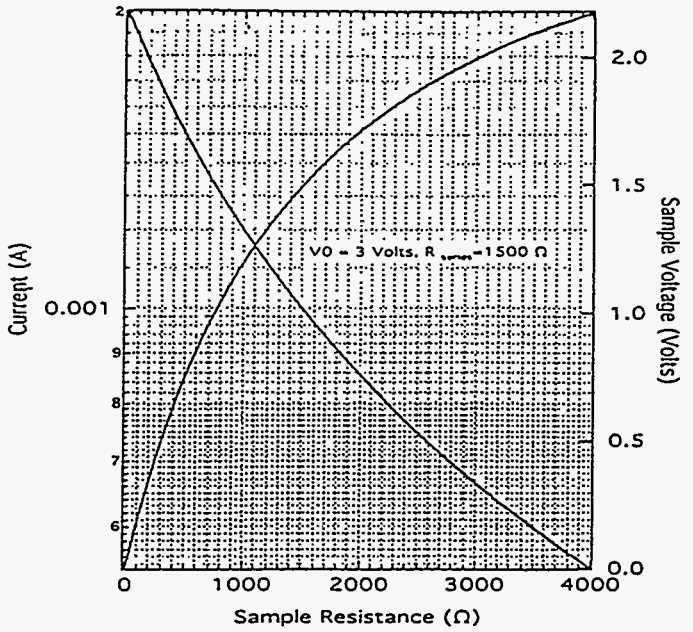

a)

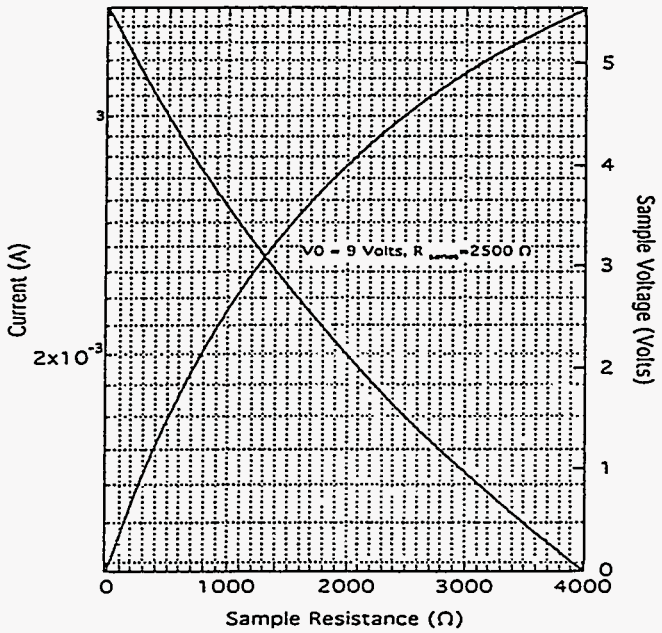

b)

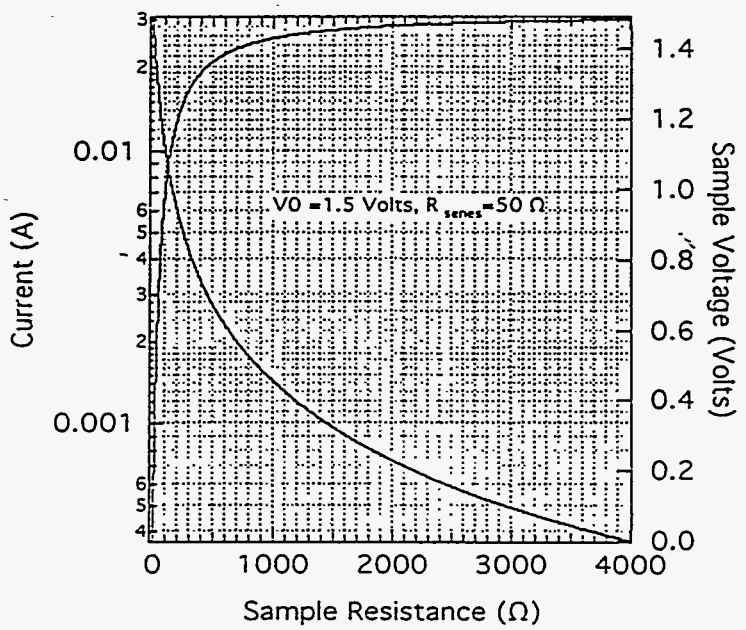

c)

Figure 13

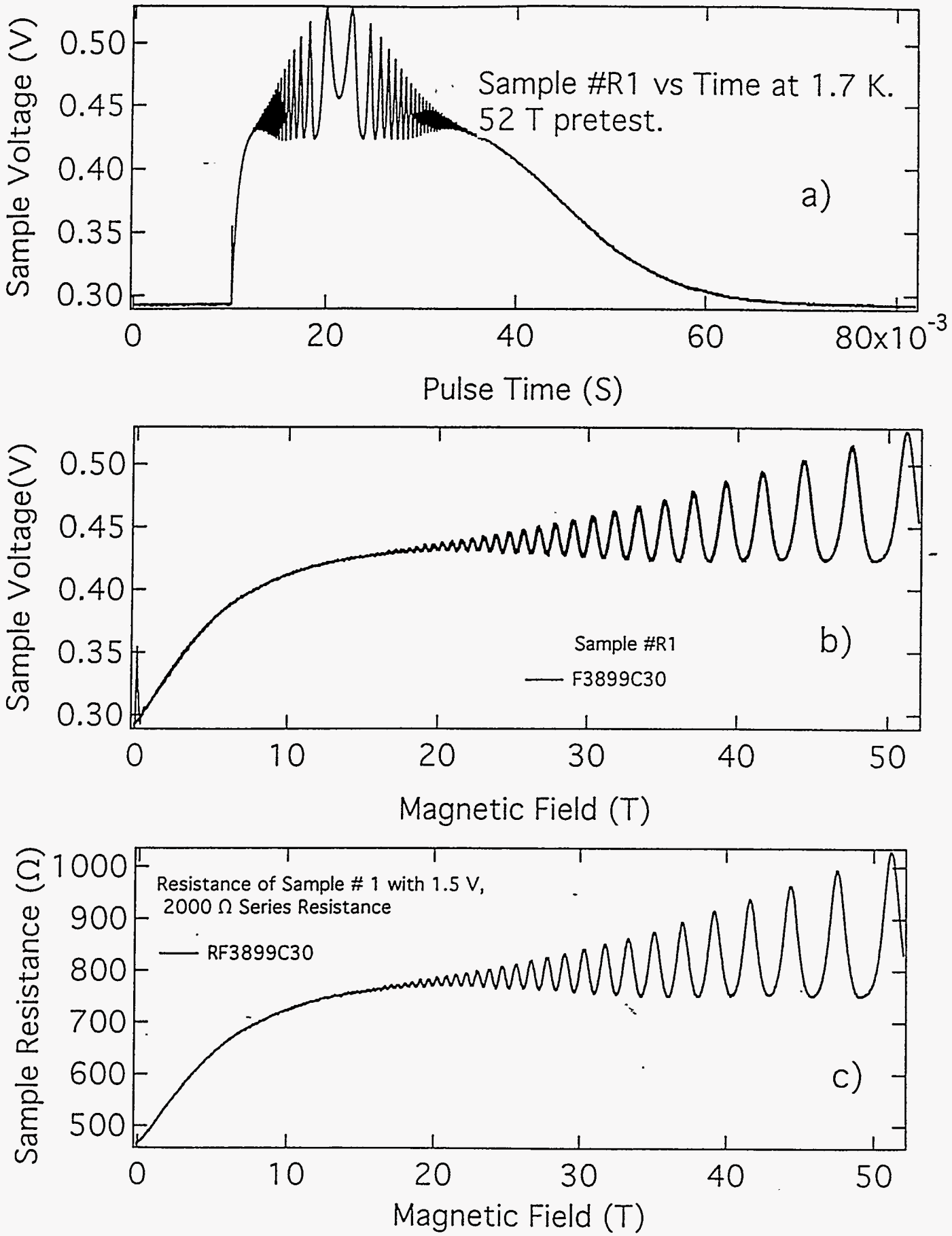

Figure 14 a,b,c

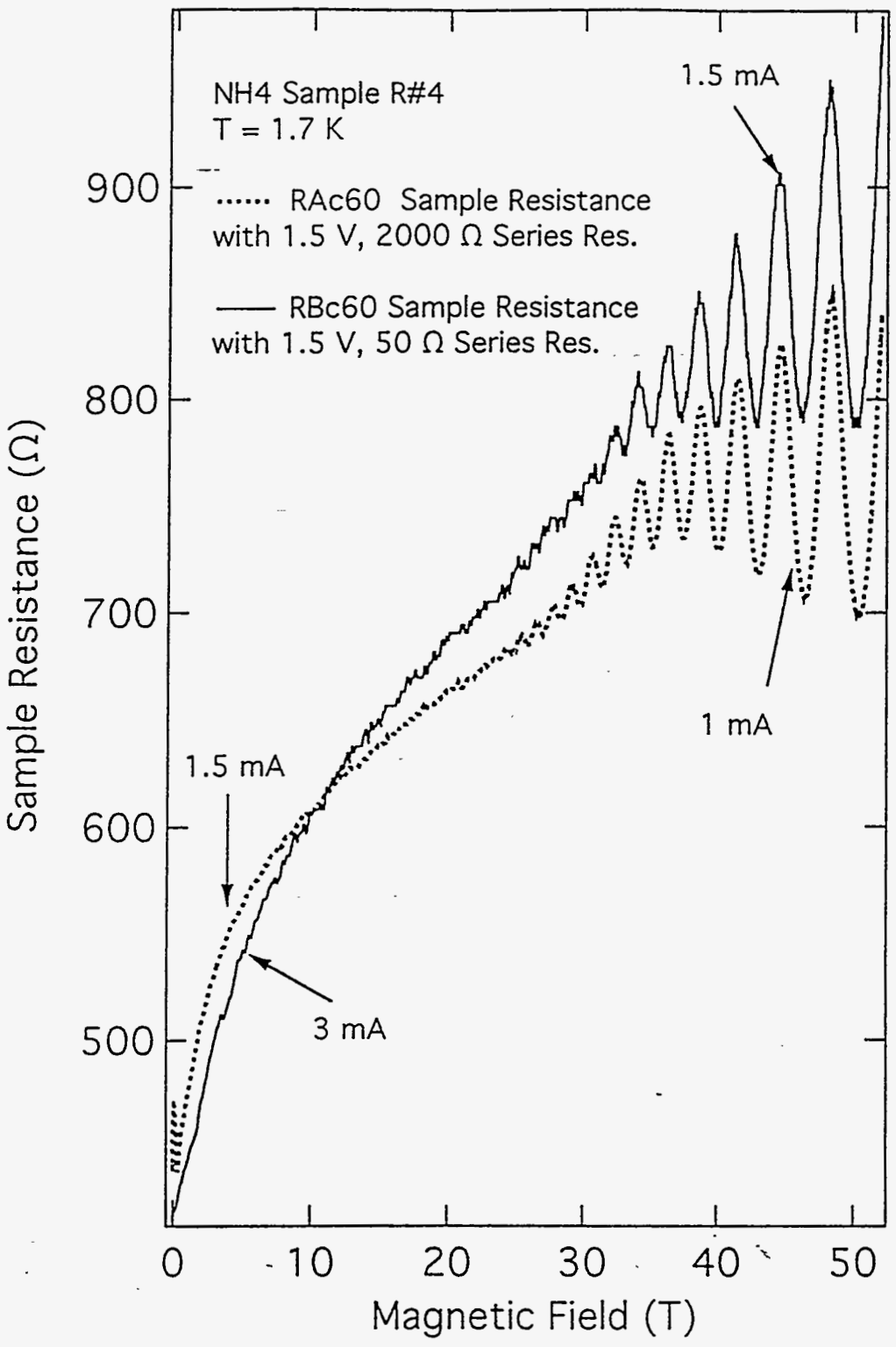
NH4 Sample R#4
T = 1.7 K
..... RAc60 Sample Resistance with 1.5 V, 2000 Ω Series Res.
—— RBc60 Sample Resistance with 1.5 V, 50 Ω Series Res.
1.5 mA
1 mA
1.5 mA
3 mA
Sample Resistance (Ω)
900
800
700
600
500
0
10
20
30
40
50
Magnetic Field (T)

Figure 15

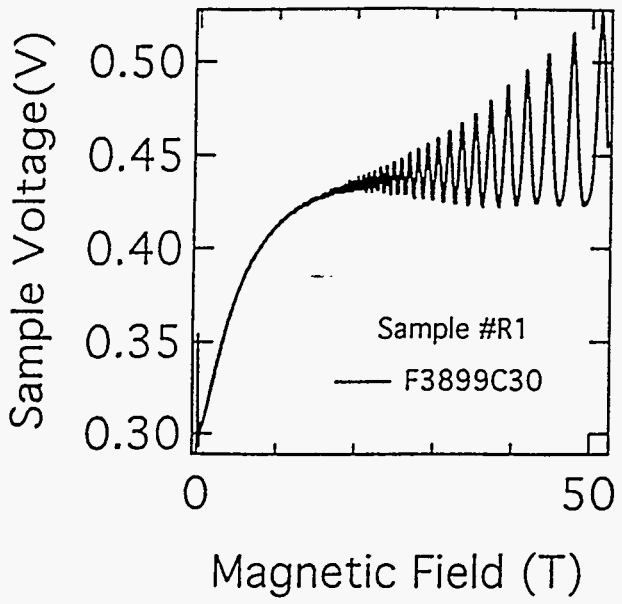
Sample Voltage(V)
0.50
0.45
0.40
0.35
0.30
0
50
Magnetic Field (T)
Sample #R1
F3899C30

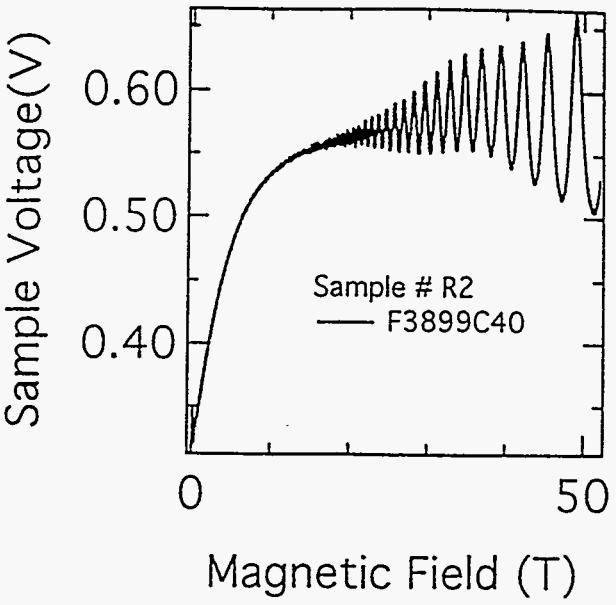
Sample Voltage(V)
0.60
0.50
0.40
0
50
Magnetic Field (T)
Sample # R2
F3899C40

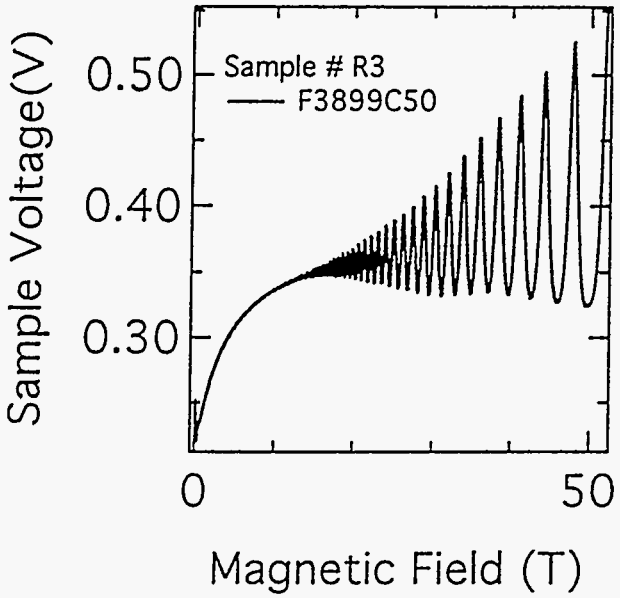
Sample Voltage(V)
0.50
0.40
0.30
0
50
Magnetic Field (T)
Sample # R3
F3899C50

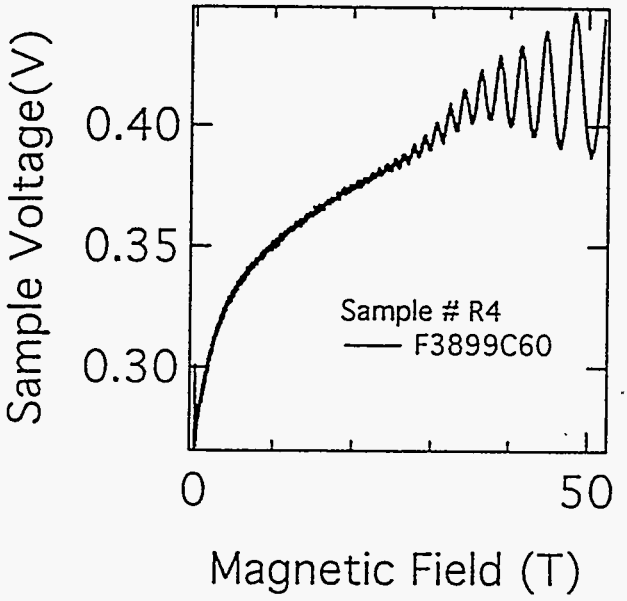
Sample Voltage(V)
0.40
0.35
0.30
0
50
Magnetic Field (T)
Sample # R4
F3899C60

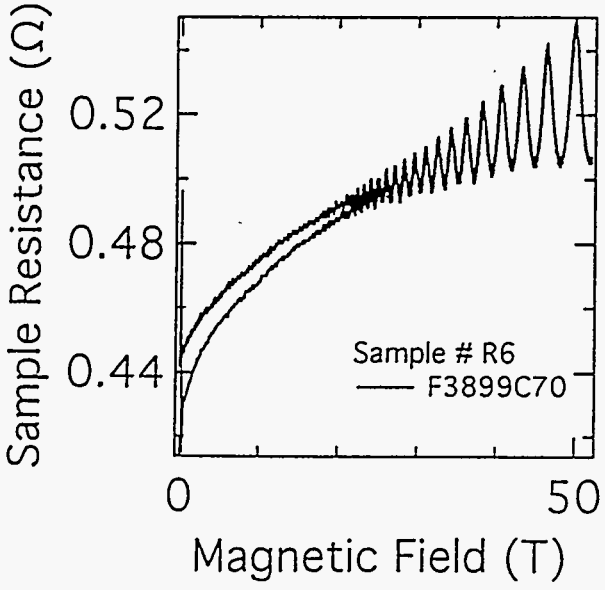
Sample Resistance (Ω)
0.52
0.48
0.44
0
50
Magnetic Field (T)
Sample # R6
F3899C70

Figure 16

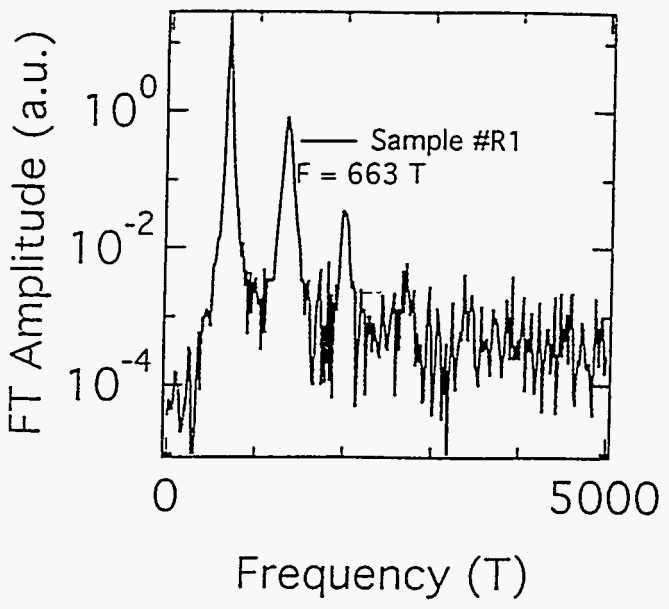
FT Amplitude (a.u.)
10^0
10^{-2}
10^{-4}
Sample #R1
F = 663 T
0
5000
Frequency (T)

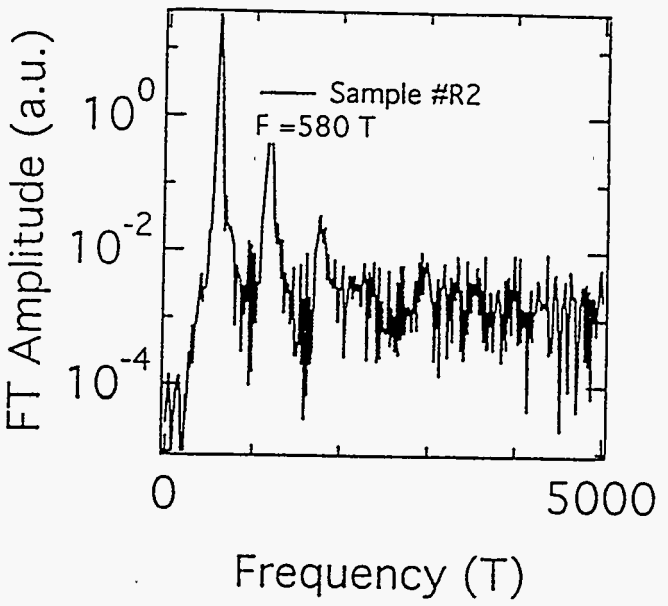
FT Amplitude (a.u.)
10^0
10^{-2}
10^{-4}
Sample #R2
F =580 T
0
5000
Frequency (T)

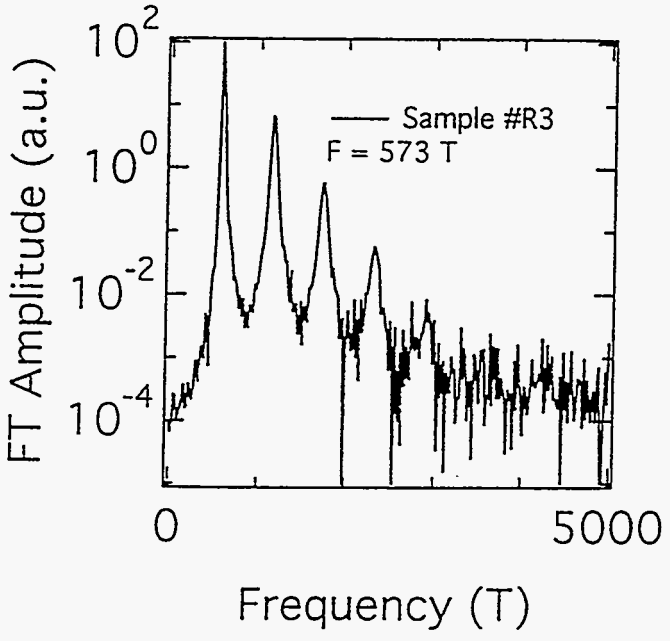
FT Amplitude (a.u.)
10^2
10^0
10^{-2}
10^{-4}
Sample #R3
F = 573 T
0
5000
Frequency (T)

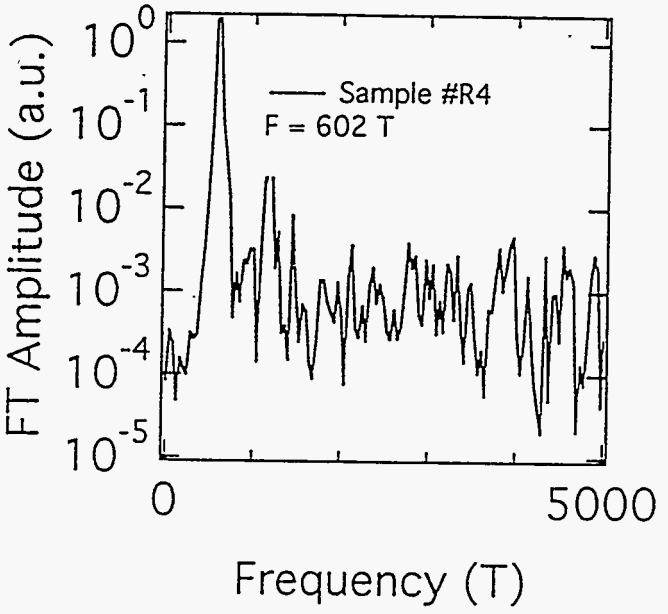
FT Amplitude (a.u.)
10^0
10^{-1}
10^{-2}
10^{-3}
10^{-4}
10^{-5}
Sample #R4
F = 602 T
0
5000
Frequency (T)

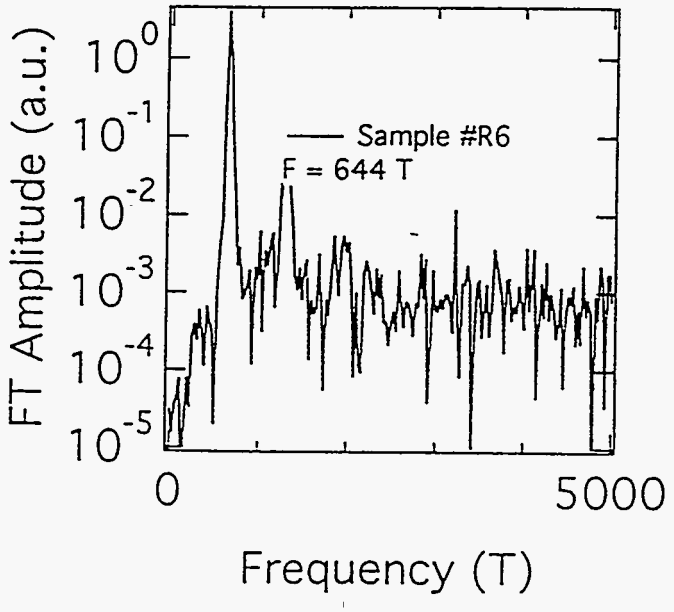
FT Amplitude (a.u.)
10^0
10^{-1}
10^{-2}
10^{-3}
10^{-4}
10^{-5}
Sample #R6
F = 644 T
0
5000
Frequency (T)

Figure 17

Note: Idea is to run 750 MHz carrier through co-planar line and the sample, and to demodulate the carrier, amplify the rectified signal, and send it via the buffer to the scope through a 50 Ω impedance.

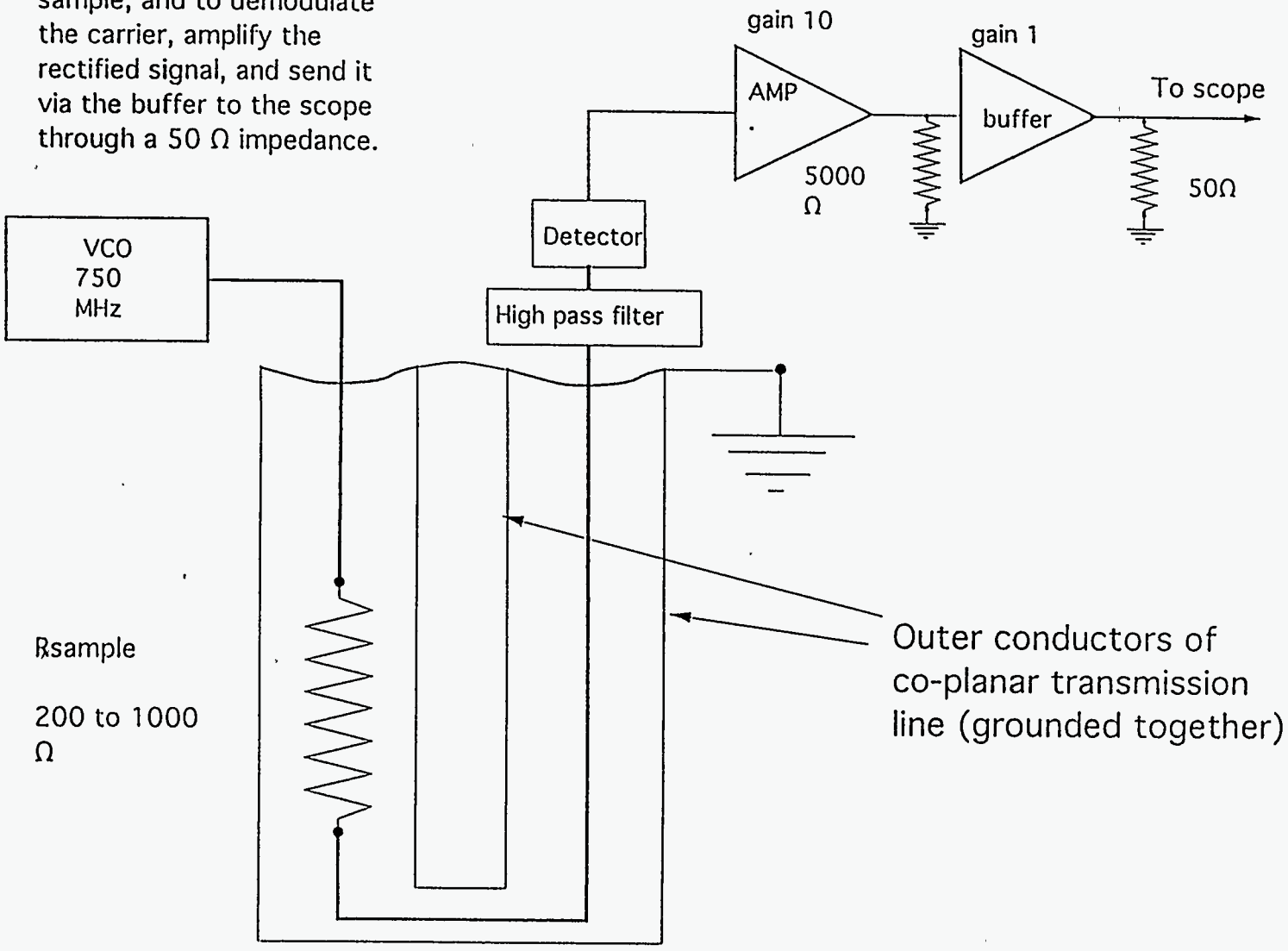

Electronics set up for MC1-C

Figure 18

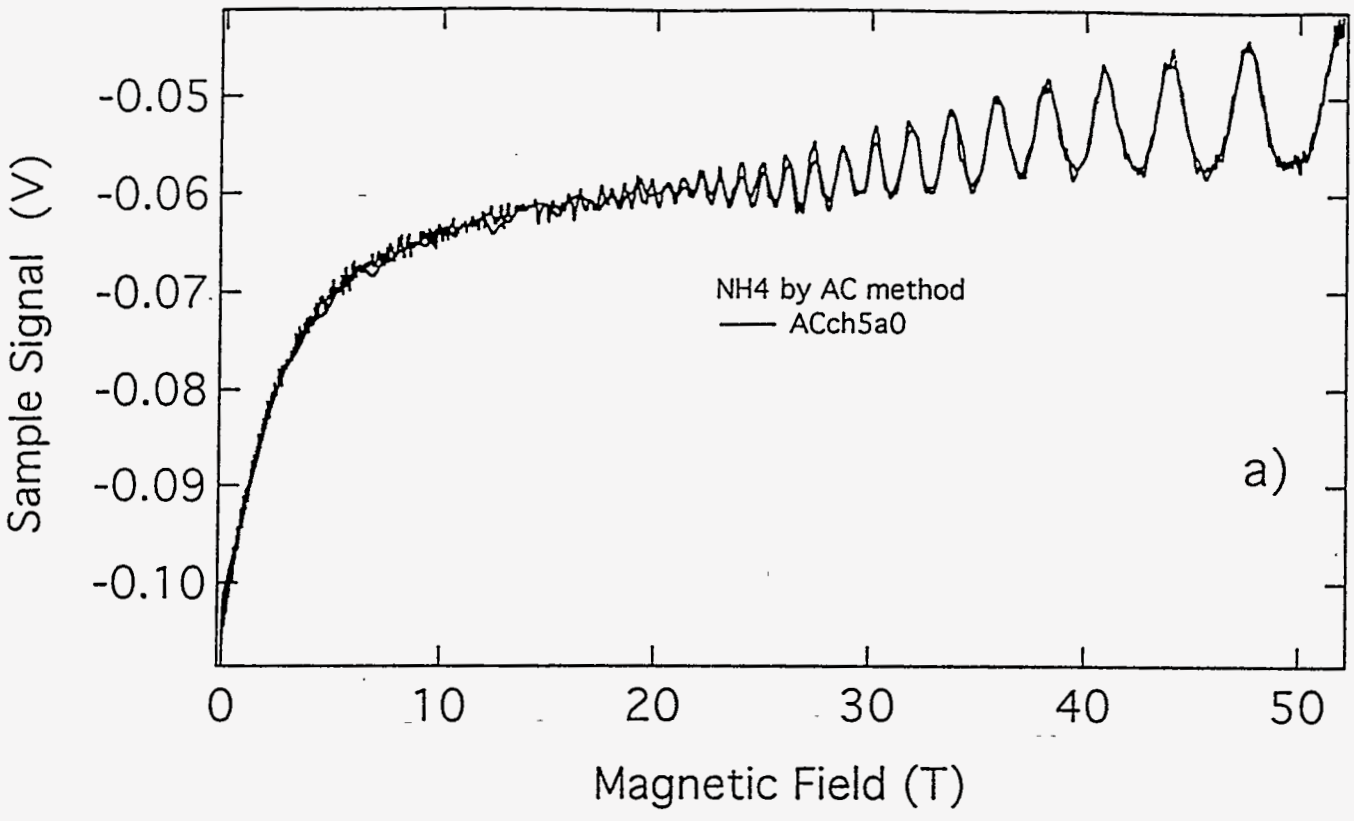
Sample Signal (V)
-0.05
-0.06
-0.07
-0.08
-0.09
-0.10
NH4 by AC method
ACch5a0
a)
0
10
20
30
40
50
Magnetic Field (T)

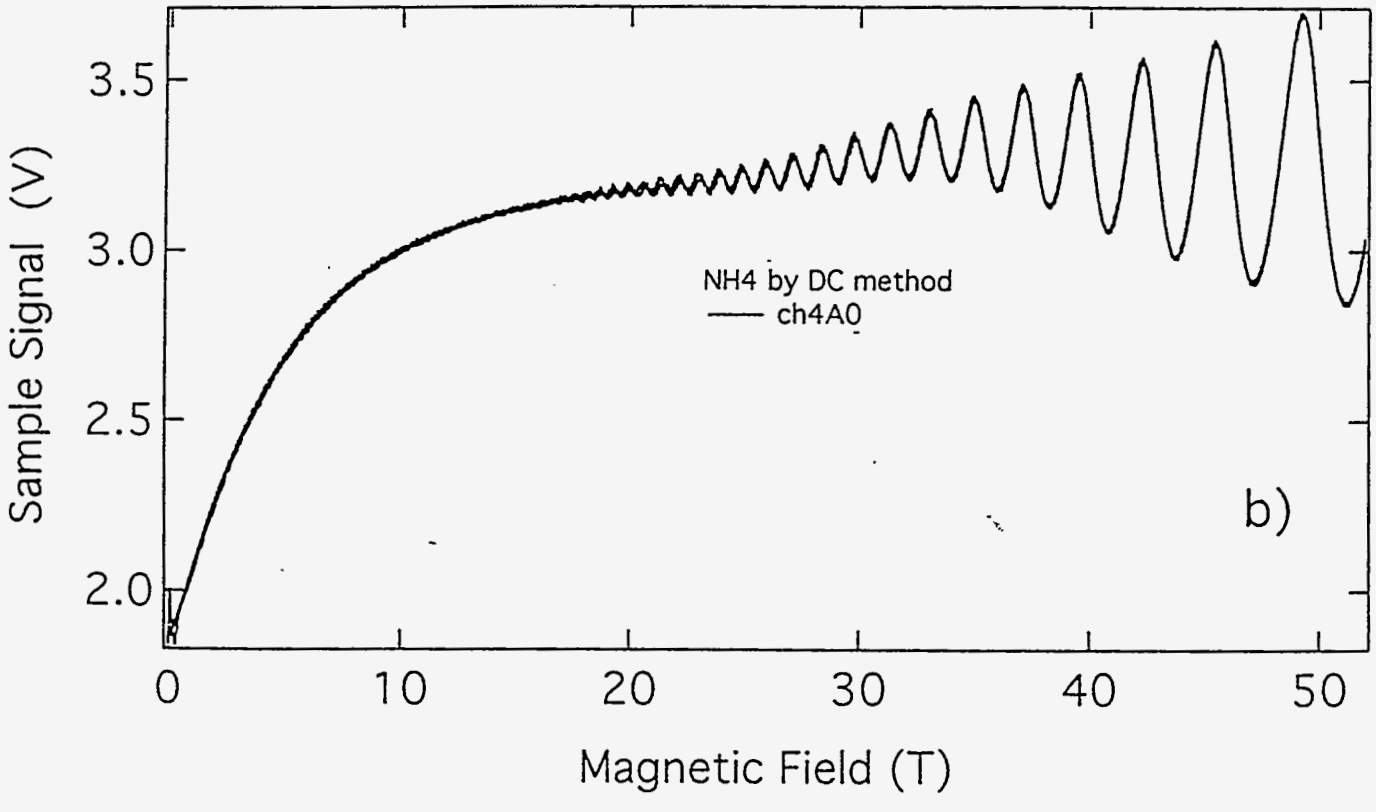
Sample Signal (V)
3.5
3.0
2.5
2.0
NH4 by DC method
ch4A0
b)
0
10
20
30
40
50
Magnetic Field (T)

Figure 19

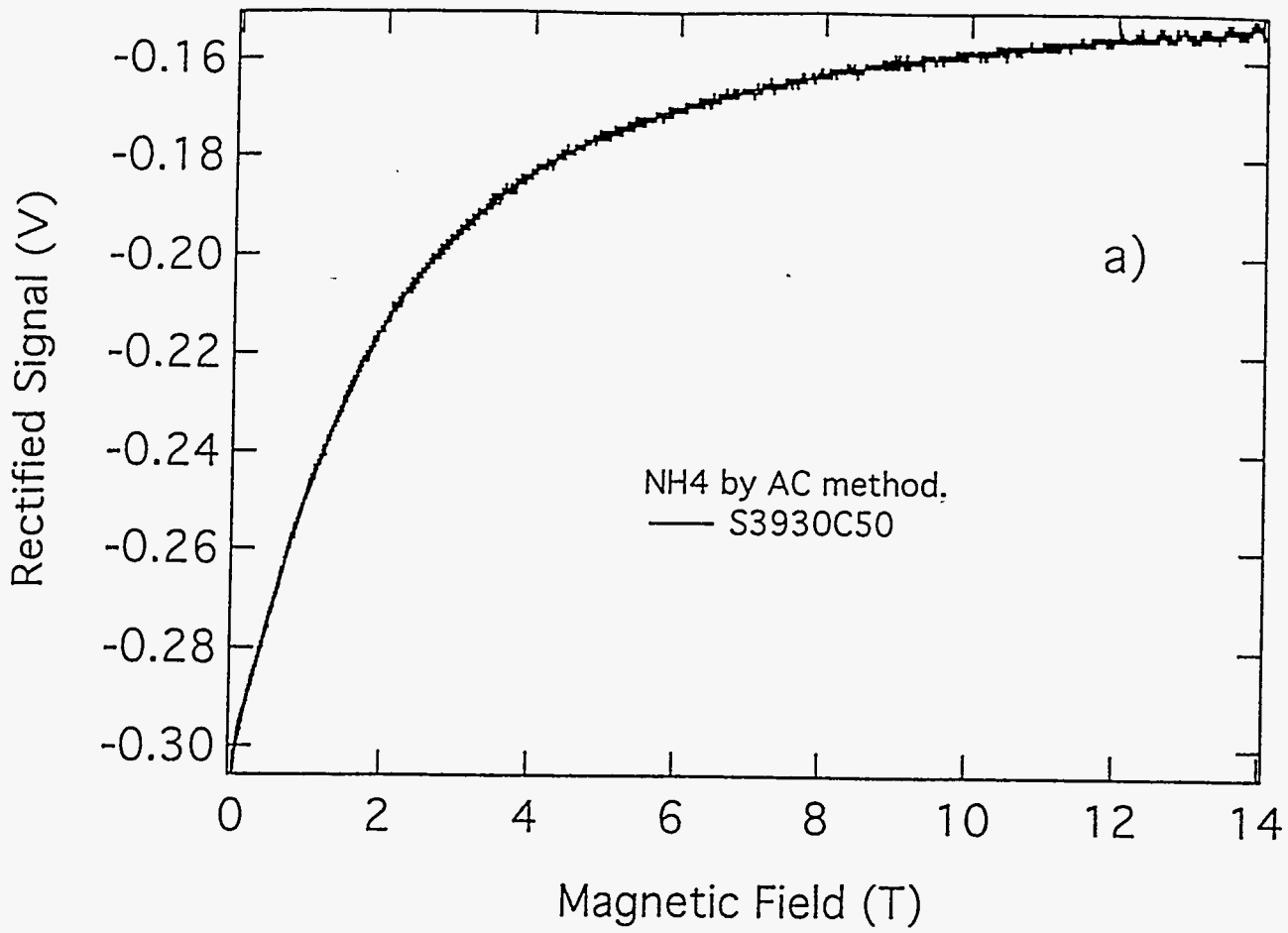
-0.16
-0.18
-0.20
-0.22
-0.24
-0.26
-0.28
-0.30
Rectified Signal (V)
a)
NH4 by AC method.
S3930C50
0
2
4
6
8
10
12
14
Magnetic Field (T)

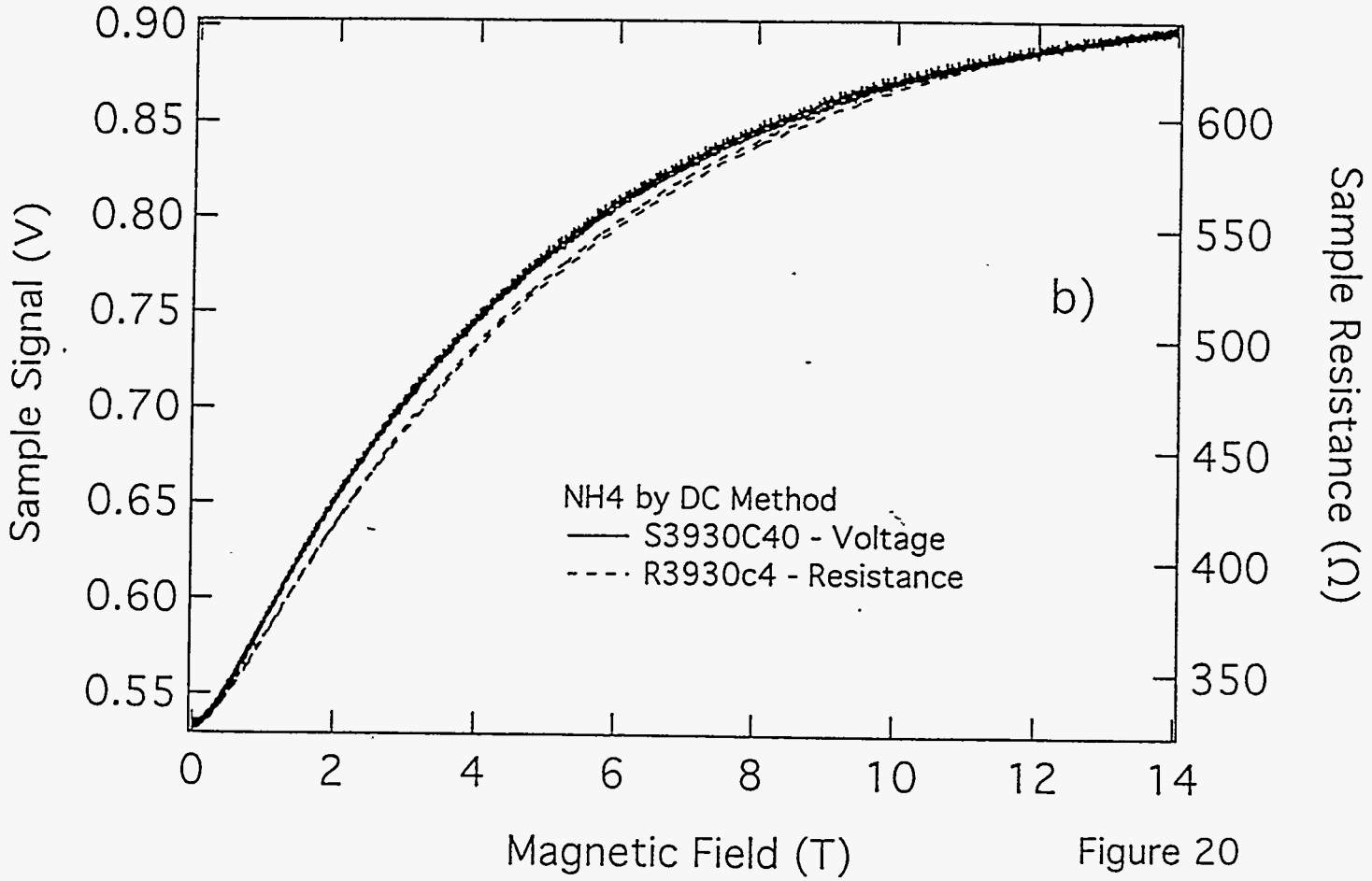
0.90
0.85
0.80
0.75
0.70
0.65
0.60
0.55
Sample Signal (V)
600
550
500
450
400
350
Sample Resistance (Ω)
b)
NH4 by DC Method
S3930C40 - Voltage
R3930c4 - Resistance
0
2
4
6
8
10
12
14
Magnetic Field (T)

Figure 20

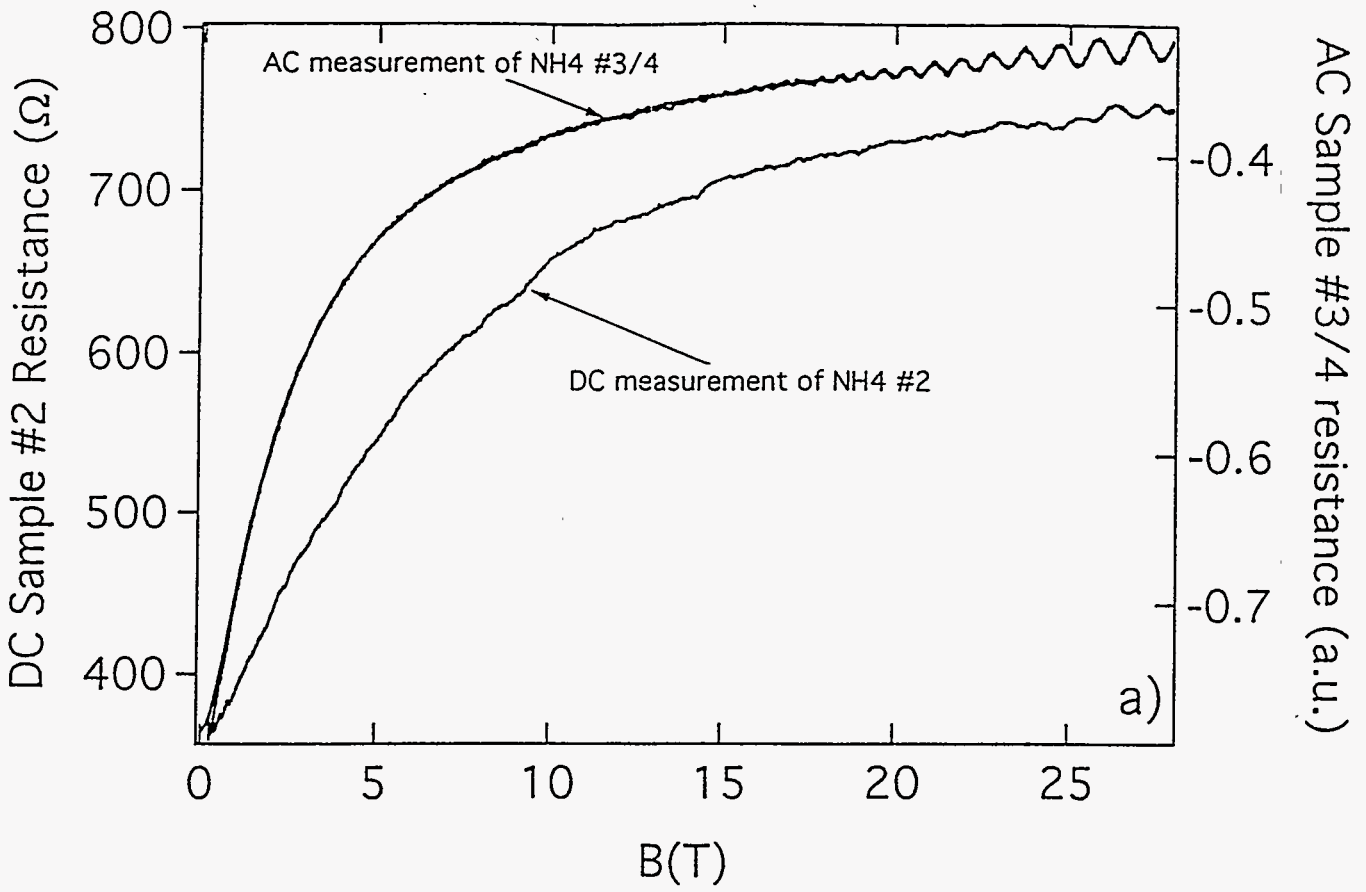
AC measurement of NH4 #3/4
DC measurement of NH4 #2
DC Sample #2 Resistance (Ω)
AC Sample #3/4 resistance (a.u.)
B(T)
a)

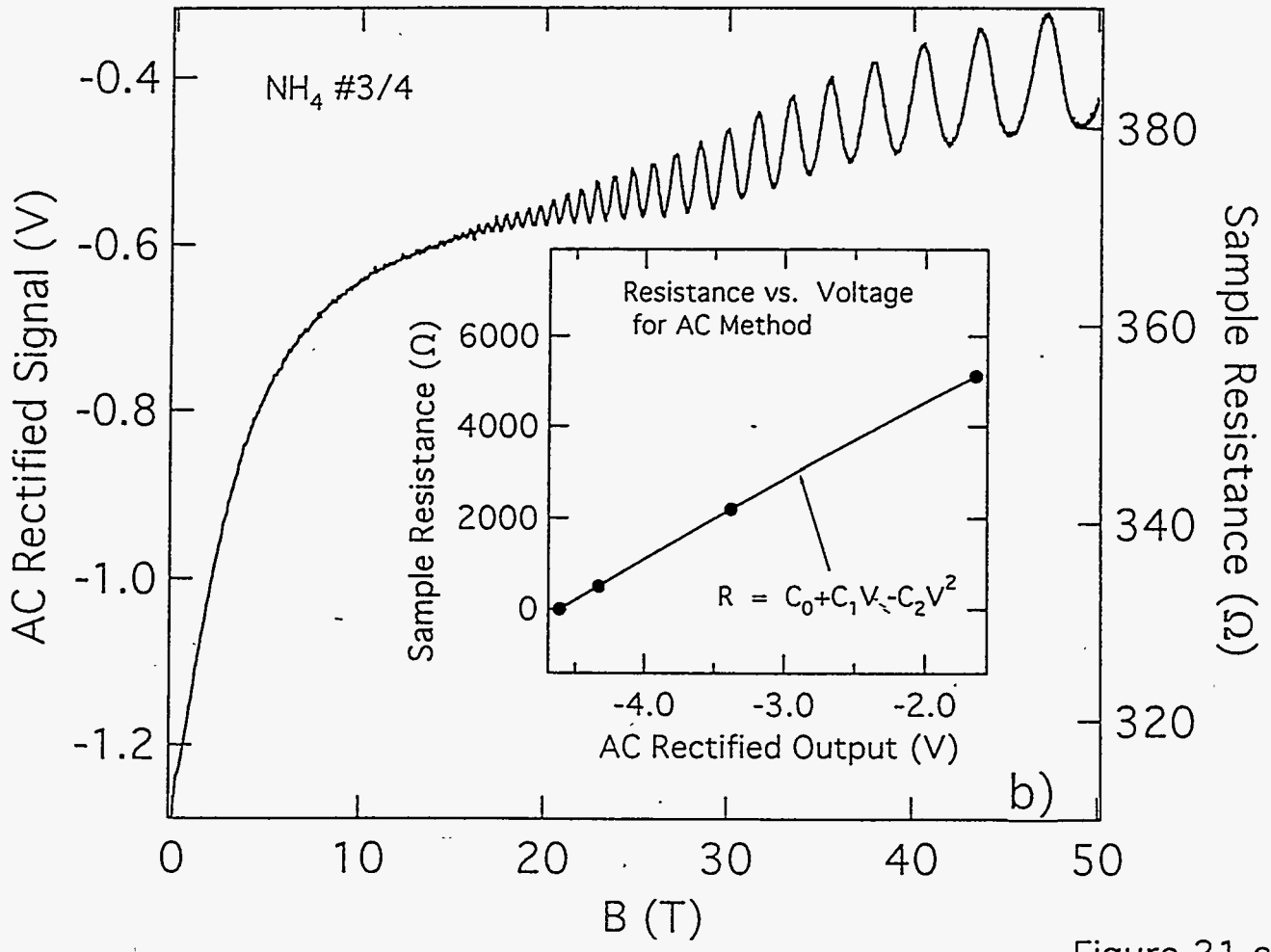
NH4 #3/4
AC Rectified Signal (V)
Sample Resistance (Ω)
B (T)
Resistance vs. Voltage for AC Method
R = C0+C1V-C2V2
AC Rectified Output (V)
b)

Figure 21 a,b

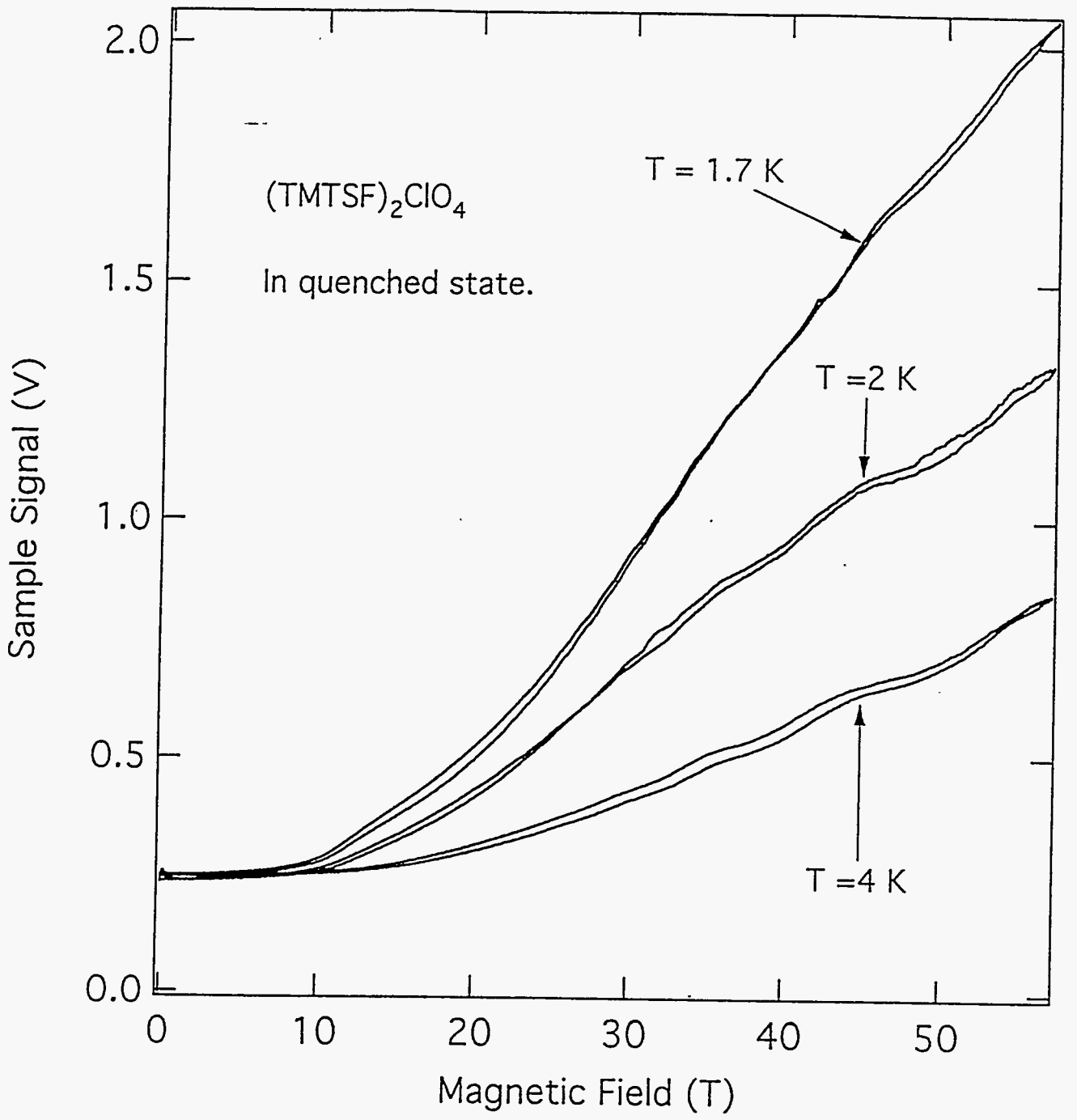
2.0
1.5
1.0
0.5
0.0
Sample Signal (V)
(TMTSF)2ClO4
In quenched state.
T = 1.7 K
T =2 K
T =4 K
0
10
20
30
40
50
Magnetic Field (T)

Figure 22

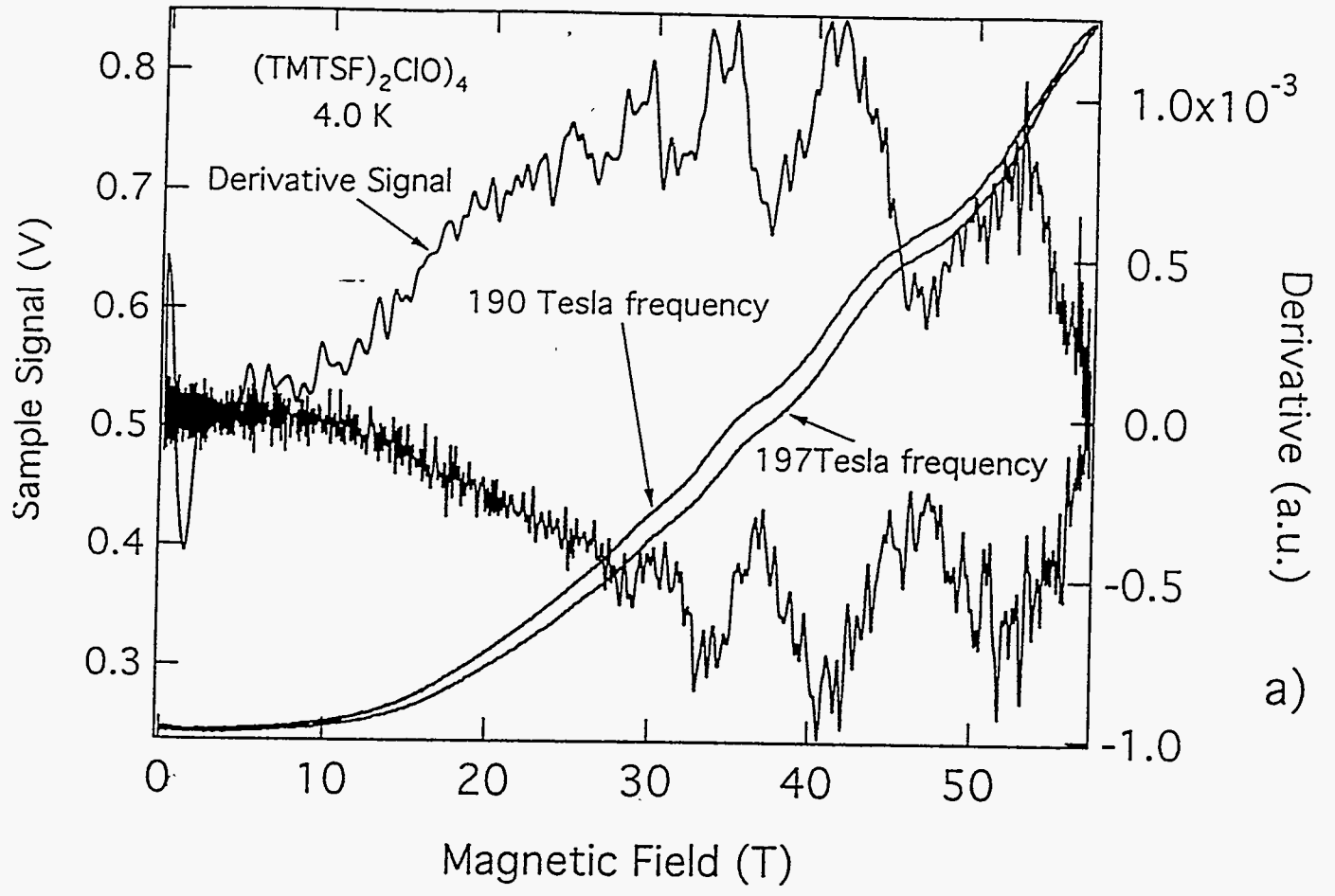
(TMTSF)2ClO)4
4.0 K
Derivative Signal
190 Tesla frequency
197Tesla frequency
Sample Signal (V)
Derivative (a.u.)
1.0x10-3
0.5
0.0
-0.5
-1.0
0.8
0.7
0.6
0.5
0.4
0.3
0
10
20
30
40
50
Magnetic Field (T)
a)

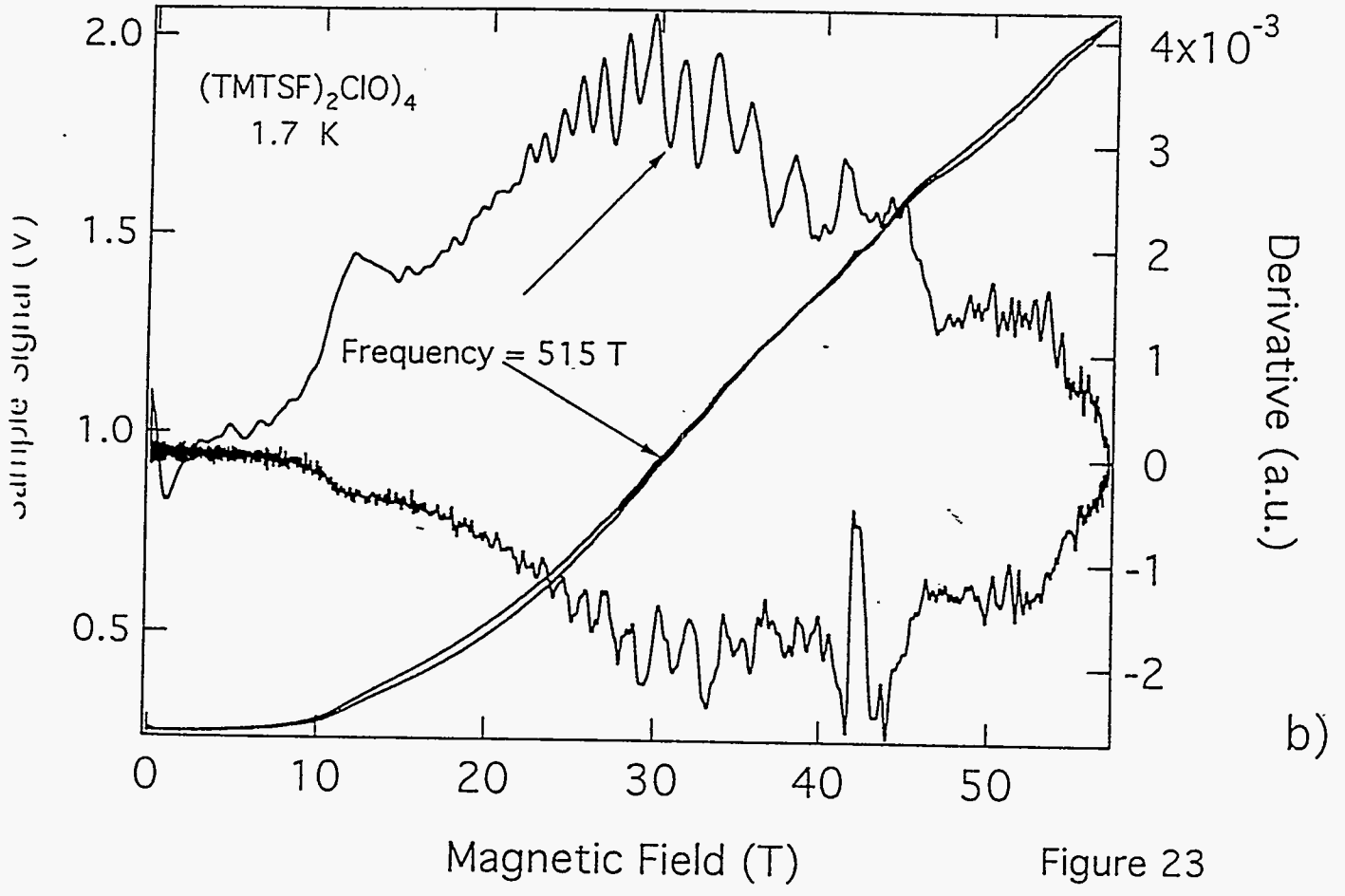
(TMTSF)2ClO)4
1.7 K
Frequency = 515 T
Sample Signal (V)
Derivative (a.u.)
4x10-3
3
2
1
0
-1
-2
2.0
1.5
1.0
0.5
0
10
20
30
40
50
Magnetic Field (T)
b)

Figure 23

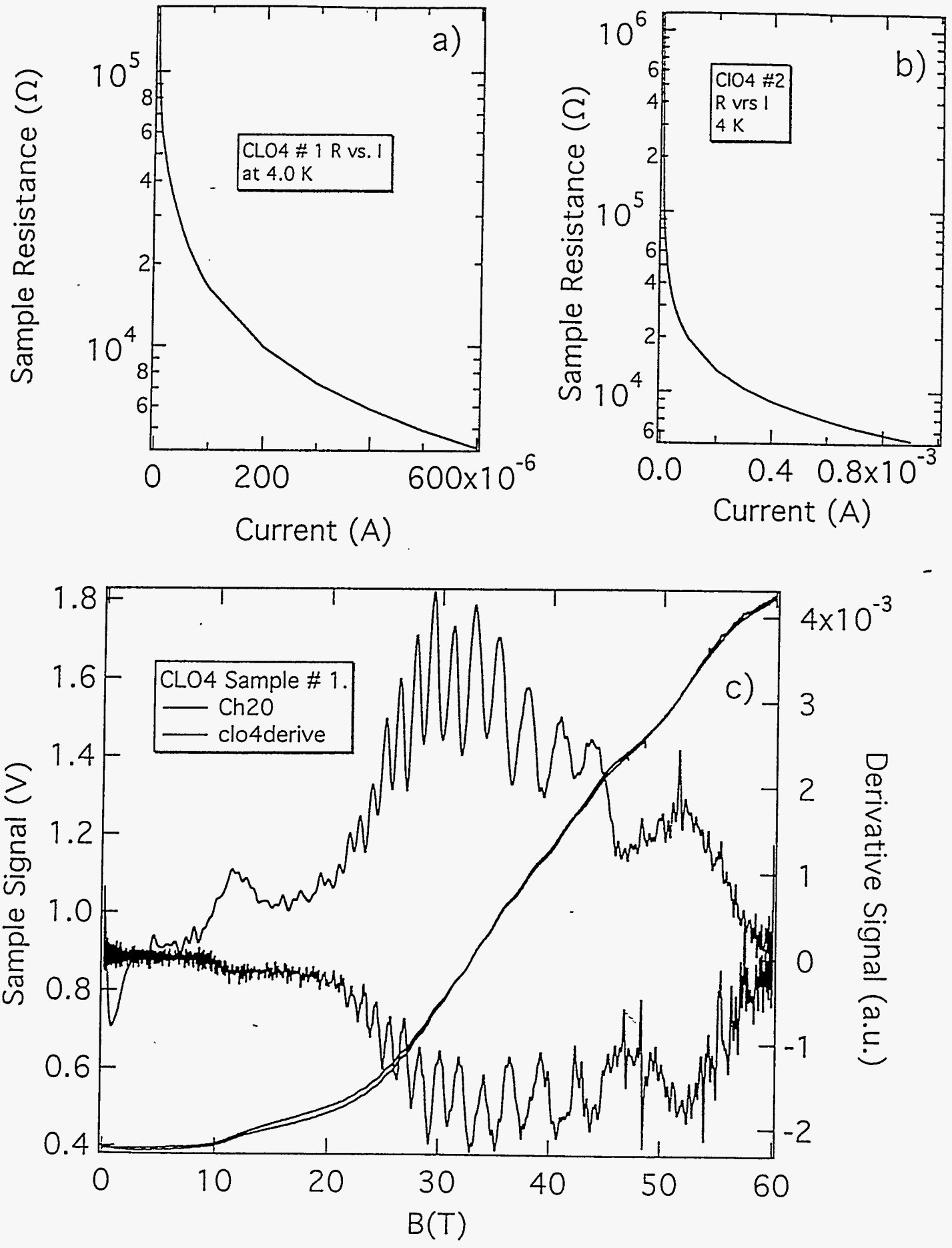

Figure 24 a, b, c

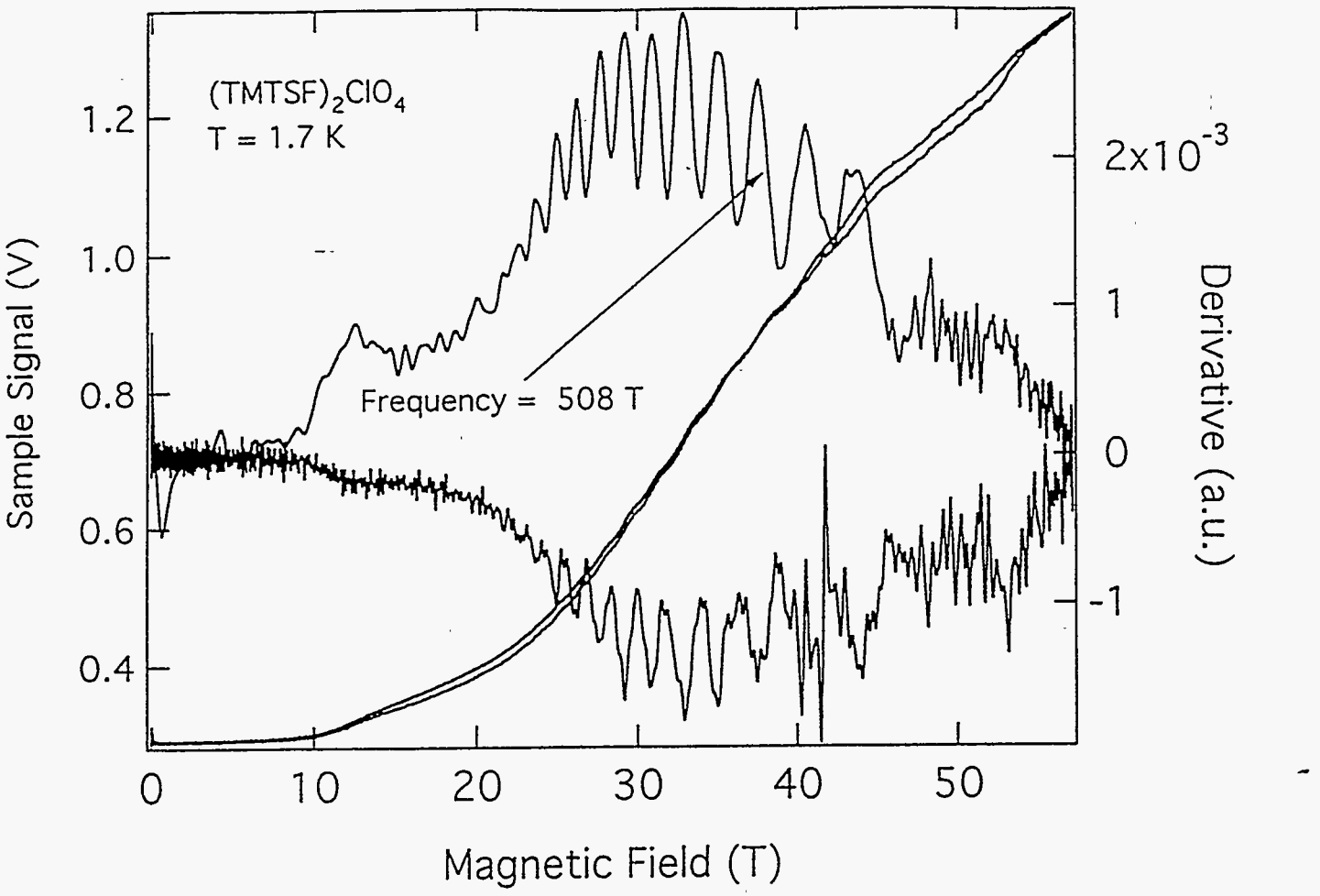
(TMTSF)2ClO4
T = 1.7 K
Frequency = 508 T
Sample Signal (V)
Derivative (a.u.)
2x10-3
1
0
-1
1.2
1.0
0.8
0.6
0.4
0
10
20
30
40
50
Magnetic Field (T)

Figure 25

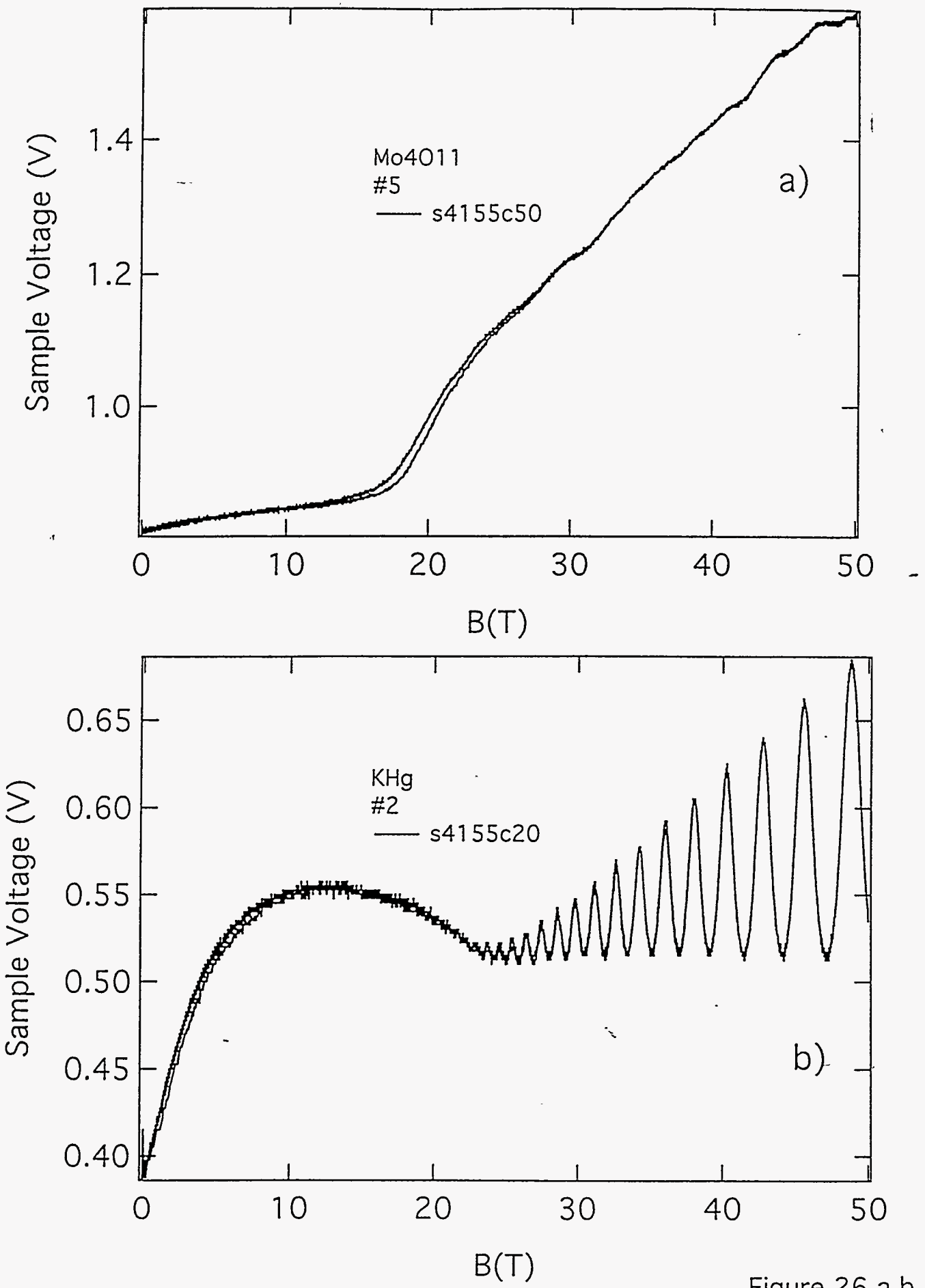
Sample Voltage (V)
1.4
1.2
1.0
Mo4011
#5
s4155c50
a)
0
10
20
30
40
50
B(T)
Sample Voltage (V)
0.65
0.60
0.55
0.50
0.45
0.40
KHg
#2
s4155c20
b)
0
10
20
30
40
50
B(T)

Figure 26 a,b

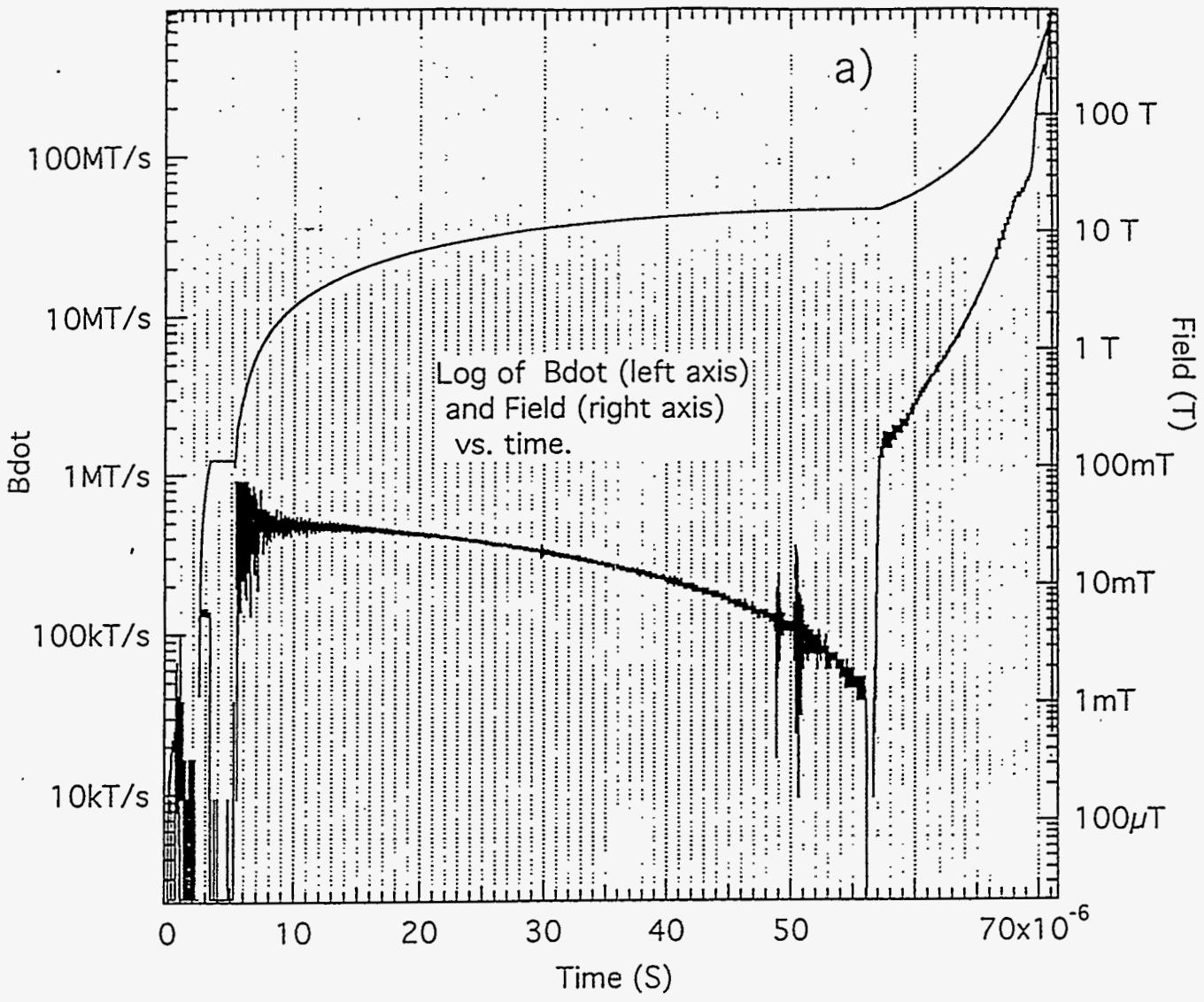
a)
100MT/s
10MT/s
1MT/s
100kT/s
10kT/s
Bdot
Log of Bdot (left axis)
and Field (right axis)
vs. time.
100 T
10 T
1 T
100mT
10mT
1mT
100μT
Field (T)
0
10
20
30
40
50
70x10-6
Time (S)

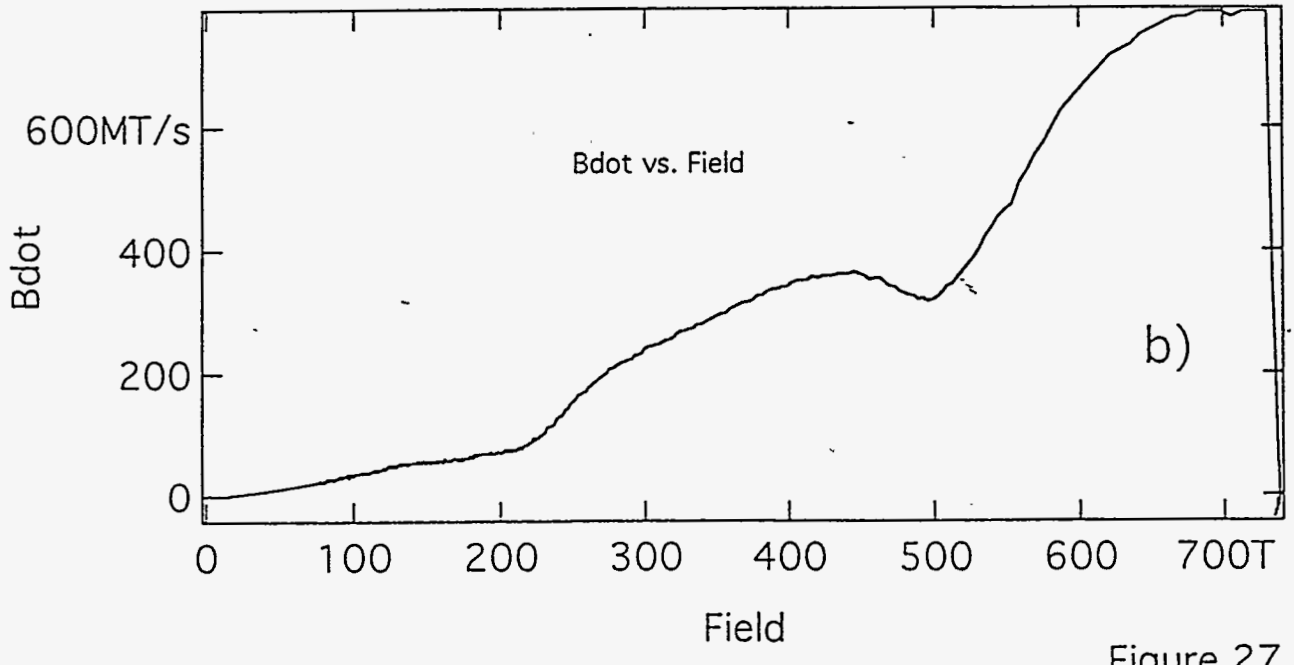
600MT/s
400
200
0
Bdot
Bdot vs. Field
b)
0
100
200
300
400
500
600
700T
Field

Figure 27 a & b

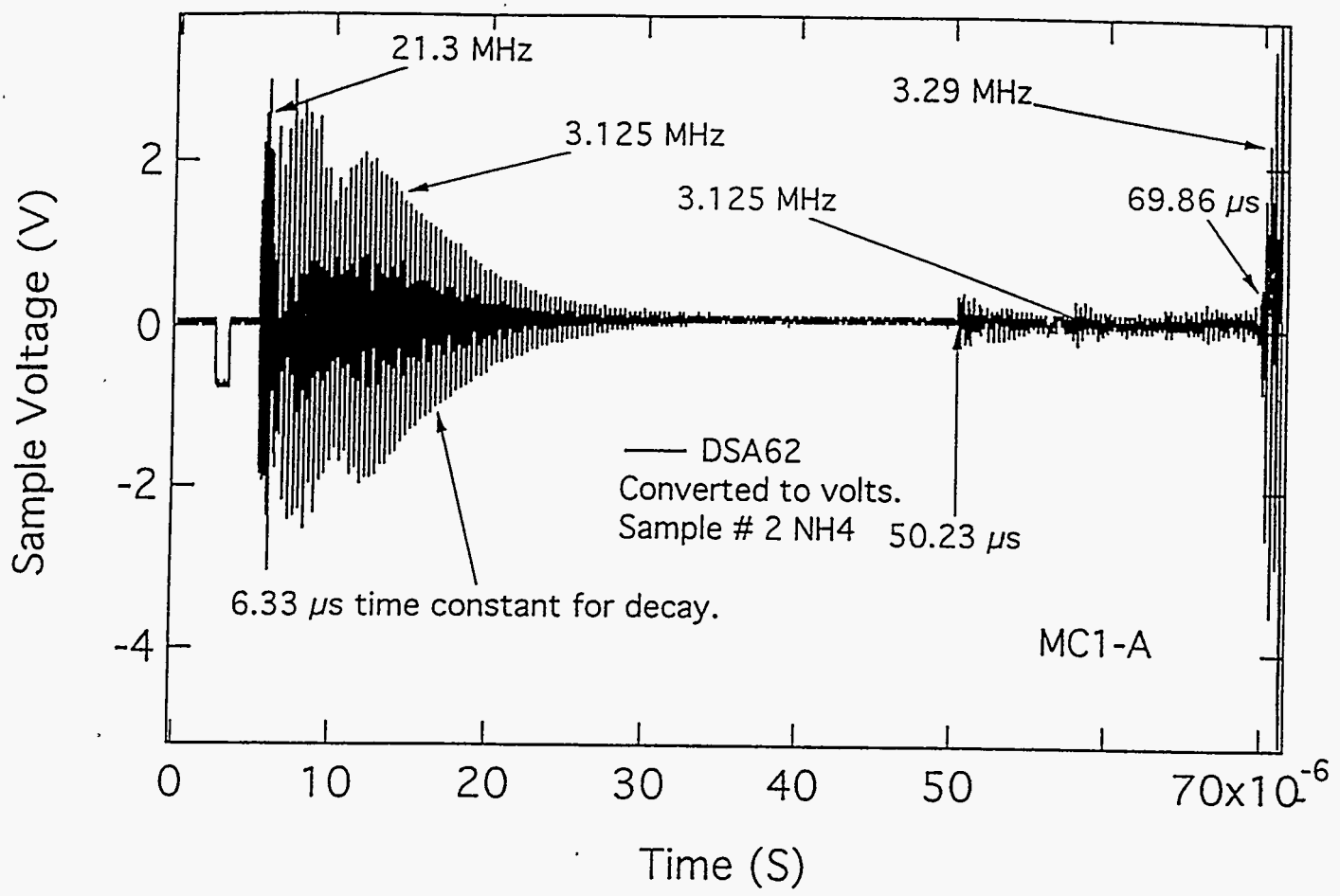
21.3 MHz
3.125 MHz
3.29 MHz
3.125 MHz
69.86 μs
DSA62
Converted to volts.
Sample # 2 NH4
50.23 μs
6.33 μs time constant for decay.
MC1-A
Sample Voltage (V)
2
0
-2
-4
0
10
20
30
40
50
70x10-6
Time (S)

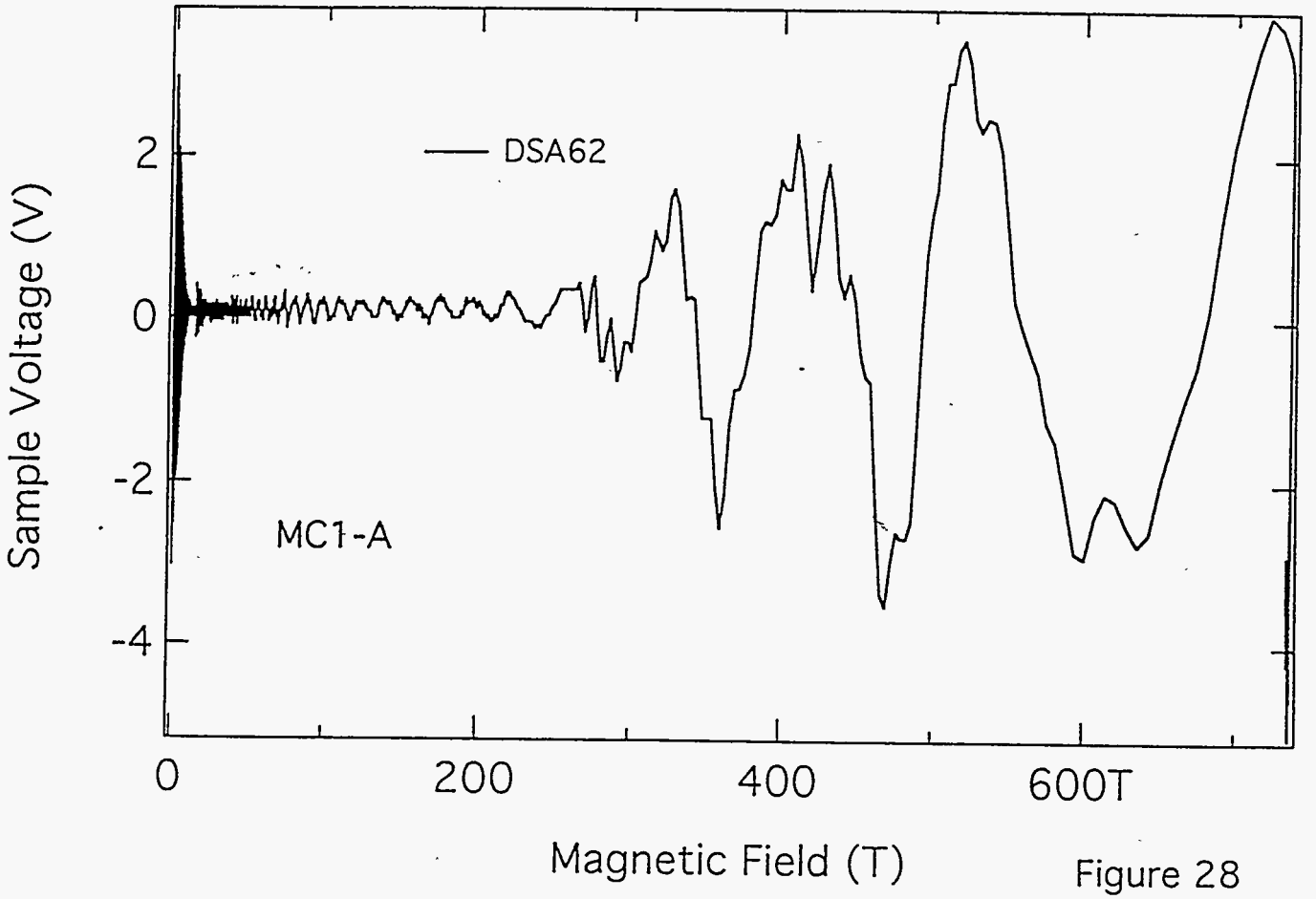
DSA62
MC1-A
Sample Voltage (V)
2
0
-2
-4
0
200
400
600T
Magnetic Field (T)

Figure 28

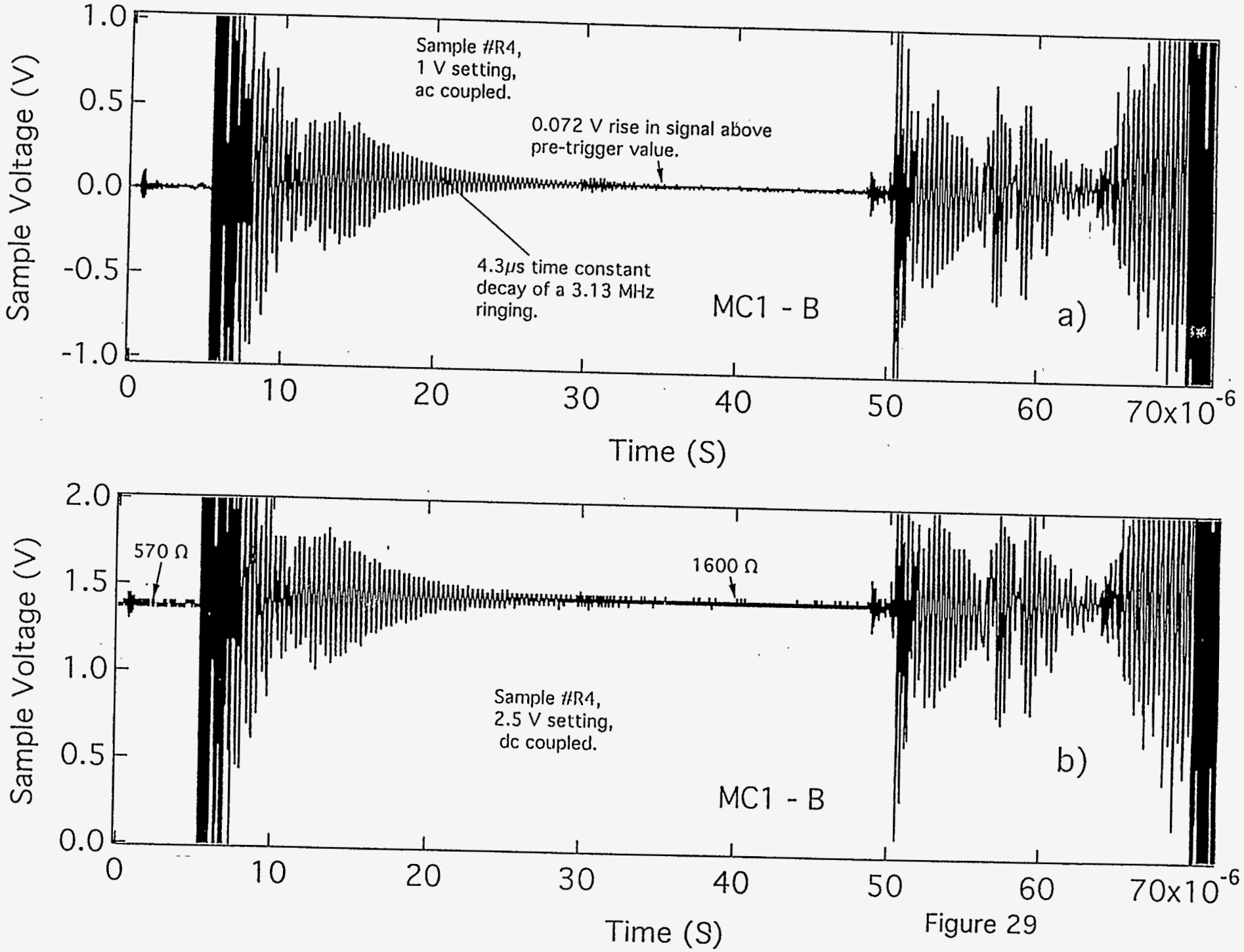
Sample Voltage (V)
1.0
0.5
0.0
-0.5
-1.0
Sample #R4,
1 V setting,
ac coupled.
0.072 V rise in signal above
pre-trigger value.
4.3μs time constant
decay of a 3.13 MHz
ringing.
MC1 - B
a)
0
10
20
30
40
50
60
70x10-6
Time (S)
Sample Voltage (V)
2.0
1.5
1.0
0.5
0.0
570 Ω
1600 Ω
Sample #R4,
2.5 V setting,
dc coupled.
MC1 - B
b)
0
10
20
30
40
50
60
70x10-6
Time (S)

Figure 29

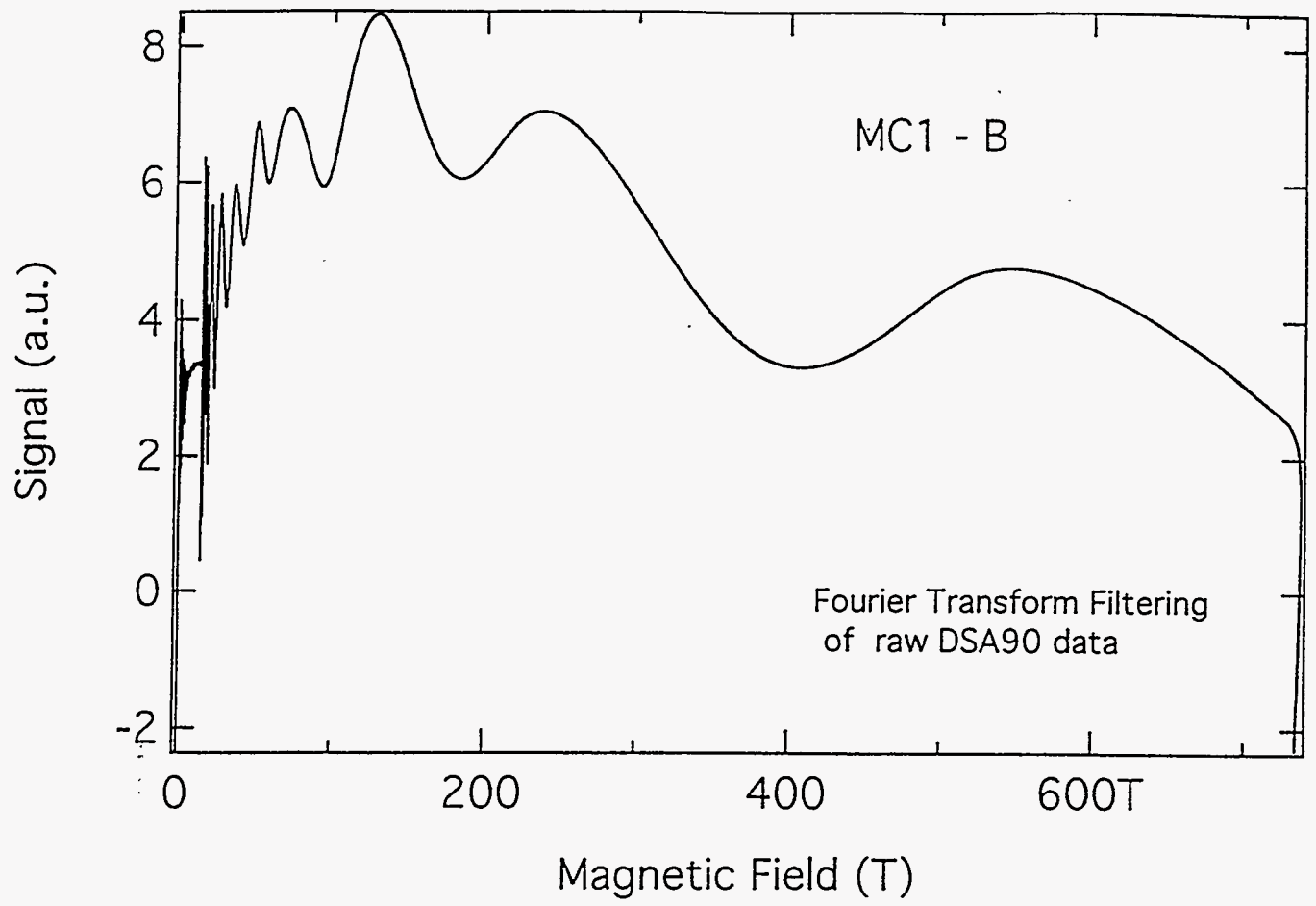
MC1 - B
Fourier Transform Filtering
of raw DSA90 data
Signal (a.u.)
8
6
4
2
0
-2
0
200
400
600T
Magnetic Field (T)

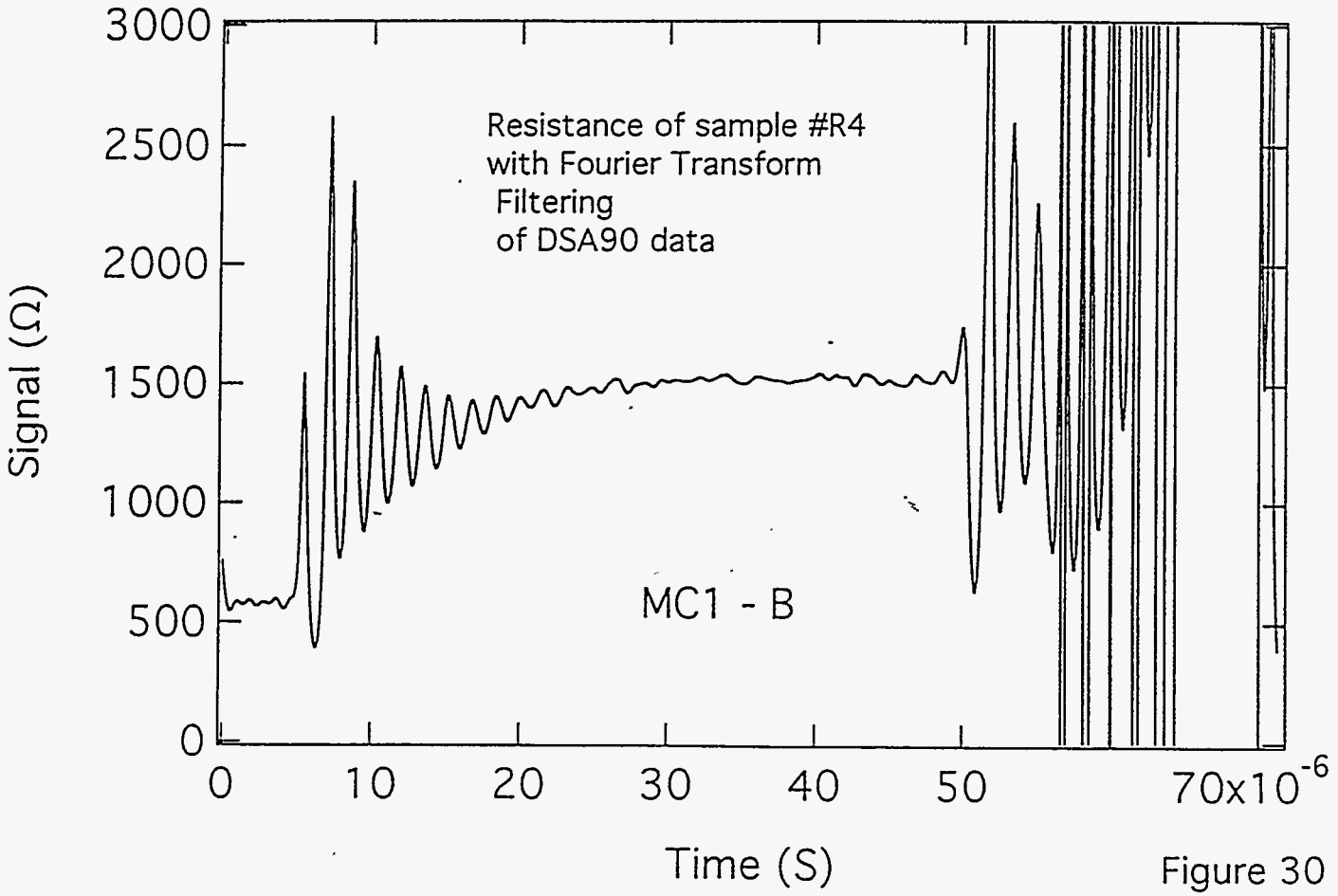
Resistance of sample #R4
with Fourier Transform
Filtering
of DSA90 data
MC1 - B
Signal (Ω)
3000
2500
2000
1500
1000
500
0
0
10
20
30
40
50
70x10-6
Time (S)

Figure 30

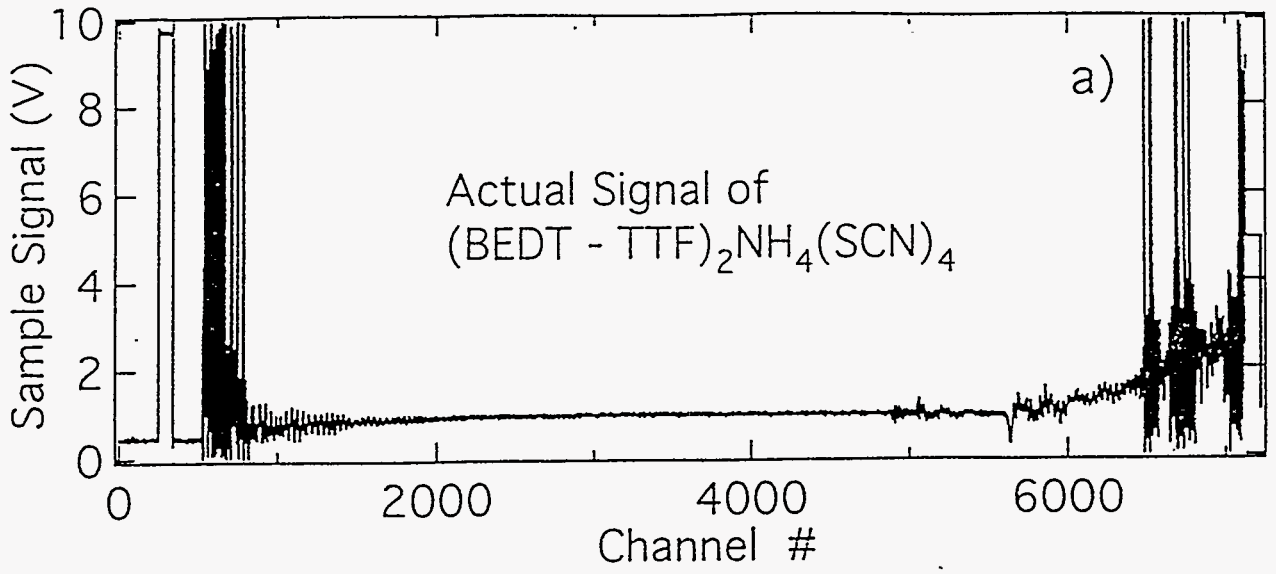
a)
Actual Signal of
(BEDT - TTF)2NH4(SCN)4
Sample Signal (V)
Channel #

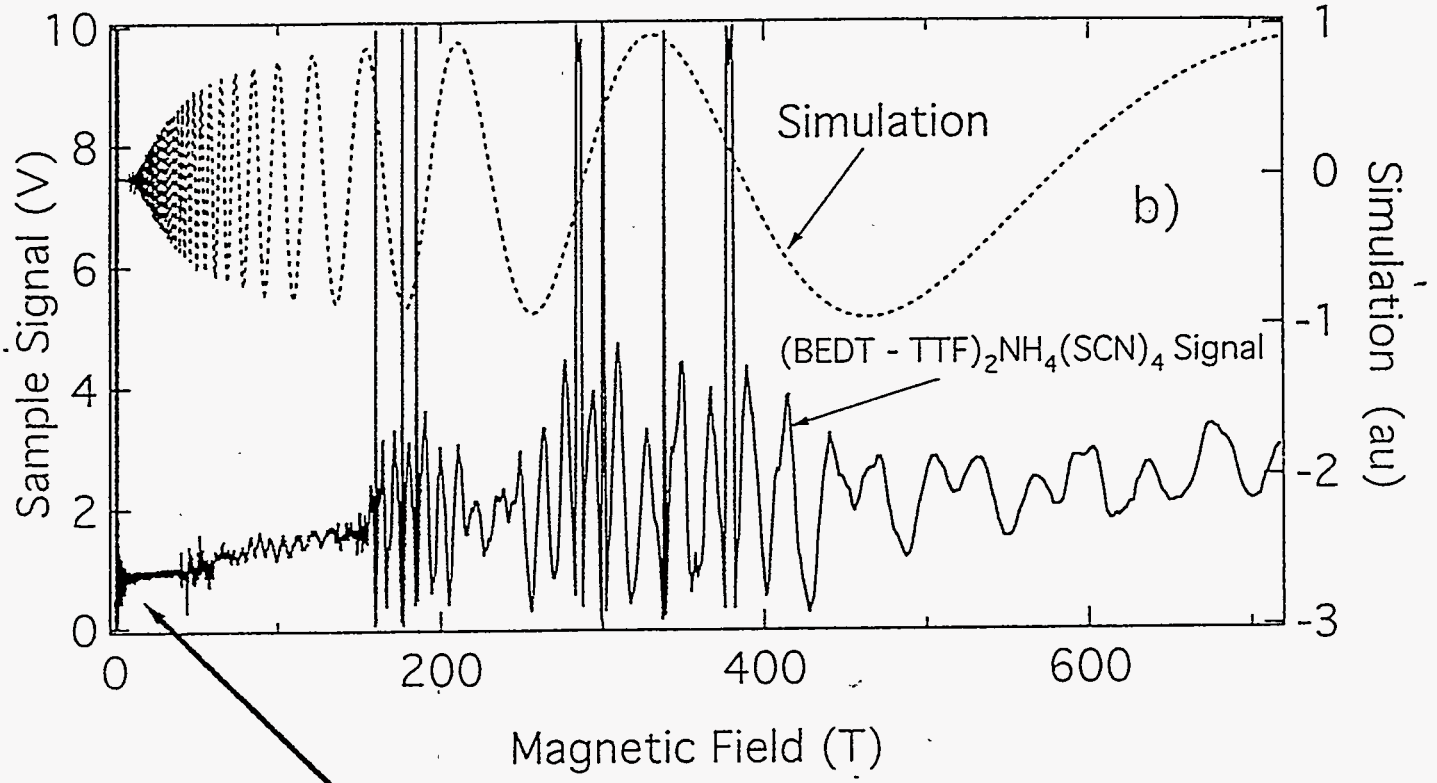
Simulation
b)
(BEDT - TTF)2NH4(SCN)4 Signal
Sample Signal (V)
Simulation (au)
Magnetic Field (T)

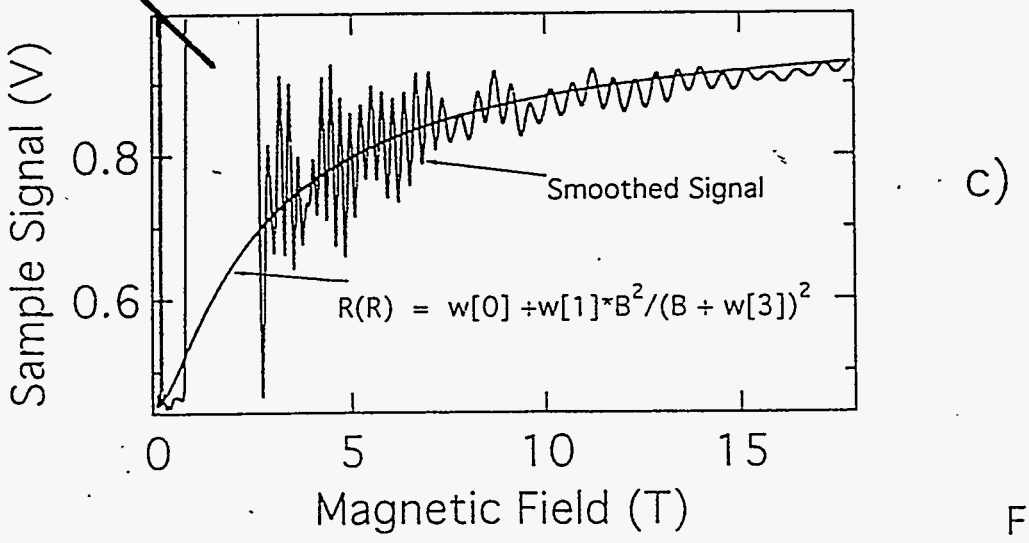
Smoothed Signal
R(R) = w[0] +w[1]*B2/(B + w[3])2
c)
Sample Signal (V)
Magnetic Field (T)

Figure 31